Stick-slip behavior of ice interacting with concrete surfaces

N. Nuus

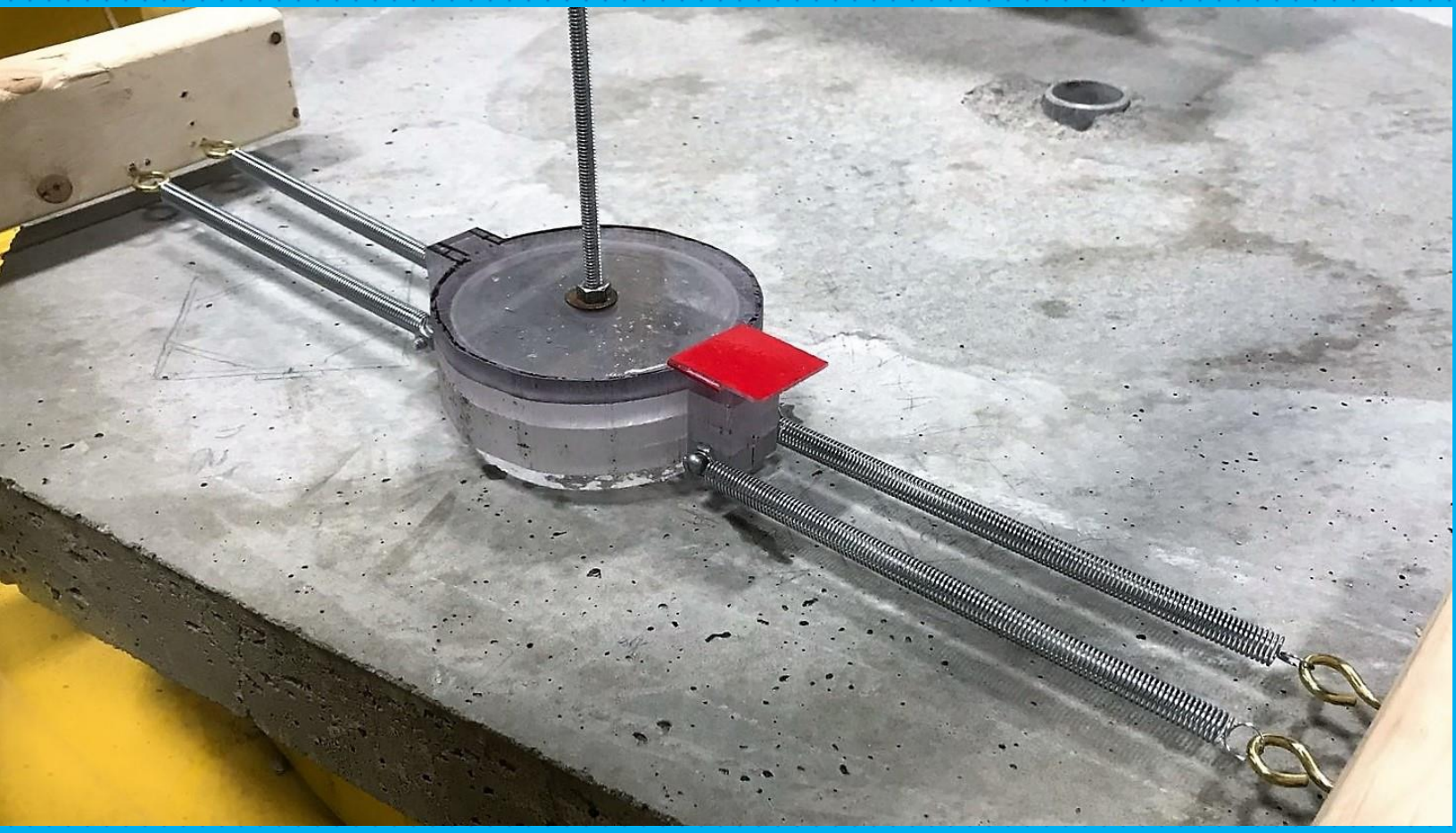

TU Delft

Memorial University

Stick-slip behavior of ice interacting with concrete surfaces

by

N. Nuus

to obtain the degree of Master of Science
in Offshore & Dredging Engineering
at the Delft University of Technology.

Student number:	4163176	
Project duration:	November 1, 2017 – November 8, 2018	
Thesis committee:	Prof. dr. A. Metrikine,	TU Delft – Chairman
	Ir. J. S. Hoving,	TU Delft
	Dr. S. E. Bruneau,	Memorial University of Newfoundland, Canada
	Dr. ir. K. N. Van Dalen,	TU Delft

An electronic version of this thesis is available at `http://repository.tudelft.nl/`.

TU Delft

MEMORIAL UNIVERSITY

Preface

Curiosity for the unknown and the ambition to challenge myself, have played a large role in the last seven years of my life. My choice to study Aerospace Engineering involved a move to the other side of the country, where I traded in a farm house for a student room and cows in my back yard for a billboard of IKEA. After finishing my bachelor, I felt the need for a change and shifted my focus to ocean related engineering challenges. I started with the MSc degree in Offshore- and Dredging Engineering with a specialization in Bottom Founded Offshore structures. When the opportunity arose to follow a two week course on the Norwegian archipelago Svalbard, in the Arctic Ocean, I jumped right in. Here, my interest for Arctic engineering and awe for remote environments was sparked. To my excitement, upon seeking advise for a graduation topic abroad, Jeroen Hoving introduced me to Stephen Bruneau, associate professor of the Civil Engineering department at Memorial University of Newfoundland in Canada.

From February to June 2018, I got the opportunity to work together with Dr. Stephen Bruneau, Dr. Bruce Colbourne, Dr. Amgad Hussein and Dr. Assem Hassan to design an experimental set-up for my graduation project. The experiment was performed in the labs of Memorial University with the guidance of Craig Mitchell, Matt Curtis and Trevor Clark. My sincere gratitude is given to everyone at Memorial University for their helpfulness. Thanks to my colleagues, Amanda Ryan, Titli Pramantik and Yiran Liu for their support and much needed coffee breaks. Many thanks goes out to my friends in St. John's for joining me on numerous adventures and making me truly feel at home.

This amazing experience and the completion of this work would never have been possible without the support of my thesis committee. Special thanks goes out to Stephen Bruneau and Jeroen Hoving for being wonderful daily supervisors. Last but not least, I would like to thank my parents for trusting me, my friends for their advice and helping me unwind, and my boyfriend Stijn for always being there and for having fruitful discussions about my work.

Executive summary

When sea or lake ice interacts with concrete offshore structures in Arctic regions, the frictional forces between the ice and the structure cause abrasion of the concrete surface of the structure. This may endanger the structural integrity when the steel reinforcement gets exposed and experiences corrosion, and must therefore be taken into account in the design process. For the design of concrete offshore structures in Arctic conditions, an accurate description and prediction of ice-structure interaction is required. The interaction between moving ice and concrete surfaces is mainly governed by friction and the so-called stick-slip phenomenon. This phenomenon has been observed during laboratory and field testing and, although the physics of this phenomenon are believed to be well understood, the corresponding static and kinetic friction coefficients reported in literature have a widespread range and are inconclusive. This thesis aims at a more accurate identification of the ice-concrete friction coefficients.

For this graduation project, an experimental set-up was designed and stick-slip tests were carried out at Memorial University of Newfoundland, Canada. Additionally, a numerical model describing stick-slip behavior between ice and concrete was created. For the experimental set-up, a cylindrical fresh water columnar ice sample with a 50 mm radius and 50 mm height was attached to four springs with the same stiffness. The springs were attached to a support structure and throughout the test campaign, the stiffness of these springs was varied between 20 - 70 N/m per spring. To simulate one-dimensional ice-concrete interaction, the ice sample was placed near the edge of a rotating concrete slab. The normal load on the ice sample was varied from 0.7 to 2 kg by adding weight. In addition the concrete velocity as experienced by the ice was varied between 0.15 and 0.82 m/s by increasing the rotational rate of the concrete slab. The static and kinetic friction coefficients were obtained from the experimental data and their dependence on normal load, velocity and spring stiffness was analyzed as well. The static friction coefficients found over the whole range of tests varied from 0.1 to 0.5. The analysis showed that the static friction coefficient decreases with increasing normal load and with increasing velocity. The kinetic friction coefficient was found to be in the range of 0.08 to 0.4 and may on average be obtained as 0.7 times the static friction coefficient. The kinetic friction coefficient, too, decreases with an increase in normal load and velocity. The influence of the spring stiffness was not clearly identified.

The friction coefficients that were calculated using the experimental data were provided as input to the numerical stick-slip model. An analysis was performed to verify that the model displays similar regression with the varied mass, velocity and spring stiffness, compared to what was observed in the experiment. The output was compared to the experimental data, and it was found that the model describes the stick-slip behavior as seen during the experiment with an accuracy between 84 and 99%. Although some further improvements to the model can be implemented, in general it is concluded that under the made assumptions, the model is valid for the prediction of stick-slip behavior as observed during the experiment.

Contents

Chapter 1

Introduction

A growing demand for oil and gas recovery in the past has lead to innovations and challenges in the industry, such as the development of offshore structures in Arctic regions. The harsh environment and influences of ice loading have inspired new designs and specialized material selection, such as artificial ice islands or gravity-based concrete structures, with a reduced diameter or a sloped surface at the water line to reduce ice loads. Concrete is often used in Arctic offshore structures, as well as bridges, ports, dikes and lighthouses. Although concrete is a favorable material because of its low cost and great load withstanding capabilities, the interaction between concrete and ice has remained a challenging subject due to the large inhomogeneity of both materials. This leads to uncertainty in the estimation of the abrasion rate. Abrasion of concrete due to friction between ice causes degradation of the material and can seriously harm the structural integrity. A typical phenomenon in friction is stick-slip, which has also been observed during the abrasion process. Stick-slip of ice interacting with concrete produces cyclic loading which may cause material fatigue and could possibly play a role in ice induced vibrations. The parameters influencing the stick-slip behavior as well as the friction parameters involved are not fully understood.

In order to gain more insight into the parameters that influence stick-slip behavior, a numerical model was developed that was validated with an experimental set-up. Figure 1.1 shows a mass-spring system, which experiences stick-slip on a conveyor belt, that was simulated with the numerical model.

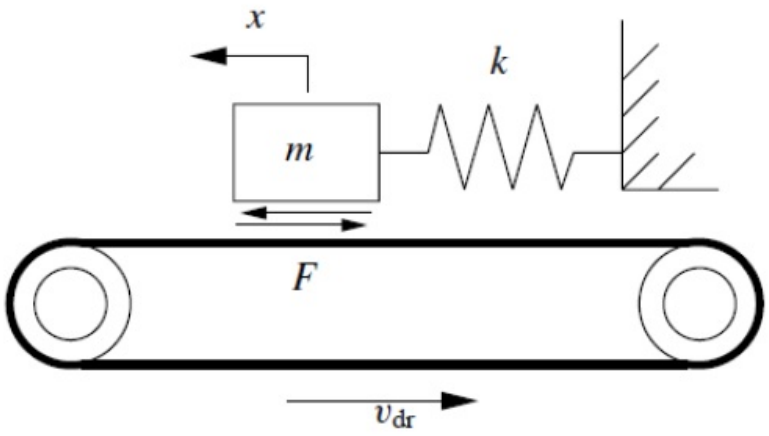

Figure 1.1: 1 DOF model with dry friction [Leine et al. 1998]

The model can be used to investigate the sensitivity of the system to different input parameters such as mass, spring stiffness or the drive velocity of the belt. The use of a model provides many benefits, as it can be used anywhere at any time, and is low in costs as opposed to laboratory or field testing. Nevertheless, in order to validate the numerical model, real testing data was required. For this purpose an experimental set-up was designed and built in the labs of Memorial University of Newfoundland in Canada. Figure 1.2 shows the experimental set-up.

An overview of the state-of-the-art of concrete-ice interaction research is presented in Chapter 2. Chapter 3 presents the experimental set-up and elaborates on the design choices made. The results obtained from the experiment are presented in Chapter 4. It shows the sensitivity of the system to various parameters and the static and kinetic friction coefficients are calculated and discussed. The numerical model is presented in Chapter 5, where the output is discussed and improvements on the model are made. The sensitivity of the model to changes of the various parameters are discussed. In Chapter 6, the experiment and numerical model are compared and discrepancies are addressed. Lastly, the conclusions and recommendations are presented in Chapter 7.

Figure 1.2: Experimental set-up

Chapter 2

State of the art of research into concrete-ice interaction

In order to establish a framework and background in which the numerical model and experimental research presented in this thesis can be placed, this chapter will elaborate on the state of the art of research into concrete-ice interaction. A general overview of findings and theories developed on the topic of concrete abrasion due to ice will be given in Section 2.1. The abrasion process is mainly governed by friction between concrete and ice and this topic will therefore be discussed in more detail in Section 2.2. Lastly Section 2.3 discusses the stick-slip behavior of ice over concrete and introduces the basis of the numerical model.

2.1 Abrasion of concrete due to ice loading

Since the construction of offshore platforms, bridges and other structures in cold regions, abrasion of concrete due to ice has been experienced. However, the characterization of this process and the correct estimation of the abrasion rate has proved a challenge. Industry often solves the abrasion problem with the use of steel or wooden protective plates, but these need regular replacement and maintenance, which can be a costly and dangerous operation.

Field investigations have indicated the risks of abrasion and provided insight into the processes involved. For example inspection of the Confederation Bridge in Canada showed exposure of aggregates after the cement paste had been worn off, see Figure 2.1.

Figure 2.1: Abrasion damage to the Confederation Bridge [Newhook and McGuinn 2007]

Because field testing in the arctic environment is expensive, complicated and dangerous, several laboratory tests investigating abrasion have been performed. Laboratory testing also allows for separation between the multiple processes involved to study the

isolated phenomena.

Itoh et al. were among the early contributers with their laboratory work investigating concrete abrasion due to sea ice [Itoh et al. 1988]. The goal of the experiment was to identify the major factors causing concrete wear, by varying parameters such as the type of aggregate, concrete strength, ice temperature, contact pressure and relative velocity between concrete and ice. An abrasion testing machine was designed to push a concrete specimen onto a back and forth sliding block of sea ice, see Figure 2.2.

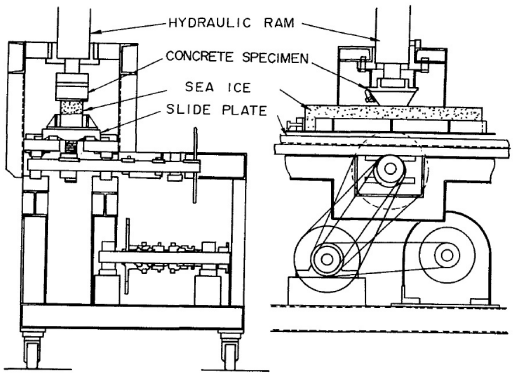

Figure 2.2: Abrasion testing machine [Itoh et al. 1988]

For concrete without surface treatment three stages of abrasion were observed:

1. Surface region: the cement paste is worn off
2. Transition region: coarse aggregates are exposed
3. Stable region: also the coarse aggregates are abraded

It was concluded that the wear rate of concrete mainly depends on ice temperature and contact pressure. Relative velocity between concrete and ice, the strength of concrete and the concrete aggregate type are also influential but not as significantly. Next to this, surface treatment that reduces the friction was found to be very effective in resisting wear due to abrasion. On the contrast, treatment which improves cement strength, such as polymer impregnation and steel fiber reinforcement, was found to be ineffective. Based on their findings Itoh et al. provided a calculation chart for wear rate based on the most important wear inducing factors, see Figure 2.3.

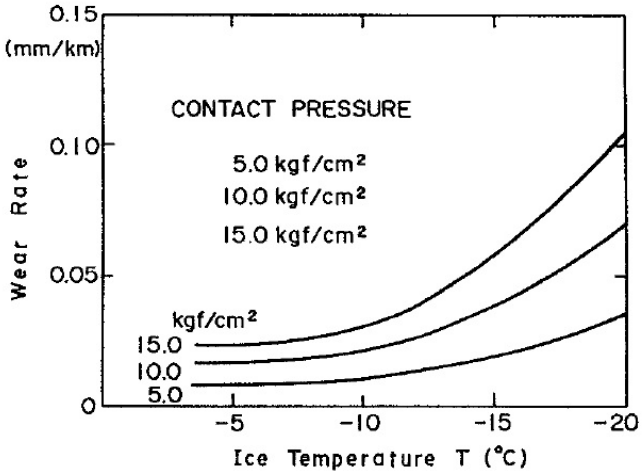

Figure 2.3: Wear rate versus contact pressure and ice temperature [Itoh et al. 1988]

Other research concluded that freeze-thaw cycles and mechanical loading of ice were most governing in the abrasion process of marine concrete in cold regions, based on a review of previous work such as laboratory tests, tests with an ice breaker, abrasion studies on Finnish lighthouses and computer calculations [Huovinen 1990]. Figure 2.4 presents the overview of all the contributing factors that were considered.

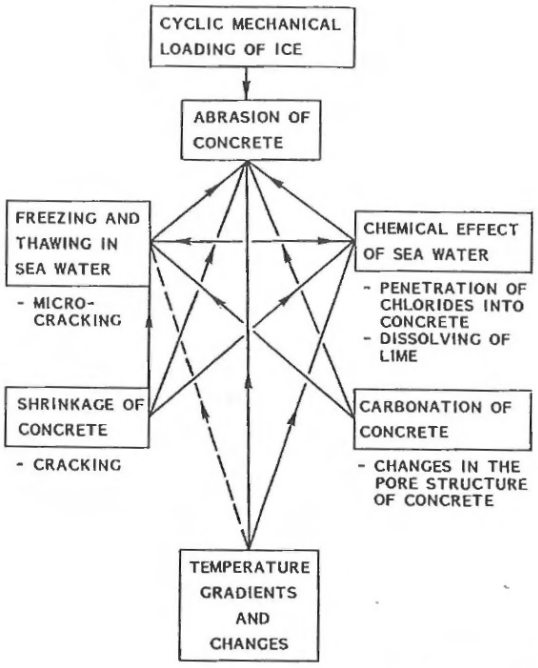

Figure 2.4: Effects causing damage to concrete in sea water [Huovinen 1990]

A more recent study investigated the influence of concrete compressive strength, ice pressure and ice temperature on the abrasion of concrete due to ice [Moen et al. 2015]. The test set-up used, shown in Figure 2.5, consisted of a stationary concrete block and a moving cylindrical ice sample with adjustable normal load.

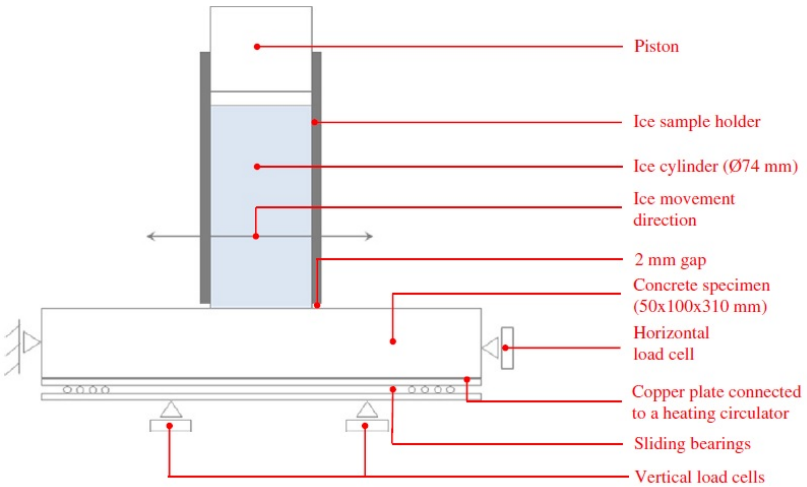

Figure 2.5: Ice abrasion test rig [Moen et al. 2015]

The experiments showed that the concrete compressive strength and ice pressure were most deteriorating, where the abrasion rate decreases with increasing concrete compressive strength and increases with increasing ice pressure. No clear relation between the ice temperature and the abrasion rate was found.

In the few examples above, it becomes clear that the findings so far have been inconclusive, ambiguous and sometimes even contradicting. For example [**Itoh)1988**] concluded that the abrasion rate mainly depends on ice temperature, where [Moen et al. 2015] finds no relation. The experiments conducted by Tijsen therefore had an exploratory character in order to identify the abrasion phenomenon and qualitatively observe the corresponding processes [Tijsen 2015].

An experimental set-up involving a horizontally oscillating concrete specimen with a laterally impinging conical ice sample was used in order to simulate the microscopic process of ice interacting on a particular point of a circular concrete pile as shown in Figure 2.6a. The results of the experimental data indicated dry and wet friction due to normal and shear loading. At low relative velocity (v_{ice} = 1.8 mm/s), which directly affected the shear loading, stick-slip loading was observed. At the surface of the concrete samples indications of wear were visible.

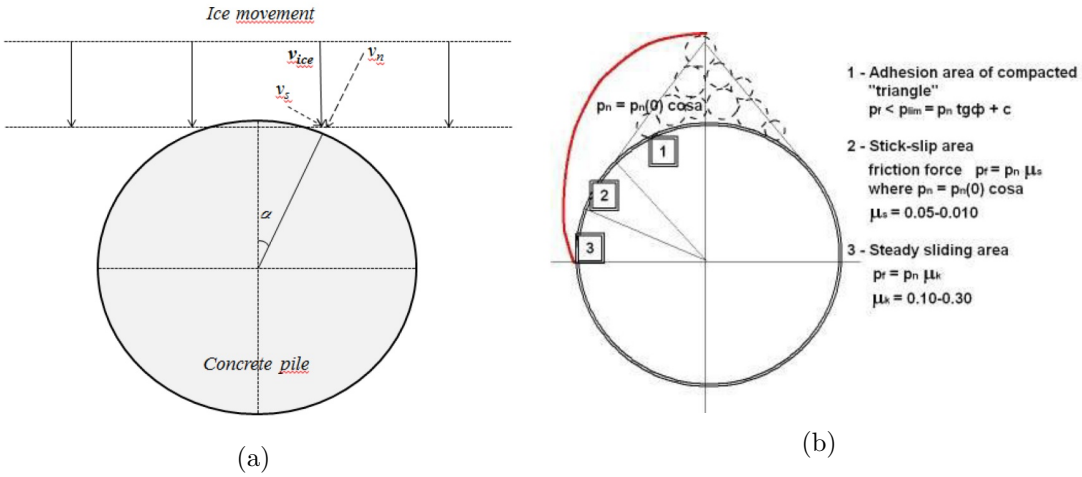

(a) (b)

Figure 2.6: (a) Real scale ice-structure interaction [Tijsen 2015], (b) Three typical abrasion regimes [Jacobsen, Kim, and Pomnikov 2012]

According to [Jacobsen, Kim, and Pomnikov 2012] three loading regimes occur on a circular pile, depending on the angle of contact, see Figure 2.6b. It was observed by Tijsen that the type of abrasive loading depends on ice velocity and angle of contact and that region I experiences highest level of abrasion. Next to that it was concluded that adhesion introduces a cyclic load on the concrete surface due to stick-slip under low ice velocities and that the stick-slip cycle depends on real contact area.

Many different test set-ups have been used for experimental research into ice-concrete abrasion over the past few decades. The need for standardized testing is emphasized in recent work [Ryan, Bruneau, and Colbourne 2017]. It is pointed out that many set-ups have been borrowed from other departments and are therefore not fully focusing on the specific factors that need to be considered in concrete-ice interaction. A rotating basin design is proposed, that has the advantage of continuous motion and testing in a submerged environment. An additional feature of this proposal will be the capability to start and stop the rotating concrete sample at planned times. This will allow the introduction and control of stick-slip action and adhesion processes.

2.2 Friction between concrete and ice

It was concluded from previous research that the ice-structure friction conditions play a large role in the contact behavior and therefore better knowledge of friction between concrete and ice is needed [Fiorio, Meyssonnier, and Boulon 2002]. For this purpose, experiments were carried out to study the influence of the parameters involved in ice-structure friction and to obtain more information about the physical mechanisms involved. A friction apparatus with alternate translation was used, with variable sliding speed (1.67 × 10-6 to 1.67 × 10-4 m/s) and variable normal stress (25-800 kPa). The friction coefficients during sliding were calculated in the initial and the final cycle of ten cycles in total, and the evolution of friction under constant load was studied. Under constant load the initial friction coefficients varied between 0.26 and 0.77 and the final friction coefficients varied between 0.37 and 0.98. The increase of the friction coefficient over time can be explained by the increase in the real contact area. Furthermore, it was found that an increase in normal stress causes a decrease in friction coefficient and an increase in sliding velocity causes an increase in friction coefficient, which is explained by visco-plasticity of ice.

In the research that was already mentioned before in Section 2.2 [Moen et al. 2015] the kinetic coefficient of friction was also determined and the research showed that the coefficient decreases with increasing ice pressure and concrete compressive strength. A comparison was made between other studies that led to the table shown in Figure 2.7.

Table 3
Summary of average kinetic ice–concrete COF and associated abrasion rates.

Publication	Kinetic COF	Abr. rate [mm/km]	f_c [MPa]	P_{ice} [MPa]	T_{ice} [°C]	V_{ice} [m/s]	Comments
Fiorio (2005)	0.46	19	24.8	0.1	−10	1.67×10^{-6}	Smooth surface.Rough surface.
	0.74	17	24.8	0.2	−10	1.67×10^{-4}	
Itoh et al. (1988)	0.085	0.010	35–70	0.2	−8	0.05	No effect of f_c on abrasion rates.
	0.050	0.009	35–70	0.2	−8	0.20	
Møen et al. (submitted for publication)[a]	0.054	0.018	60.4	0.5	−10	0.21–0.37	V_{ice} varied according to Fig. 6.
	0.039	0.002	72.8	0.5	−10	0.21–0.37	

[a] Part I, present study.

Figure 2.7: Kinetic ice-concrete friction coefficients [Moen et al. 2015]

Another experimental investigation into the static and kinetic friction coefficients between ice and concrete was performed in 1986 and in this study the most influential parameters were found to be the relative velocity, the sea ice temperature and the surface roughness [Saeki et al. 1986]. It was found that the coefficients of friction decreased with increasing relative velocity, as shown in Figure 2.8.

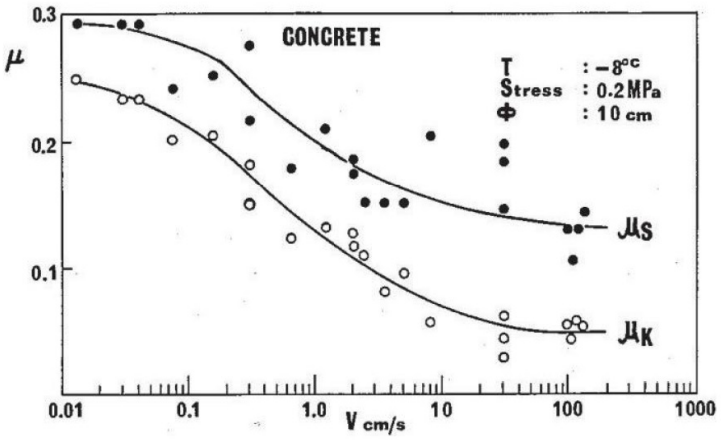

Figure 2.8: Influence of relative velocity on the friction coefficients between ice and concrete [Saeki et al. 1986]

The coefficients were found to be relatively independent of contact area and normal stress. The coefficient of kinetic friction remained constant while increasing the normal stress, whereas the static friction coefficient decreased until it reached a constant value. Also the presence of sea water at the interface or the direction of growth of the ice sample did not greatly affect the coefficients of friction.

Nakazawa et al. investigated which factors influence the coefficients of friction between ice and various other materials [Nakazawa et al. 1993]. It was concluded in their previous work that the coefficients are dependent on relative contact area, normal stress, velocity, ice temperature and surface roughness by having various plates of steel and one concrete plate. In this paper the different studies are compared to draw conclusions about how these factors influence the coefficient of friction. For the concrete plate, it is concluded that both static and kinetic friction coefficients are independent of contact area. The dependence on normal stress was not investigated. Increasing the relative velocity between the two surfaces is causes a decrease in the friction coefficients, approaching a constant at about $v_{concrete} = 0.3$ m/s. It is stated that in general, μ_{stat} increases with decreasing temperature due to the increase of the ice shear strength with decreasing temperature, while μ_{kin} is not affected significantly.

As discussed above, it was noticed by Fiorio et al. that the friction coefficient increases with time due to the increase in real contact area. Schulson and Fortt elaborated on this phenomenon with their research into static strengthening, which is the difference between the static and kinetic coefficient: $\Delta\mu = \mu_s - \mu_k$. [Schulson and Fortt 2013]. It is stated that static friction has received less attention with respect to the kinetic friction and therefore it is studied in this paper more closely. It has been concluded in the past, that a long holding time can increase the static friction coefficient by a factor 2, however the nature of this phenomenon is unknown. In order to investigate the phenomenon, systematic slide-hold-slide (SHS) tests were performed using a double shear device. The coefficient of static friction is defined as: $\mu_s = \tau_p/\sigma_n$, where τ_p is the peak shear stress, which increases with increasing holding time, and σ_n is the normal stress which is constant. The coefficient of static friction is greater than the coefficient of kinetic friction, as has been observed before. Figure 2.9 shows the relation between the static friction coefficient and holding time.

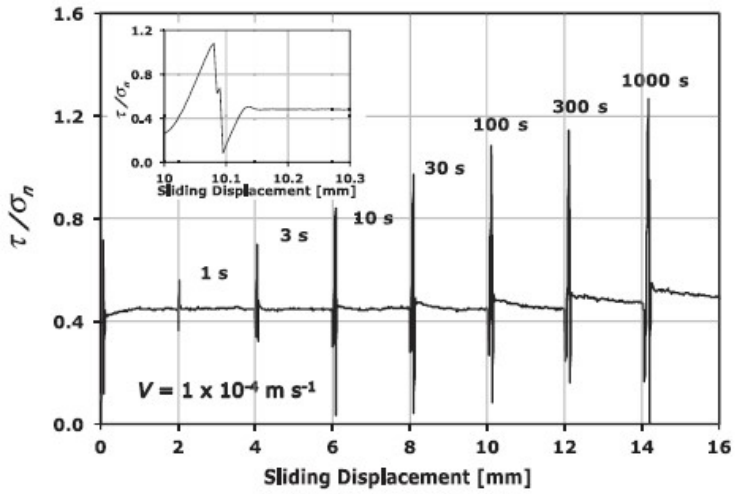

Figure 2.9: Static strengthening [Schulson and Fortt 2013]

Several notes that were made with respect to static strengthening are:

- Static strengthening can be detected only after a certain threshold value for the holding time. The threshold period decreases with increasing velocity.

- Static strengthening increases approximately logarithmic with increasing holding time.

- Static strengthening increases with increasing velocity

2.3 Stick-slip phenomenon

In Section 2.2, regarding the subject of friction between ice and concrete, the difference between static and kinetic friction, or in other words the *initiation* and *continuation* of sliding, is mentioned several times. The process of initiation and continuation of sliding is also referred to as the stick-slip phenomenon. Stick-slip vibrations are friction induced self-sustained oscillations experienced in many engineering systems as well as everyday life. This phenomenon has been observed in abrasion testing and numerical modeling of the stick-slip effect has been studied.

In an experimental study researching the friction of ice over concrete at the centimeter scale, a series of friction tests using a shear box apparatus in a cold room at -10 degrees Celsius were carried out [Fiorio and Meyssonnier 1997]. The tests performed were similar to those explained in Section 2.2 [Fiorio, Meyssonnier, and Boulon 2002]. The analysis of the results indicated stick-slip behavior, where some tests exhibited a stick-slip phenomenon during their whole duration and some during only part of it. In the study three stages in the stick-slip phenomenon are identified:

1. Adhesion of ice on concrete

2. Increase of the tangential stress until the ice-concrete bond reaches its failure point

3. Breaking of the bond followed by displacement of the ice relative to the concrete together with a decrease of the tangential stress

Over time the tangential stress decreases to zero, and the velocity of the ice relative to the concrete becomes zero, which leads to stage 1 again. When this process is repeated it leads to a stable stick-slip regime. It was observed that stable stick-slip was influenced by the normal load, the velocity of the ice relative to the concrete, and the roughness of the plate. In case of high roughness an increase in normal load and velocity tended to favor stable stick-slip. In case of low roughness an increase in normal load also favored stable stick-slip, however the velocity did not play a significant role in the occurrence of stick-slip.

A single degree-of-freedom conveyor-belt model has been used in several applications in order to investigate stick-slip behavior between materials, see Figure 2.11. For example it has been used for a simplistic simulation of the dynamics of sysmic faults [Galvanetto and Bishop 1994] or for bowed instruments [Oestreich, Hinrichs, and Popp 1996]. On the other hand, a discrete lattice model consisting of kinematic Bingham-Kelvin-Voigt (BKV) elements is proposed by [Hoving 2019]. The upper part of the BKV element as shown in Figure 2.10 consists of the Kelvin-Voigt element which combines a spring and a dashpot in parallel. The lower element is the Bingham element that consists of a damper and a dry-friction element.

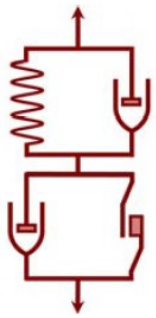

Figure 2.10: Bingham-Kelvin-Voigt element [Hoving 2019]

The dry-friction element is only activated if the forces on the particle are larger than the critical friction force. In the motion state *stick* the Bingham element is not activated and when the forces on the element overcome the critical friction force, the motion state transitions from *stick* to *slip*. During slip, the force is equal to the critical friction force, and thus the difference between the static and kinetic friction forces is not accounted for in this model. Because in slip the applied force is equal to the friction force, the moment of slip-to-stick transition can not be determined from the force that is applied to the element. Therefore it is determined based on the relative motion between the two degrees of freedom.

The numerical stick-slip model presented in this thesis is based on an alternate friction model of a mass attached to a spring, that is positioned on a conveyor belt, see Figure 2.11 [Leine et al. 1998]. In this model dry friction is assumed to occur between the mass and the conveyor belt. The state equation for this 1 degree of freedom system is defined as follows:

$$\dot{\underline{x}} = \begin{bmatrix} \dot{x} \\ -\frac{k}{m}x + \frac{F}{m} \end{bmatrix} \tag{2.1}$$

Where $\underline{x} = [x\ \dot{x}]^T$.

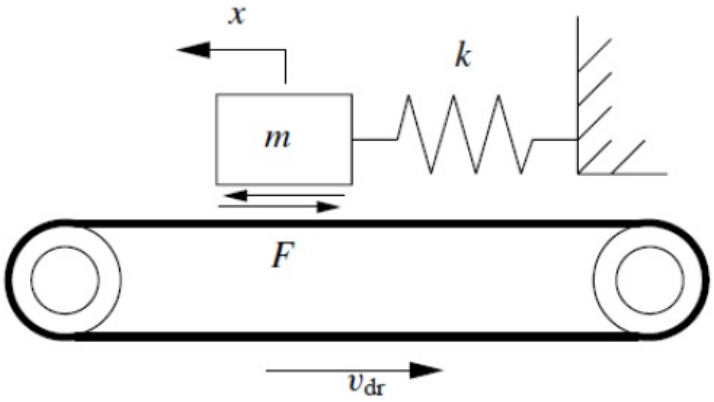

Figure 2.11: 1 DOF model with dry friction [Leine et al. 1998]

The friction model presented by Leine et al. reads:

$$F(v_{rel}, x) = \begin{cases} F(x) = & min(|F_{ex}(x)|, F_s)\text{sgn}F_{ex}(x), & v_{rel} = 0 \text{ stick}, \\ F(v_{rel}) = & -\frac{F_s \text{sgn} v_{rel}}{1+\delta|v_{rel}|}, & v_{rel} \neq 0 \text{ slip}. \end{cases} \tag{2.2}$$

During *stick*, the friction force F_s is equal to the external force F_{ex} applied to the mass, until the critical static friction force is reached. The external force is applied by the springs and the critical friction force in this model is assumed to be 1 N. The friction force applied to the mass during *slip* is a function of the static friction force and depending on the relative velocity as well as a constant δ. The relative velocity between the mass and the belt is formulated as $v_{rel} = \dot{x} - v_{dr}$ where v_{dr} is the drive velocity of the belt.

As mentioned above, the information in literature that is available, related to the static and kinetic friction coefficients between ice and concrete is not complete. Therefore, stick-slip experiments were carried out during this thesis and from the experimental data the friction coefficients were calculated. Next to that, a numerical model based approach was taken to investigate the possibility of simulating the behavior observed in the experiments, with the obtained friction coefficients. The conveyor belt model was chosen as a basis because of its transparency and straightforwardness. To explicitly incorporate the friction coefficients, the friction model (Equation 2.2) was adapted to:

$$F = \begin{cases} min(|F_{ex}(x)|, F_{stat})\text{sgn}F_{ex}(x), & v_{rel} = 0 \text{ stick}, \\ -F_{kin}\text{sgn}v_{rel}, & v_{rel} \neq 0 \text{ slip}. \end{cases} \tag{2.3}$$

Where $F_{stat} = \mu_s mg$ and $F_{kin} = \mu_k mg$. This way the static and kinetic friction coefficients are a direct input parameter in the model.

Chapter 3

Experimental set-up for analyzing stick-slip behavior of ice interacting with concrete surfaces

To research the stick-slip behavior between concrete and ice, a test set-up was designed at the Memorial University of Newfoundland, Canada. Based on the review of the state of the art of research into concrete-ice interaction, a preliminary numerical model and the facilities at hand, requirements were set up and different designs were considered. In this chapter the final test set-up is presented after which the design considerations will be discussed in more detail. Lastly the test plan is presented which describes the combination of test variables used, and the order in which they were tested.

3.1 Test setup

Figure 3.1 presents the top view of the experimental set-up. The test set-up consists of an ice sample connected to springs, resting on a rotating concrete slab. The tests were carried out in a cold room where the temperature was kept at -2 °C (± 1 °C).

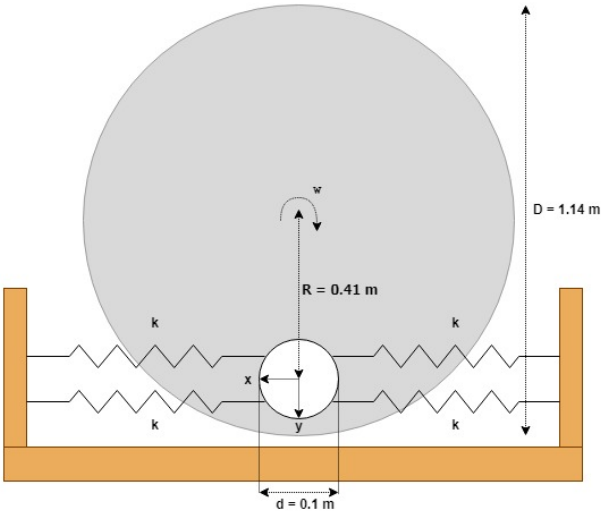

Figure 3.1: Top view of the test setup

The diameter of the concrete is 1.08 m and the diameter of the ice sample is 0.1 m. The center of the ice sample is located a distance 0.41 m away from the center of rotation of the concrete slab that rotates with angular velocity ω. The ice sample is free to move in x- and y-direction and is attached to two springs on both sides that have the same stiffness k.

The rotational velocity of the concrete was varied between 3.6 - 19.2 RPM, the normal load on the ice was varied between 0.6 - 2 kg and the spring stiffness was varied between 20-70 N.

The preliminary version of the numerical stick-slip model presented in Chapter 2 describes the behavior of a block of ice with mass m attached to a single spring with spring constant k, resting on a conveyor belt. This conveyor-belt model formed a strong starting point for the design of the experiment. However, a concrete conveyor belt was not a feasible design option and other ideas were considered, bearing the facilities at hand in mind. The final design was based around an ice-cone shaper cart that was previously used to shape large ice cones. In this experiment, a concrete slab was placed on top of the turntable. The turntable was able to rotate, providing a constant motion like a conveyor belt.

A difference with the conveyor belt model was the rotational motion as opposed to a purely uni-directional motion. However, it was assumed the rotational motion is negligible with respect to the displacement in x-direction. Figures 3.2 and 3.3 provide a frontal view of the set-up by means of a sketch and a picture, respectively.

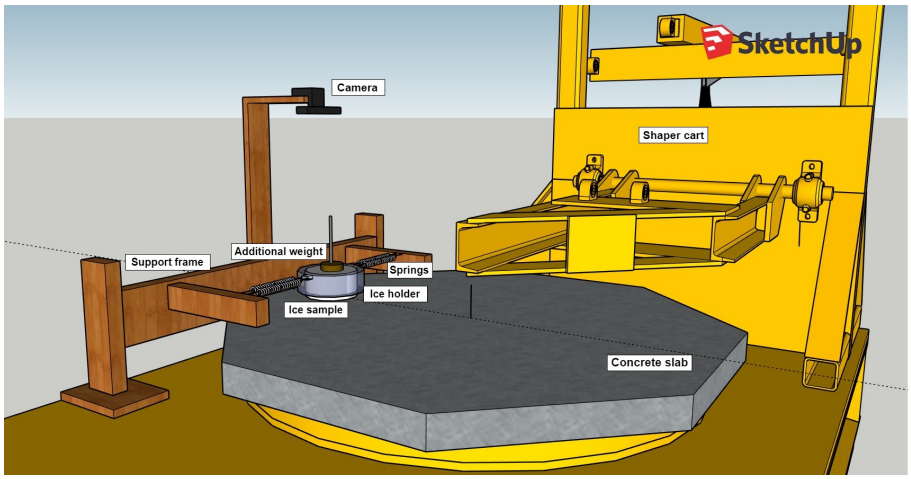

Figure 3.2: Final sketch of the test setup

Figure 3.3: Picture of the actual test setup

3.2 Design and considerations of experimental set-up

Figure 3.2 labels the different elements of the experimental set-up. The design process of the individual elements underwent multiple stages and in this section each of the components is elaborated on:

- ice-cone shaper cart;
- concrete slab;
- support frame;
- ice sample;
- ice holder;
- set of springs;
- set of additional weights;
- a camera.

3.2.1 Ice-cone shaper cart

The shaper cart was previously used to shape large cylindrical ice samples into cones. The surface of the cart had been corroded and therefore it was brushed and painted, see Figure 3.4. It is seen in Figure 3.4a that the metal arm that was previously used to hold the shaping blade is up, while in Figure 3.4b it is down. This was done to investigate the possibility to use the metal arm as support for the test set-up. This would have obstructed the view on the ice sample and therefore a support structure was designed.

(a) Shaper cart before paintjob (b) Shaper cart after paintjob

Figure 3.4: Shaper cart before and after paintjob

Another update of the shaper cart was the adjustment of the motor to set it up for controllable variable speed or in other words, to allow the turntable on the shaper cart to rotate at various speeds instead of one. The motor was replaced by a 3 phase 2hp which was compatible with the frequency controller needed to control the rotational speed. The controller was placed outside of the cold room to avoid corrosion of the control box. Through an opening in the wall of the cold room an extension chord connected the controller to the shaper cart. Lastly, casters were attached to the cart to allow for flexibility with moving the cart in and out of the cold room.

3.2.2 Concrete slab

An octagonal wooden form work was manufactured to facilitate the pouring of a concrete slab reinforced with 15 mm diameter reinforcement bars, as shown in Figure 3.5.

(a) Concrete pouring form work (b) Concrete slab in mold

Figure 3.5: Concrete mold making process

The side of the concrete slab that had faced the form work was of low roughness due to the fact that the bottom plate was designed specifically for concrete pouring. The experiments were conducted on the smooth side of the concrete. This side was chosen in order the prevent damage to the ice due to bumps and an uneven sliding surface. The type of concrete chosen was a low performance type as described in Table 3.1 that was used in previous research [Tijsen 2015]. This type of concrete was chosen, because the materials were readily available and the integrity and strength of the concrete were not the main focus of this experiment. The dimensions of the concrete slab are shown in Figure 3.6a. Figure 3.6b shows that the concrete slab extends 3 centimeters over the turntable when placed on top.

(a) Dimensions of concrete octagon (b) Concrete slab on turntable

Figure 3.6: Dimensions of concrete slab and turntable

A steel pipe was placed in the middle of the slab to help align the center of the slab with the center of the turntable, see Figure 3.7.

Figure 3.7: Concrete slab positioning on turntable

Table 3.1: Concrete mixture [Tijsen 2015]

	HP Concrete Mix	LP Concrete Mix
Air volume	3 - 5	3 - 5
SCM	8	0
Binder	500	300
C/F	1.2	1.2
W/B	0.33	0.5
Absorption	0.01	0.01
Portland cement	460	300
SF	40	0
C.A. (8 - 16 mm)	952.09	1070.39
F.A. (0 - 8 mm)	793.41	891.99
W	165	150
TW	182.46	169.62

3.2.3 Support frame

The wooden support frame located on the side of the cart, as shown in Figure 3.8, supported the springs and provided for the ability to attach a camera for displacement measurements. The arms to which the springs were attached were secured with a metal hook and two bolts to limit movement and vibrations in the support frame itself. The spacing between the arms could be adjusted to allow for more extension in the springs, depending on the spring stiffness.

Figure 3.8: Support frame

3.2.4 Ice sample

Cylindrical plastic molds (normally used to make concrete samples) with a diameter of 100 mm and a height of approximately 200 mm were filled with crushed ice and flooded with purified, deaerated water in accordance with the ice specimen preparation described by Bruneau et al. [Bruneau, Dillenburg, and Ritter 2012]. An insulating styrofoam jacket, which covered the top and exposed the bottom of the cylinder, was put over these cylinders to support uni-directional growth of the ice, see Figure 3.9a. The samples were removed from the plastic holders by drilling a hole in the bottom of the plastic and pressurizing it with an air gun. Figure 3.9 shows two ice samples, the left ice sample was prepared without insulating jacket whereas the right ice sample was prepared with the insulating jacket. This test proved the need for the insulating jacket as cracks can be seen, that formed due to lateral growth of the ice.

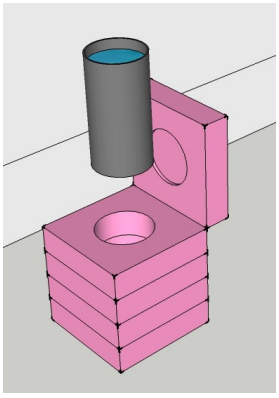

(a) Insulating jacket

(b) Ice samples

Figure 3.9: Ice sample preparation

The ice cylinder was sawed in slices of 50 mm inside the cold room to obtain the desired ice samples and to smooth the edges, see Figure 3.10. The final ice sample had a weight of 0.33 kg. Figure 3.11 shows a horizontal thin section of the ice sample, showing the distributed grain size and orientation.

Figure 3.10: Sawing an ice sample

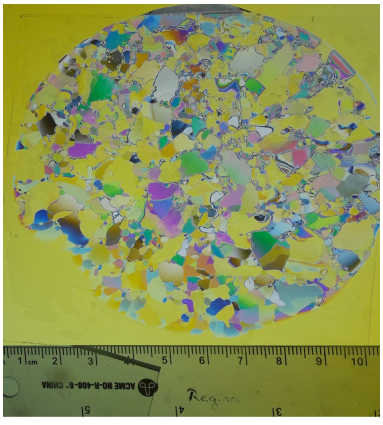

Figure 3.11: Horizontal thin section

3.2.5 Ice holder

The ice holder is shown in Figure 3.12. The holder was needed to provide attachment points for the springs and a rod in the middle was used to put additional weight on top of the ice sample to vary the normal load. The red marker on the right was used for data acquisition using the camera, see Section 3.2.8. The ice holder was made out of thick

sheets of plastic that were glued together. The shape of the ice holder was made as thin as possible in order to make it as light as possible. The final weight of the ice holder was 0.27 kg.

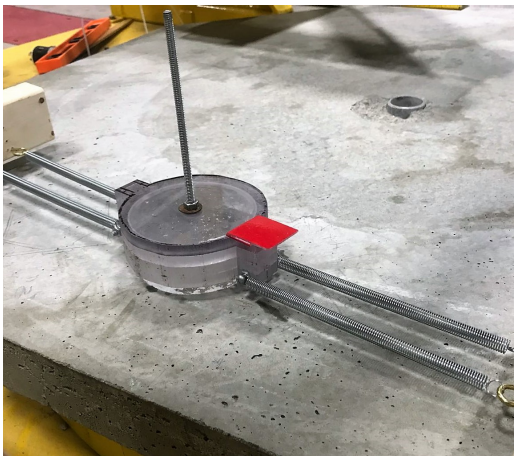

Figure 3.12: Ice holder

3.2.6 Additional weights

Additional weights were placed over the rod on top of the ice holder in order to investigate the influence of the normal load on stick-slip behavior. Combinations were made with the available weights of 0.2 kg, 1 lbs and 2 lbs.

3.2.7 Springs

The preliminary numerical model that was presented in Chapter 2 was used to analyze stick-slip behavior prior to the experiment, to determine the the range of springs that needed to be used and ordered. The weight of the ice sample and the ice holder were known and a limited set of additional weights was available. The velocity of the turntable was bound by its operational limits and the friction coefficients were assumed between 0.1 and 0.6. The only unknown in the input parameters of the model at that point was the spring stiffness. However, the maximum displacement was known through the geometry of the concrete slab. On the position of R = 0.41 the maximum distance in x-direction was measured to be 35 cm, before the ice sample would fall off. Using this constraint and the minima and maxima in the range of normal load an concrete velocity, the range of spring constants was determined to be between 20-80 N/m. Multiple springs were ordered and tested, and the four most suitable were chosen based on their performance and geometry to fit easily into the set-up, see Table 3.2. The spring stiffness was re-calculated by hand, by extending the springs horizontally over a range of known loads and measuring the extension of the spring, see Figure 3.13.

Figure 3.13: Measuring the spring constant for horizontal extension

3.2.8 Camera

On the long post of the support frame a camera was mounted to track the motion of the ice sample. The camera was connected to a computer with object-tracking software that was able to detect the red square on the ice holder and store this information [Bose 2013]. This delivered a displacement over time curve, in both horizontal and vertical direction.

3.3 Test plan

The test sequence was based on varying the spring constant, the additional weight and the rotational speed of the concrete slab. Section 3.2.7 has explained how the springs were chosen and an overview of the different spring constants involved is given in Table 3.2.

Table 3.2: Spring constants for the different springs used

	k_1	k_2	k_3	k_4
k [N/m]	20.17	38.50	49.83	68.22

On top of the ice sample and ice holder, which had a combined weight of 0.67 kg, additional weights were placed as explained in Section 3.2.6. Table 3.3 shows the different additional weights that that were used to vary the normal load.

Table 3.3: Additional masses

	m_1	m_2	m_3	m_4	m_5	m_6	m_7
m [kg]	0.00	0.20	0.40	0.45	0.65	0.91	1.36

Lastly, the different local concrete velocities that were used during testing are shown in Table 3.4.

Table 3.4: Local concrete velocity

	v_1	v_2	v_3	v_4	v_5	v_6
v [m/s]	0.15	0.25	0.37	0.50	0.63	0.82

These local velocities were calculated using the RPM of the turntable and the radial position of the ice sample with respect to the center of rotation. The angular velocity of the concrete was measured using a tachometer. A piece of reflective tape was taped on the outside rim of the steel turntable, on top of which the concrete was placed. The laser of the tachometer was pointed on the tape and it measured the rate at which the light is reflected back as a measure of the speed and displayed the RPM. Typically three rotations or in other words three reflections were needed for the tachometer to obtain the speed accurately. The *local velocity of the concrete*, which is the speed that the ice sample experienced is defined as the velocity of the concrete surface at the location of the center of the ice sample. The center of the ice sample was measured to be at a distance $R = 0.41$ m from the center of rotation and using the RPM measurement the local velocity was calculated as follows:

$$v_{local} = \frac{RPM \cdot 2 \cdot \pi \cdot R}{60} \tag{3.1}$$

The measured RPM's are displayed in Table 3.5. The tachometer had an accuracy of 0.1 RPM and this means that 3.6 RPM could be any value between 3.55 - 3.64. This has some influence on the interpretation of the results which will be addressed in Chapter 4.

Table 3.5: Angular concrete velocity

	v_1	v_2	v_3	v_4	v_5	v_6
v (RPM)	3.6	5.8	8.7	11.7	14.7	19.2

Combinations between k, v and m were chosen empirically. This resulted in test plans that show which combinations of k, m and v were tested and in which order. Figures 3.14, 3.14, 3.14 and 3.14 show the four test plans that were used.

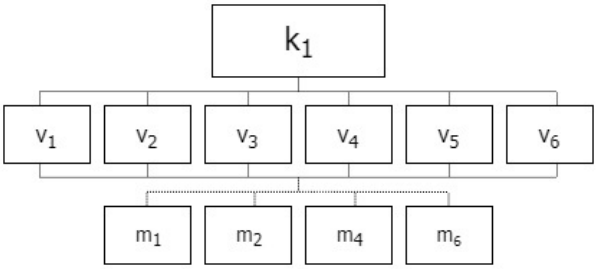

Figure 3.14: Test plan for k_1

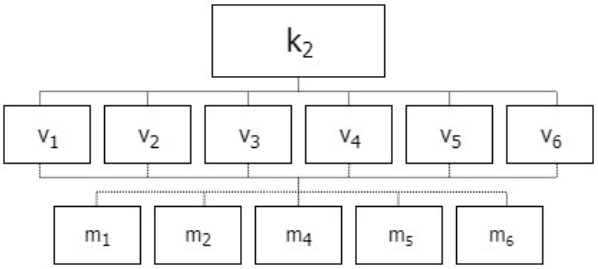

Figure 3.15: Test plan for k_2

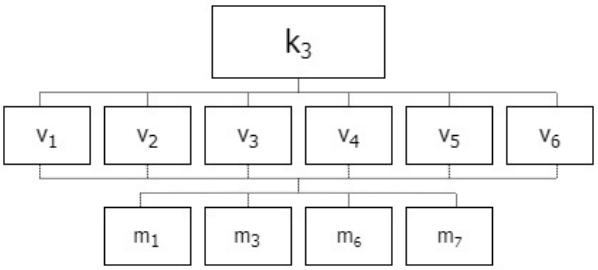

Figure 3.16: Test plan for k_3

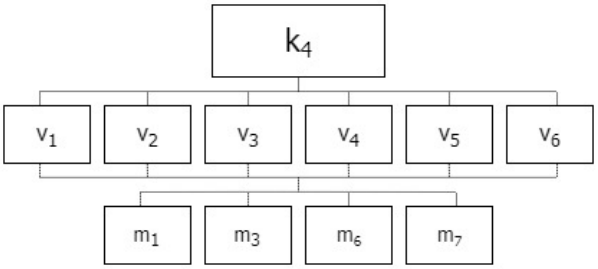

Figure 3.17: Test plan for k_4

All the tests in one diagram were performed with one particular spring type. After attaching the right spring type the speed was set. Starting off with no additional weight, the added weight was slowly increased. This was done for all speeds, until the whole test plan for one spring type was completed. This same process was completed for the other spring types. It is seen that for example m_7 is used for spring types k_3 and k_4 and not in combination with k_1 and k_2. The weaker springs could not carry this heavier load and caused the ice sample to adhere to the concrete surface, which caused to much tension in the springs. Some tests were performed multiple times to verify that the experiment is reliable and repeatable.

Chapter 4

Analysis of experimental data

The experimental data is analyzed and discussed in this chapter. The experimental data consists of displacement measurements over time that were captured with a camera and object-tracking software. The top view of the experimental set-up was shown in the previous chapter in Figure 3.1 and the displacement referred to in the experimental data analysis is the displacement in x-direction, since the displacement in y-direction was assumed negligible. From the displacement measurements, the velocity and acceleration were calculated, providing the complete set of information about the motion of the ice sample. In section 4.1 the influence of the spring stiffness (k), the concrete velocity (v) and the normal load (m) on the motion of the ice sample is analyzed. Section 4.2 elaborates on the calculation of the static and kinetic friction coefficients from the experimental data, and their dependence on k, v and m.

4.1 Influence of k, v and m on the motion of the ice sample

In this section, a typical data set is presented and three parameters that are used to characterize each data set are introduced. The influence of k, v and m on these characteristic parameters is identified, in order to verify that the experiment complies with what it was set up to do: show stick-slip behavior. A typical data set from the stick-slip experiments describes the displacement, velocity and acceleration of the ice sample. Figures 4.1 presents the displacement for the data set $k_1v_1m_1$, a typical example from the test plan (see Section 3.3).

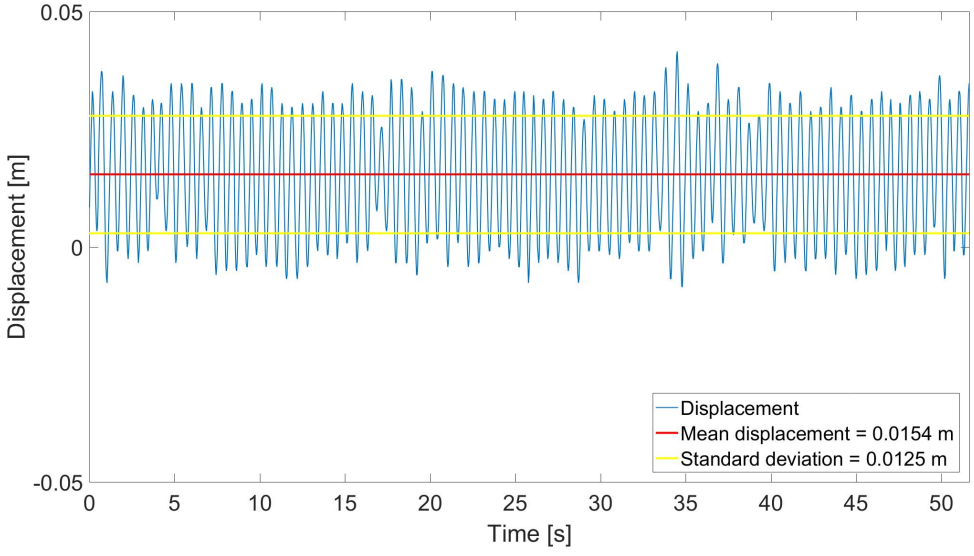

Figure 4.1: Displacment over time for data set $k_1v_1m_1$

The displacement curve shows the back and forth sliding of the ice sample. The mean displacement indicates the offset from the equilibrium position ($x = 0$) around which the ice sample oscillates with an amplitude equal to what is referred to as the standard deviation of the displacement. Differentiating the displacement over time led to the velocity curve as shown in Figure 4.2.

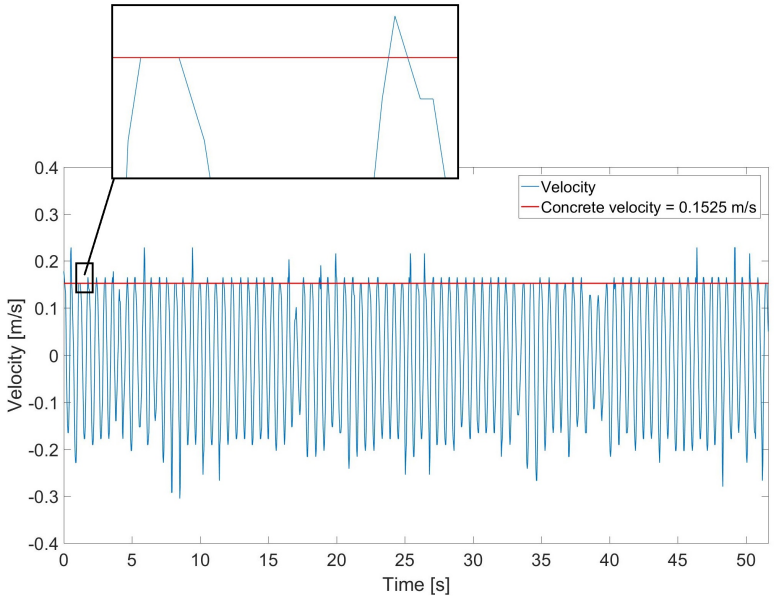

Figure 4.2: Velocity over time for data set $k_1v_1m_1$

In the velocity curve, periods of stick can be observed. The velocity of the ice sample is equal to the concrete velocity for at least a period 0.033 seconds, which is the time between two data points. For example, stick can be observed in the second oscillation in Figure 4.2. Possible explanations for the peaks above the concrete velocity are discussed in Section 4.2.1. Taking the gradient of the velocity over time leads to the acceleration of the ice sample as shown in Figure 4.3.

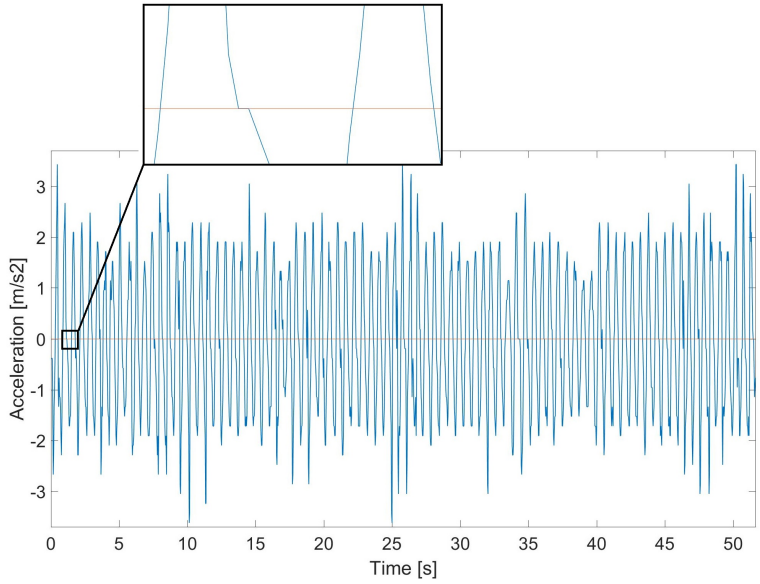

Figure 4.3: Acceleration over time for data set $k_1v_1m_1$

In theory, when the velocity is constant the acceleration should be zero. This is seen when looking at the second oscillation in Figure 4.3. When analyzing the data carefully, it

can be noticed that not every time the velocity is constant, corresponds to zero acceleration. This is because taking the gradient causes a computational error. The error needs to be taken into account but is assumed small enough to be able to perform the data analysis.

To interpret the influence of the spring stiffness, the concrete velocity and the normal load on the stick-slip behavior of the ice sample, the following characteristics of the motion of the ice sample were calculated for each test combination $k_i v_j m_k$ from the test plan:

- x_{mean}: the mean displacement of the ice sample [m], which represents the offset from the equilibrium position around which the ice sample oscillates
- x_{SD}: the standard deviation of the displacement of the ice sample [m], which represents the amplitude with which the ice sample oscillates around x_{mean}
- f_{peak}: the oscillating frequency of the ice sample [Hz]

In Figure 4.1 already an example of the mean and standard deviation of the displacement were given. Figure 4.4 shows the frequency spectrum for the data set $k_1 v_1 m_1$. The frequency corresponding to the peak, f_{peak}, is the dominant frequency of the system, the frequency with which the ice sample oscillates around the mean displacement.

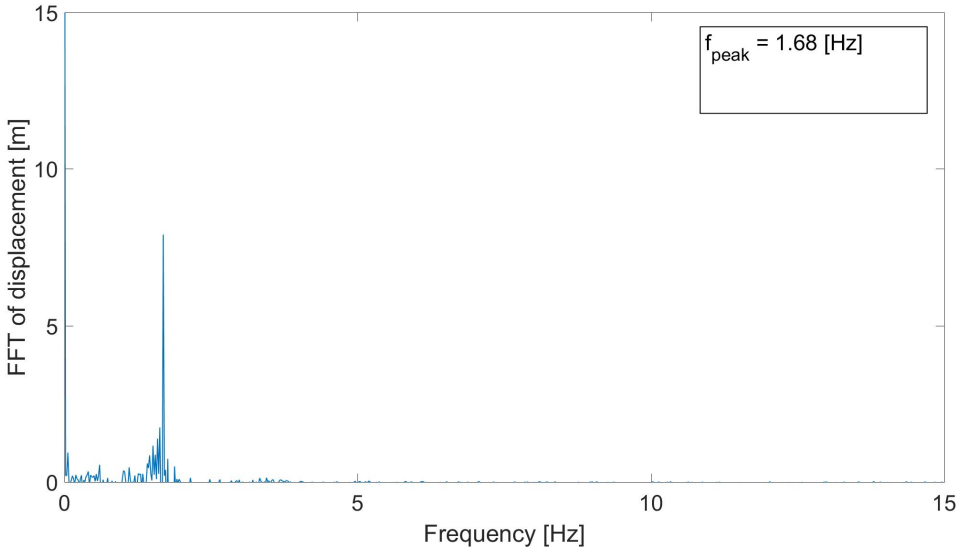

Figure 4.4: An example of the frequency spectrum, for data set $k_1 v_1 m_1$

The parameters x_{mean}, x_{SD} and f_{peak} were calculated for all the tests that were presented previously in the test plan, see Section 3.3. The influence of the testing variables k, v and m on these characteristic parameters of the ice sample will be elaborated on in the following section.

4.1.1 Influence of k, v and m on the mean and standard deviation of the displacement

In this section the mean and standard deviation of the displacement in relation to k, v and m are discussed simultaneously, because the two parameters are inherent to each other. Figures 4.5 and 4.6 display the mean and standard deviation over a range of masses for velocities $v_1 - v_6$ at constant spring stiffness k_1, corresponding to the test plan shown in Figure 3.14. Figures 4.7 until 4.12 shows the same for spring constants k_2, k_3 and k_4. Note that the mass starts at 0.6 kg, since this is the combined weight of the ice sample and the ice holder.

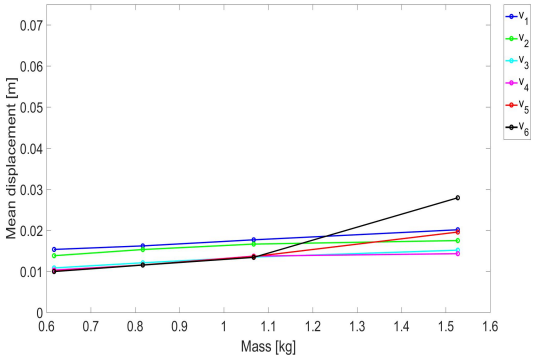

Figure 4.5: x_{mean} for k_1

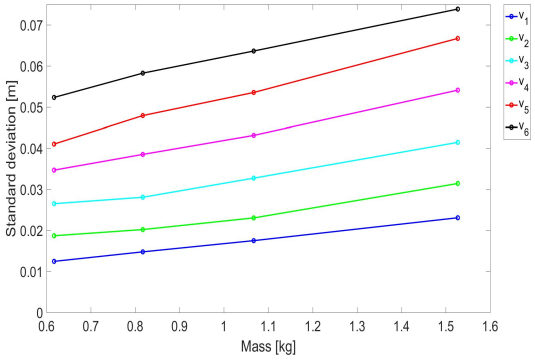

Figure 4.6: x_{SD} for k_1

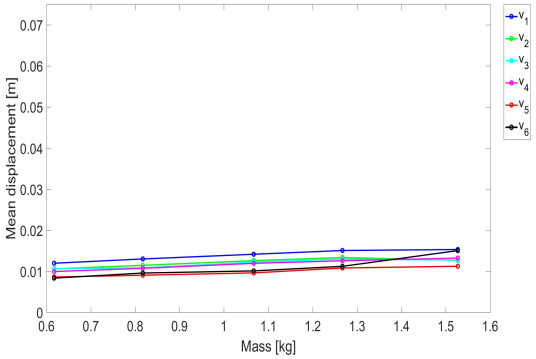

Figure 4.7: x_{mean} for k_2

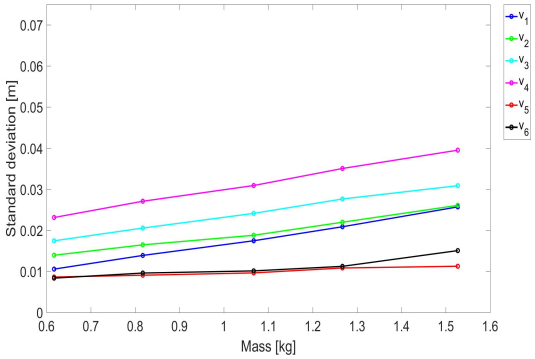

Figure 4.8: x_{SD} for k_2

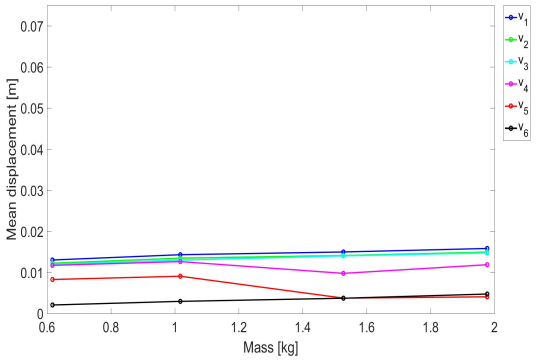

Figure 4.9: x_{mean} for k_3

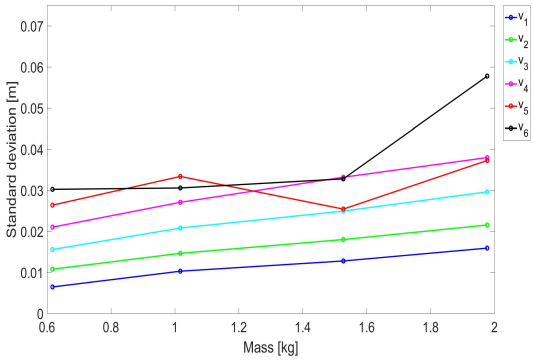

Figure 4.10: x_{SD} for k_3

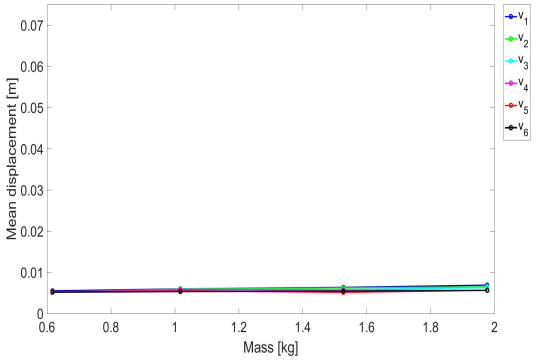

Figure 4.11: x_{mean} for k_4

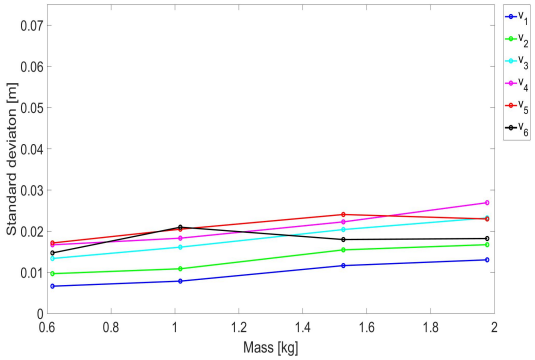

Figure 4.12: x_{SD} for k_4

In Figures 4.5, 4.9, 4.10, and 4.12 it can be seen that for the highest velocities, v_5 (shown in red) and v_6 (shown in black), do not behave in the same fashion as the curves for $v_1 - v_4$. It is known that stick-slip is a phenomenon that occurs at lower sliding velocities and an explanation for what is observed in the figures above, might be that in fact these tests did not exhibit stick-slip behavior. Another explanation might be the limitation of the number of frames per second the camera could record (30 fps). The higher the velocity, the less accurate the measurements. Therefore, the data points corresponding to a velocity of v_5 or v_6 have been removed from the data set for further data analysis. Figures 4.13 until 4.20 show the curves without v_5 and v_6.

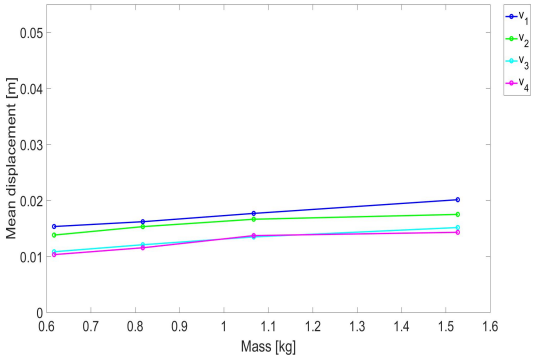

Figure 4.13: x_{mean} for k_1

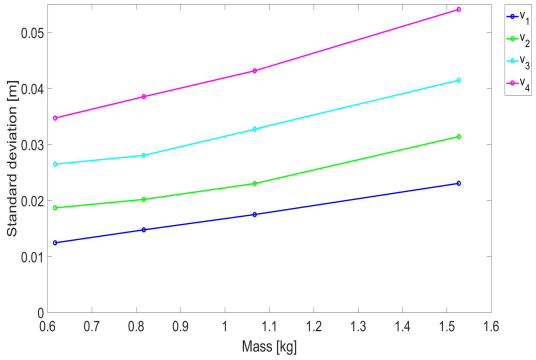

Figure 4.14: SD for k_1

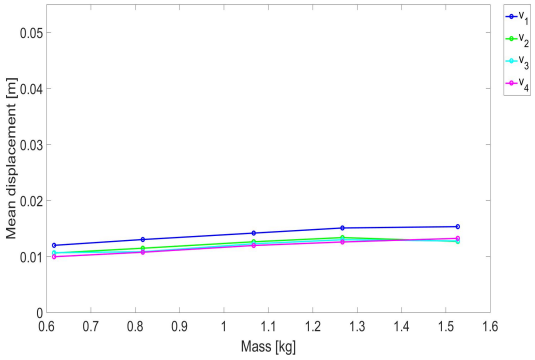

Figure 4.15: x_{mean} for k_2

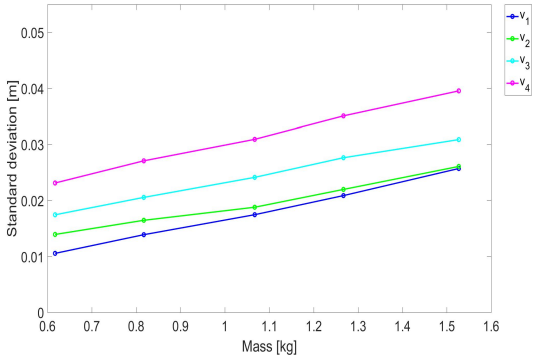

Figure 4.16: SD for k_2

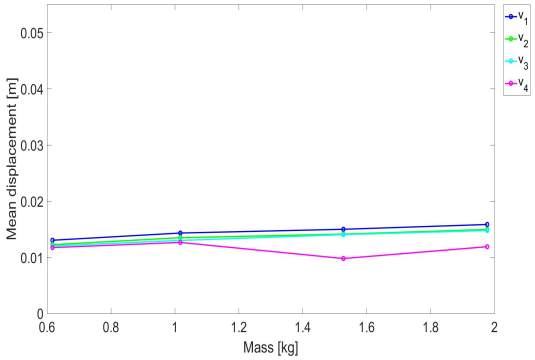

Figure 4.17: x_{mean} for k_3

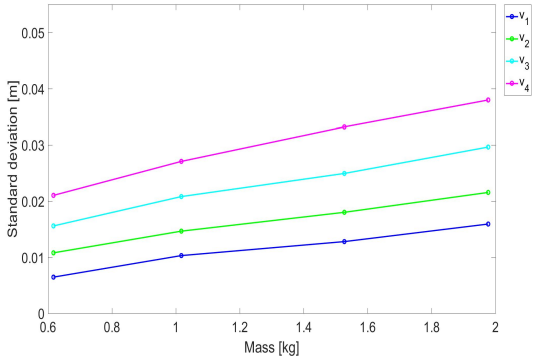

Figure 4.18: SD for k_3

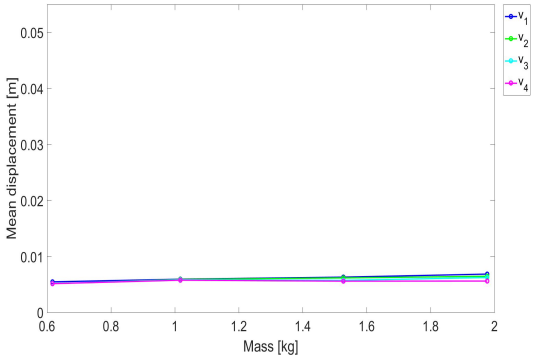

Figure 4.19: x_{mean} for k_4

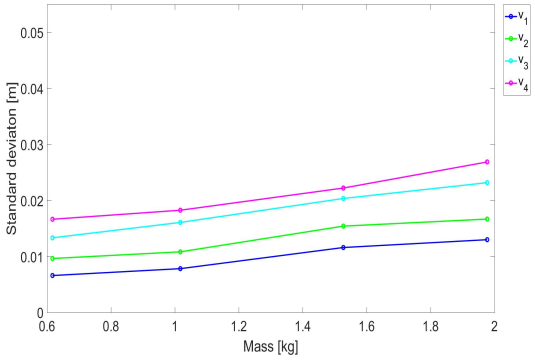

Figure 4.20: SD for k_4

Influence of normal load on mean and standard deviation of the displacement

Figures 4.13, 4.15, 4.17 and 4.19 show the mean displacements measured for all the tests from the test plan (Section 3.3) with the data corresponding to velocities v_5 and v_6 discarded. In Figure 4.13 slightly upward trends are observed, indicating an increase in mean displacement with increasing normal load on the ice sample. The standard deviation of the displacement as seen in Figure 4.14 shows a steeper increase with increasing normal load. Similar trends are observed for spring constants $k2$, k_3 and k_4 in Figures 4.15 until 4.20. The increase of both the mean and standard deviation of the displacement with an increase in normal load physically makes sense: the larger the normal force, the greater the resistance against sliding. Since the ice sample was situated on a moving surface, this translates to a larger displacement of the ice sample because more force is required to make it slip and pull it backwards.

Influence of velocity on mean and standard deviation of the displacement

Again looking at Figure 4.13 and focusing on the difference between the four curves v_1, v_2, v_3 and v_4 it can be concluded that an increase in velocity causes a decrease in the mean displacement. The lowest velocity, v_1, displays the highest values for the mean displacement, while $v_2 - v_4$ sequentially show lower values. On the contrary, Figure 4.14 shows an increase in the standard deviation of the displacement with respect to an increase in velocity. The standard deviation is now the lowest for v_1 and the highest for v_4. Similar behavior of the mean and standard deviation of the displacement with respect to the velocity of the concrete is visible in Figures 4.15 to 4.20.

An increase in velocity intuitively should only influence the system in slip mode, since the force balance in stick mode stays the same: $k \cdot x_{transition} = \mu_s \cdot m \cdot g$. This means that the location where stick-to-slip transition happens ($x_{transition}$) should stay the same. However, this is assuming that μ_s is constant and not depending on the relative velocity. In reality, an increase in velocity could cause a decrease in friction due to, for example, frictional heating which is especially valid for ice. This would cause a decrease in $x_{transition}$ which could explain the decrease in mean displacement with increasing velocity. The effect on the slip mode is more transparent because the initial conditions change: the velocity increases and a larger deceleration is needed. Figures 4.21 and 4.22 show the accelerations of the ice sample for two typical data sets $k_1v_1m_1$ and $k_1v_2m_1$. When the velocity increases from v_1 to v_2, larger accelerations are observed. It takes longer for the ice sample to slow down and return in the opposite direction, which makes it travel further and that explains the increase in standard deviation of the displacement with increasing velocity.

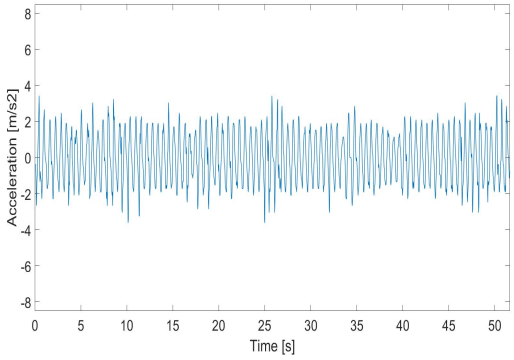

Figure 4.21: Acceleration $k_1 v_1 m_1$

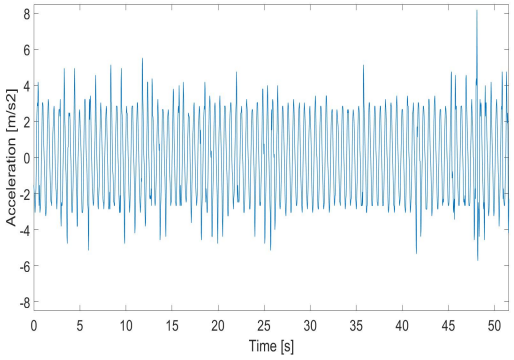

Figure 4.22: Acceleration $k_1 v_2 m_1$

Influence of spring stiffness on mean and standard deviation of the displacement

Figures 4.13, 4.15, 4.17 and 4.19 show that the mean displacement is not affected significantly by the increase in spring stiffness. Figures 4.14 (lowest stiffness, k_1) to 4.16 (for $k_2 > k_1$) to 4.18 (for $k_3 > k_2$) to 4.20 (highest stiffness, k_4) show that the standard deviation in general decrease with increasing stiffness. Where the maximum standard deviation calculated for spring k_1 is about 0.054 m, it is 0.040 m for k_2, 0.038 m for k_3 and 0.027 m for k_4. Figures 4.23 and 4.24 show that an increase in spring stiffness leads to higher accelerations in slip mode for the same concrete velocity and additional mass. The motion in slip mode is defined by $m\ddot{x} + kx = \mu_k mg$, and assuming μ_k, m and g are constants this also suggests a decrease in the displacement.

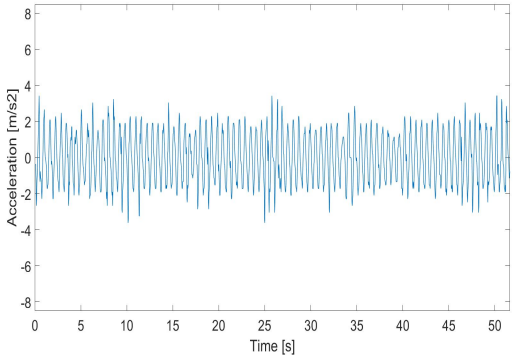

Figure 4.23: Acceleration $k_1 v_1 m_1$

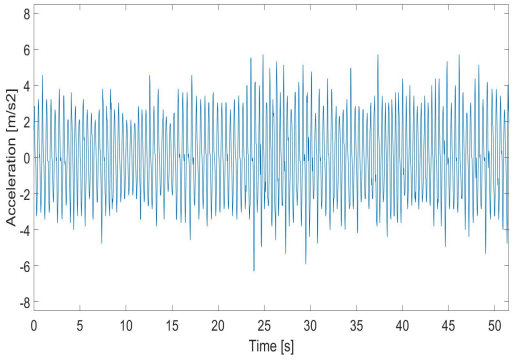

Figure 4.24: Acceleration $k_2 v_1 m_1$

4.1.2 Influence of k, v and m on the peak frequency of the ice sample

For each data set a Fast Fourier Transform analysis was performed which showed the frequency spectrum as shown before in Figure 4.4. For each spectrum the peak frequency was calculated, which represents the frequency of the oscillation of the ice sample. The influence of normal load, velocity of the concrete and the spring stiffness on the peak frequency was analyzed and is shown in Figures 4.25 - 4.28.

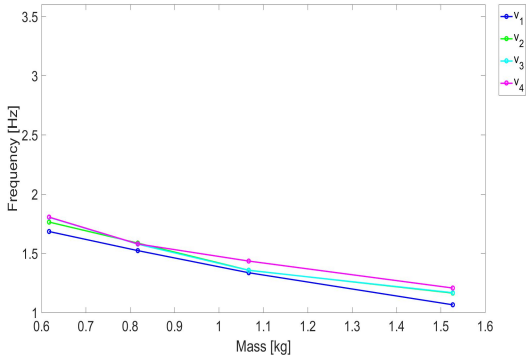

Figure 4.25: f_{peak} for k_1

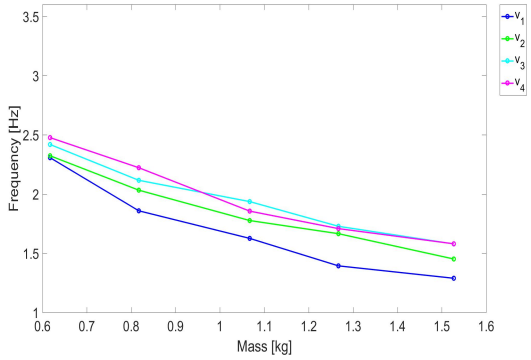

Figure 4.26: f_{peak} for k_2

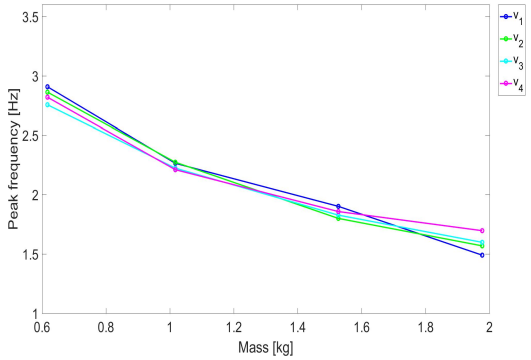

Figure 4.27: f_{peak} for k_3

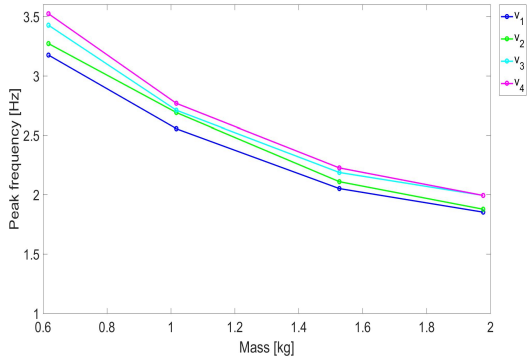

Figure 4.28: f_{peak} for k_4

Influence of normal load on peak frequency

The data sets corresponding to the tests performed with spring stiffness k_1, see Figure 4.25, show that an increase in mass leads to a decrease in the oscillating frequency. For the cases k_2, k_3 and k_4 the same downward trends are observed. Intuitively this behavior makes sense, as a heavier object takes more time to switch directions. This corresponds with what was seen above in Section 4.1.1, an increase in mass causes larger displacements. Therefore, if the normal load increases, and when the same concrete velocity and spring stiffness is considered, the frequency becomes lower.

Influence of velocity on peak frequency

In Figures 4.26 and 4.28 it can be seen that an increase in the concrete velocity causes an increase in peak frequency: the lowest velocity v_1 corresponds to the blue curve that shows the lower frequencies. The curves corresponding to v_2, v_3 and v_4 show a sequential increase in peak frequency. The same effect, although less clearly, can be observed in Figure 4.25 for spring stiffness k_1. The behavior of the ice to oscillate with a higher frequency when the velocity of the concrete is increased, intuitively makes sense. However, for the test data of k_3 this effect is not seen. This could be explained by the fact that an increase the velocity changes the initial conditions in slip mode and increases the displacement, as was explained above in Section 4.1.1. The fact that the ice sample has to travel further, may cause it to take longer to switch directions and thereby decreasing the frequency and canceling out the increase in f_{peak} due to the increase in velocity.

Influence of spring stiffness on peak frequency

The influence of spring stiffness is observed clearly when comparing the average minima and maximima of the trends shown in Figures 4.25, 4.26, 4.27 and 4.28. Respectively, the

minimum and maximum frequencies observed for the cases k_1, k_2, k_3 and k_4 are: 1.1 - 1.8, 1.3 - 2.5, 1.5 - 2.9 and 1.9 - 3.5. In conclusion, an increase in spring stiffness causes an increase in frequency. This is to be expected: the stronger the springs, the less freedom for movement and the faster the ice sample will be pulled back and switch directions.

The behavior of the ice sample under the influence of different spring stiffness, concrete velocity and normal load can be explained physically. Therefore, it has been verified in this section that the experiments have performed stick-slip behavior between ice and concrete accurately.

4.2 Analysis of static and kinetic friction coefficients

Now that the experimental output has been verified, the next step is to calculate the static and kinetic friction coefficients, and to analyze their dependence on k, v and m. The Coulomb law of friction is a widely accepted approximation to describe dry friction between two solids. It describes the friction process by distinguishing between *static* and *kinetic* friction. The static friction force is the critical force that needs to be overcome before two surfaces start moving with respect to each other. This force is proportional to the normal force:

$$F_s = \mu_s F_N \tag{4.1}$$

where μ_s is the static friction coefficient. After the static friction force is overcome and the surfaces start sliding over each other, a kinetic friction force acts on the body in the direction that is opposite to the velocity. The kinetic friction force is also proportional to the normal force:

$$F_k = \mu_k F_N \tag{4.2}$$

where μ_k is the kinetic friction coefficient. Generally, it is assumed that the static and kinetic friction coefficients depend on the two materials in contact, slightly depend on relative sliding velocity and are independent of contact area and surface roughness [Popov 2017].

A lot of uncertainty exists about the frictional properties between concrete and ice. Therefore, the aim of this section is to calculate the static and kinetic friction coefficients from the experimental data and investigate their dependence on the testing variables k, v and m. To be able to do so, first, the stick and slip modes need to be identified in the data, as μ_s follows from stick mode and μ_k from slip mode. Section 4.2.1 discusses the definition of stick and slip mode and elaborates on possible explanations why stick mode is not represented in every oscillation of the ice sample and how this is dealt with in the calculation of the friction coefficients. Sections 4.2.2 and 4.2.3 elaborate on the calculation of the static and kinetic friction coefficients, respectively, as well as their dependence on k, v and m.

4.2.1 Identification of stick and slip modes

The definition that is used to identify the stick and slip modes is as follows:

- During *stick*, the velocity of the ice sample is equal to the local concrete velocity: $v_{ice} = v_{concrete}$
- During *slip*, the velocity of the ice sample is not equal to the local concrete velocity: $v_{ice} \neq v_{concrete}$

During slip, the velocity of the ice is usually smaller than the velocity of the concrete. Because, when the force in the springs overcomes the static friction force, the net force is opposite to the direction of motion which means the ice sample should slow down and the velocity should *decrease*. However, the experimental data has shown that this is not always the case. Figure 4.29 shows an example of the ice sample velocity for a typical data set, which is compared to the local concrete velocity.

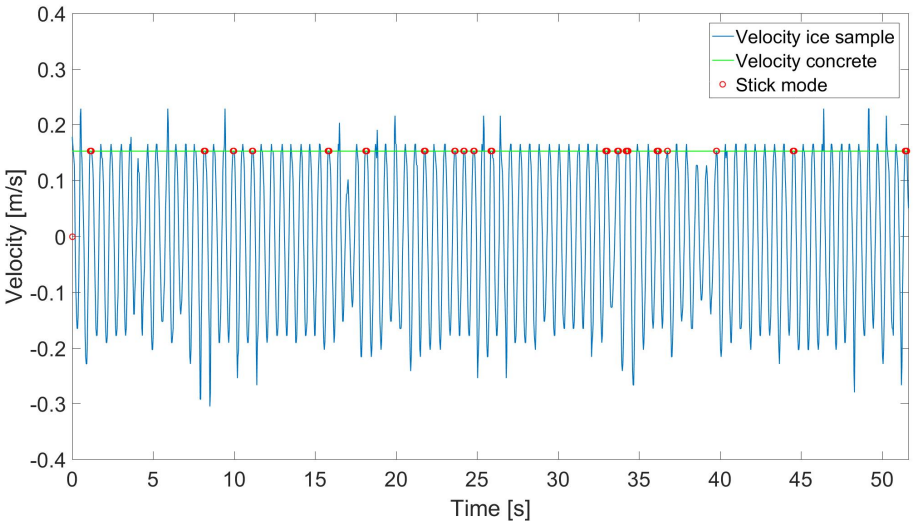

Figure 4.29: Identification of stick mode based on velocity

To be able to speak of a *stick mode*, multiple data points on the $v_{concrete}$ curve are needed, as seen in Figure 4.30, which is an enlargement of a section from Figure 4.29.

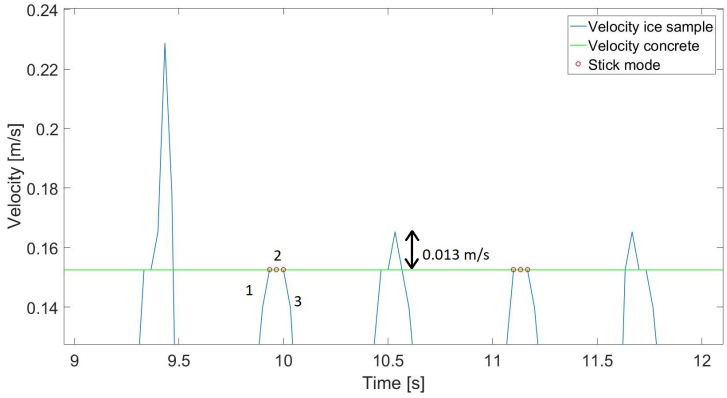

Figure 4.30: Identification of stick mode based on velocity, enlargement

Indeed in Figure 4.30 the second and fourth peak show stick behavior. Three stages can be identified as shown for the second peak. In stage 1 the ice sample is in slip mode and the velocity increases. Considering the 1D situation (i.e. negligible movement in y-direction), the moment that the velocity of the ice sample is equal to the local velocity of the concrete, the relative velocity between the ice and the concrete is zero and stick mode is entered: stage 2. When the critical static friction force is overcome by the spring force, the ice sample gets pulled back in and enters stage 3: slip mode. These three stages thus explain the stick-slip behavior of the ice sample. However, one can distinguish multiple peaks far above $v_{concrete}$, some smaller peaks that extend beyond $v_{concrete}$ all with the same value of 0.013 m/s, and also some peaks that do not reach $v_{concrete}$, see again Figure 4.29. This could be explained on the basis of:

- Error in measurement technique or equipment error

- 2D behavior, such as rotation of the ice sample

The hypotheses that can explain the velocity peaks will be highlighted in the following sections.

Error in measurement technique or equipment error

The measurement technique itself can have caused errors in the data. The post on which the camera was constructed was not very rigid, as well as the way the camera was attached to the post. Bumping into the post and or camera could have caused errors with respect to scaling. Next to that, on some occasions it was experienced that the concrete was sliding against the support frame, causing vibrations in the whole support frame including the camera, influencing the data recording. Also, it was noticed that the camera was slightly sensitive to the lightning conditions. Shadows over the red square on the ice holder sometimes caused the camera not to pick up on the (full) colored square (see Chapter 3). Another cause for error may have been the sampling frequency of 30 data points per second, dictated by the number of frames per second recorded by the camera. Peak frequencies of the stick-slip behavior (as shown in Section 4.1.2) were found to be up to 3.5 Hz, which means that one stick-slip cycle takes roughly 0.3 seconds. A measurement accuracy of 30 frames per second leads thus to 10 frames (data points) to describe the behavior of one stick-slip cycle. It can be questioned if this is sufficient. Another error may have been introduced by the interpretation of the velocity. The velocity was found to be the same every rotation, but the velocity within one rotation may have varied. It would be expected however, that these fluctuations would result in periodic effects, which are not observed in the data as presented in Figures 4.1, 4.2 and 4.3.

2D behavior

Even though it was assumed that the ice sample only moves in x-direction and therefore the behavior is 1D, in reality this is not the case. The concrete slab is rotating, and thus the ice sample will also rotate with respect to the center of rotation. Since the ice sample is connected to springs that pull it back in slip mode and resist the motion in y-direction, the ice sample follows an elliptical path as is shown in Figure 4.31. The local velocity as experienced by the ice sample was calculated as: $v_{local} = \frac{RPM \cdot 2 \cdot \pi \cdot R}{60}$ as was explained in Section 3.3. As was also explained in this section, the RPM measurement device was accurate at one decimal behind the delimiter. Next to that, due to the elliptical motion, the ice sample does not stay perfectly stable at the location R, as was assumed.

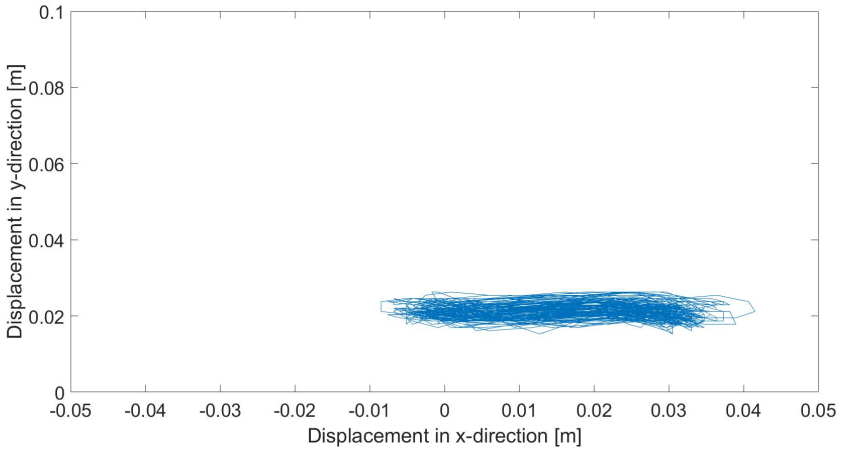

Figure 4.31: Displacement in x versus displacement in y direction for data set k_1, v_1, m_1

For the typical data set represented in Figure 4.31, it can be measured that the maximum difference in y-displacement is about 11 millimeters. Translating this to the local velocity, combined with the error that is possible in the RPM measurement, creates the following range for $v_{concrete}$:

$$v_{concrete_{min}} = \frac{3.55 \cdot 2 \cdot \pi \cdot 0.399}{60} = 0.1483 m/s \tag{4.3}$$

$$v_{concrete_{max}} = \frac{3.64 \cdot 2 \cdot \pi \cdot 0.421}{60} = 0.1605 m/s \tag{4.4}$$

From the experimental data it was deduced that the local velocity of the concrete was 0.152 m/s, because that is the velocity where the flat segments in the curve occur. It can be concluded that the large peaks that go beyond 0.20 m/s can not be explained only by the effect of the displacement in y-direction. The smaller peaks could perhaps be explained by this difference. However, a lot of the smaller peaks have a value of 0.165 m/s and the fact that this value repeats itself throughout the data set raises the question if a change in position R could cause this repetitive result.

Another 2D effect is the rotation of the ice sample around its own center of rotation. This happened because the concrete was rotating but also because a velocity gradient existed over the diameter of the ice sample. Rotation would have caused the red square to travel over a larger distance then the center of the ice sample. Therefore, it could have happened that even though the ice sample was in stick mode, this is not observed in the data. Figure 4.32 shows the ice sample in its straight position and Figure 4.33 shows the position of the ice sample when it has rotated.

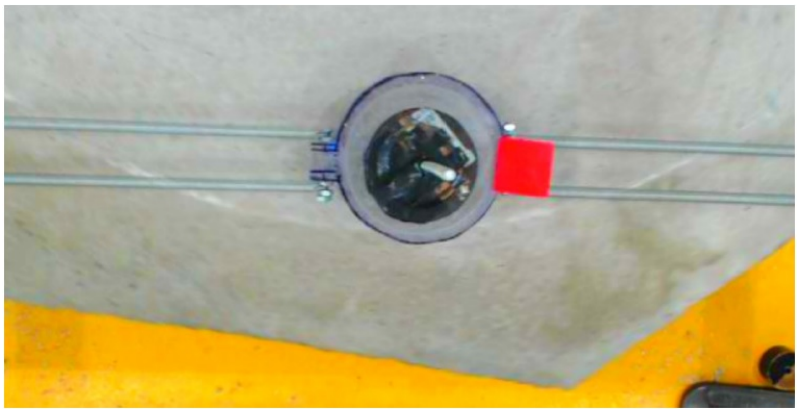

Figure 4.32: Snapshot start

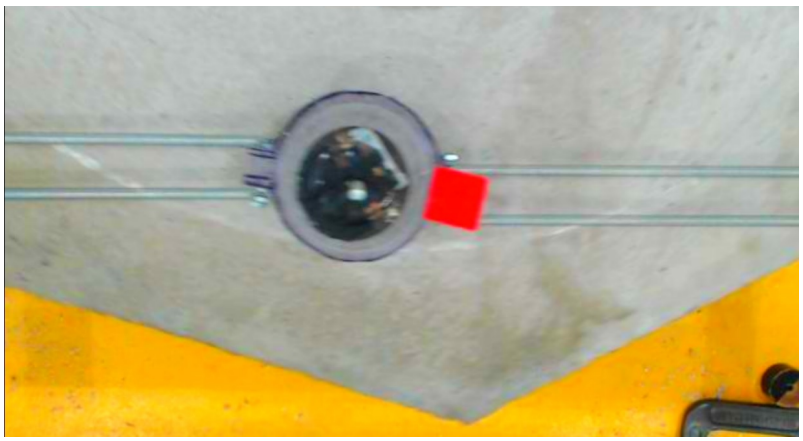

Figure 4.33: Snapshot after rotation

From Figures 4.32 and 4.33, it was estimated that the angle of rotation was 20 degrees. The position of the center of the red square with respect to the center of rotation of the ice sample was measured to be 65 mm. As shown in Figure 4.34 the increase in displacement due to a rotation of 20 degrees is: $\Delta x_{twist} = 65 - 65 \cdot \cos(20) = 65 - 61 = 4$ mm.

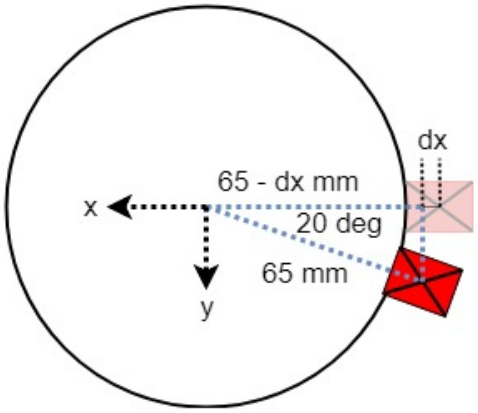

Figure 4.34: Increase of displacement, dx, due to twist

From video playback, it was estimated that the rotation took around 0.33 seconds. Therefore, the increase in velocity that was measured solely due to the rotating mechanism is in the order of: $\Delta v_{rot} = \frac{\Delta x_{rot}}{\Delta t_{rot}} = \frac{0.004}{0.3} = 0.013$ m/s. The small peaks in the experimental data had an offset of 0.165 - 0.153 = 0.013 m/s with respect to the local velocity of the concrete. It is therefore concluded that the rotation of the ice sample is likely to have caused the repetitive small peaks in the data.

Conclusions on how to identify stick and slip modes in the data

After considering the explanations for the peaks, the following is concluded:

- The calculation of the influence of rotation suggests quite strongly that the small peaks in velocity occur due to rotation of the ice sample. Thus, the ice sample was in stick mode even though the data does not show this
- Since none of the explanations above on their own could explain the large peaks it is concluded that the large peaks are due to a combination of multiple factors that have influenced the data.

The following way of dealing with the peaks in the analysis of the static and kinetic friction coefficients is proposed:

- All flat regions at $v_{concrete}$ are in *stick mode*
- All data points for which $v < v_{concrete}$ are in *slip mode*
- All data points for which $v > v_{concrete}$ are disregarded in the analysis of the static and kinetic friction coefficients

4.2.2 Calculation of the static friction coefficient

From the Coulomb model for friction it is known that at the moment of stick to slip transition, the critical static friction force is reached, where: $F_{crit} = \mu_s \cdot F_N = \mu_s \cdot m \cdot g$. Since the velocity during stick is constant, there is no acceleration. The external force on the ice sample consists of the spring forces, which gives the force balance:

$$\begin{aligned} F_{ex} &= F_{crit} \\ 4 \cdot k \cdot x_{transition} &= \mu_s \cdot m \cdot g \end{aligned}$$

Rewriting gives the following expression for the static friction coefficient:

$$\mu_s = \frac{4 \cdot k \cdot x_{transition}}{m \cdot g} \tag{4.5}$$

Where k is the spring stiffness of one spring in N/m, m is the mass of the ice sample plus the mass of the ice holder and the mass of the additional weights, and g is the gravitational acceleration of 9.81 m/s. The only unknown is $x_{transition}$: the displacement at the moment of stick to slip translation. Using the identification of the stick and slip modes from the velocity curve of the experimental data, this can be calculated. The data points where the stick mode is identified as was shown for the example case $k_1 v_1 m_1$ in Figures 4.29 and 4.30, are translated to the displacement curve, leading to the result shown in Figure 4.35.

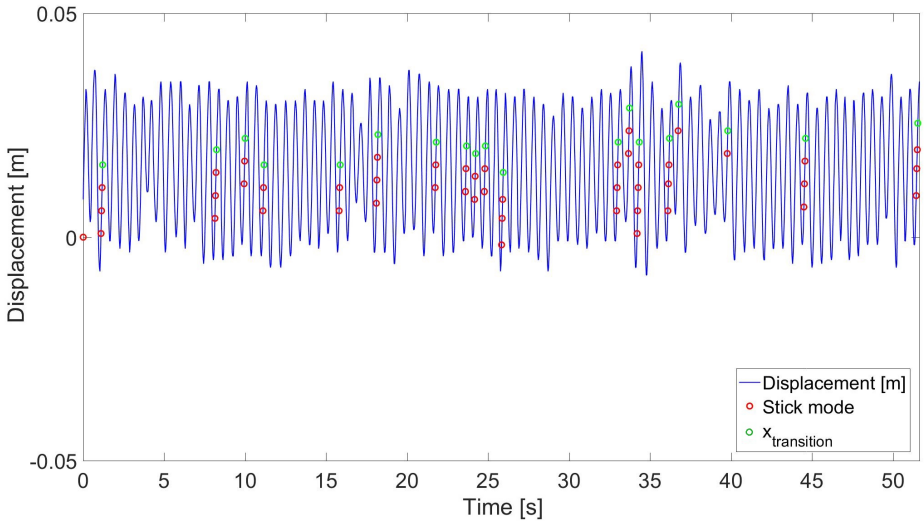

Figure 4.35: Identification of stick mode in displacement curve

The last data point identified in stick mode indicates the stick-to-slip transition and therefore the green circles in Figure 4.35 all indicate $x_{transition}$. From the definition of friction and Equation 4.5 it would be expected that μ_s and therefore $x_{transition}$ are constant during one specific test run. However, this is not the case. This can be explained by:

- The surface roughness of the concrete is not exactly the same everywhere.
- The surface roughness of the ice sample changes over time.
- Frictional heat might influence the thin water layer between ice and concrete.

This leads to a fluctuation in μ_s and therefore a fluctuation in $x_{transition}$ as observed in Figure 4.35. Therefore, the mean and standard deviation of the static friction coefficient were calculated for each data set. Some test results could not be used for this analysis, because not enough stick modes could be identified throughout the test. It was decided that at least 5 stick modes had to be visible in a data set in order to get representative values for the static friction coefficient. Appendix B contains an overview of all the static friction coefficients that were calculated.

Figure 4.36 shows the variation of the mean of the static friction coefficient over a range of masses for different velocities, for a constant spring type k_1. Figures 4.37 shows the variation of the standard deviation of the static friction coefficient over a range of masses for different velocity for constant spring type k_1. Figures 4.38 until 4.43 show the same variation for the different spring types k_2, k_3 and k_4 respectively.

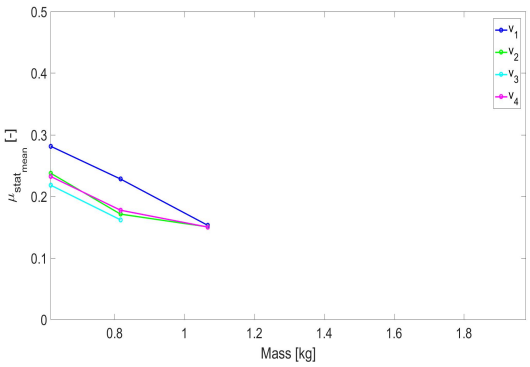

Figure 4.36: $\mu_{s_{mean}}$ for k_1

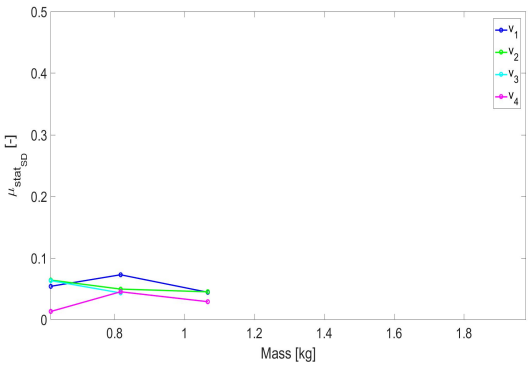

Figure 4.37: $\mu_{s_{SD}}$ for k_1

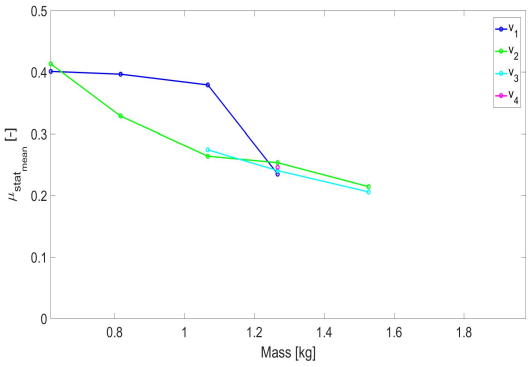

Figure 4.38: $\mu_{s_{mean}}$ for k_2

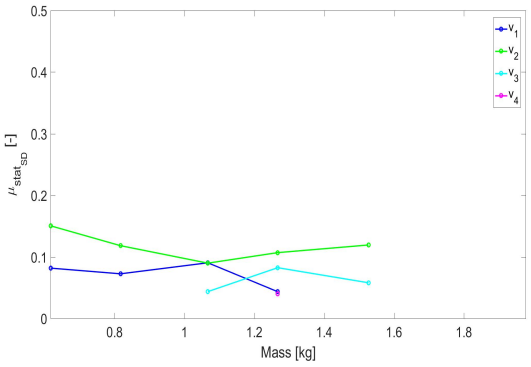

Figure 4.39: $\mu_{s_{SD}}$ for k_2

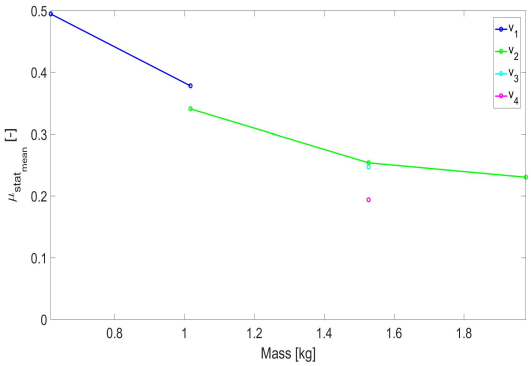

Figure 4.40: $\mu_{s_{mean}}$ for k_3

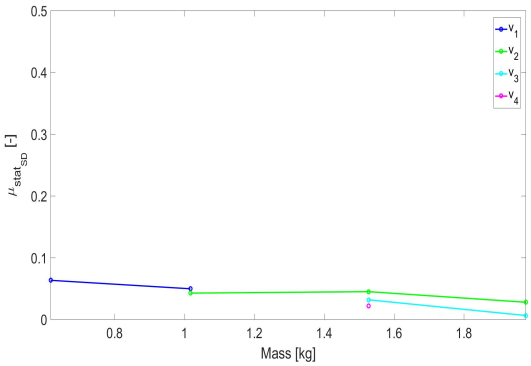

Figure 4.41: $\mu_{s_{SD}}$ for k_3

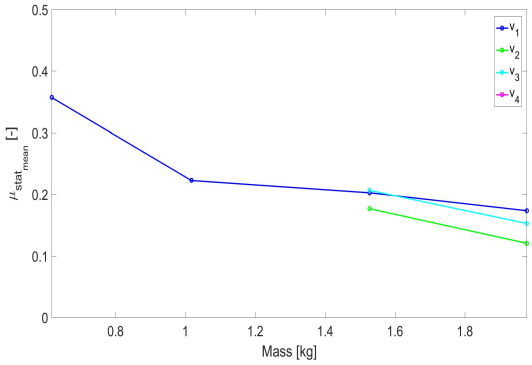

Figure 4.42: $\mu_{s_{mean}}$ for k_4

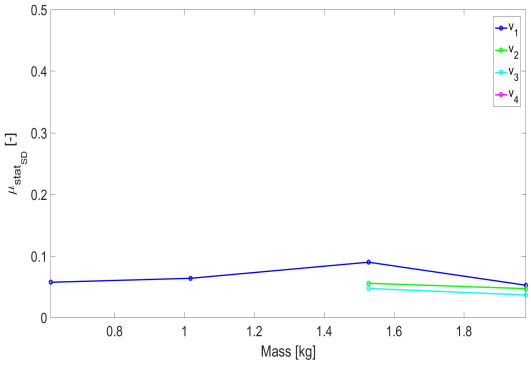

Figure 4.43: $\mu_{s_{SD}}$ for k_4

Based on the figures above, some conclusions about the behavior of the mean and standard deviation of the static friction coefficient can be drawn. Focusing on Figure 4.40 it can be observed that:

- The downward trend indicates that an increase in mass causes a decrease in the mean static friction coefficient
- When comparing between velocities $v_1 - v_4$ it is noticed that an increase in local concrete velocity slightly decreases the mean static friction coefficient

Similar trends are visible for spring constants k_1, k_2 and k_4 as shown in Figures 4.36, 4.38 and 4.42, respectively. In literature, no references to the influence of normal load on the static friction coefficient for ice-concrete contact were found. It was found however that for steel-ice interaction, an increase in normal load caused a decrease in static friction coefficient, upon approaching a constant above a normal stress of 0.5 MPa [Nakazawa et al. 1993]. According to Nakazawa et al., an increase in normal stress on the surface would cause the asperities to break off and smooth the surface, therefore decreasing the static friction coefficient. This could possibly explain the result that has been observed in Figures 4.36 - 4.42, where the maximum normal stress was: $\sigma_{N_{max}} = \frac{m_{max} \cdot g}{\pi \cdot (r_{ice})^2} = \frac{1.36 \cdot 9.81}{\pi \cdot (0.05)^2} = 0.02$ MPa.

A decrease of the static friction coefficient caused by an increase in sliding velocity was observed by [Saeki et al. 1986]. The effect was attributed to the fact that the actual contact area diminishes at higher velocities, where the surfaces start riding over each other. This is also in line with the effect of static strengthening: a higher velocity means less time for the asperities to lock into eachother and therefore lower friction coefficients [Schulson and Fortt 2013].

To analyze the influence of the spring stiffness, a comparison is made between the mean displacements for k_1, k_2, k_3 and k_4, as shown in Figures 4.36, 4.38, 4.40 and 4.42 respectively. Going from the lowest stiffness k_1 to k_3, is seen that an increase in spring stiffness causes an increase in the mean static friction coefficient. However, this trend does not continue to k_4. The influence of the spring stiffness on the static friction coefficient is therefore not identified.

The standard deviation of the static friction coefficient is small compared to the mean and does not seem to be influenced by spring stiffness, velocity or mass in a certain trend.

4.2.3 Calculation of the kinetic friction coefficient

As mentioned previously in Section 4.2, the data is interpreted such that the Coulomb model of friction applies. For kinetic friction the following statements hold:

- The kinetic friction force acts in the direction opposite to the direction of slipping
- The magnitude of kinetic friction is: $F_{kin} = \mu_k \cdot F_N$, where μ_k is the coefficient of kinetic friction, and F_N is the normal force

In slip mode, the external force on the body consists of the inertia plus the contribution of the springs. In other words, in slip mode the following relation holds:

$$m\ddot{x} + kx = F_k \cdot -sign(\dot{x}) \tag{4.6}$$

Note that it is assumed that the damping coefficient is zero. Rewriting the equation above leads to the following expression for the kinetic friction coefficient:

$$\mu_k = \frac{m\ddot{x} + kx}{mg} \tag{4.7}$$

The mass, spring constant and gravitational acceleration are known and thus the acceleration and displacement during slip need to be found. As was shown in Figure 4.29, the stick and slip modes were identified by comparing the velocity of the ice sample with the local velocity of the concrete. Following the definition given earlier all data points for which $v < v_{concrete}$ are in slip-mode. Translating the data points that were identified in the velocity curve as being in slip mode, to the displacement and acceleration curves gives the information needed to calculate μ_k. The same as for the static friction coefficient, the kinetic friction coefficient is not constant during one test run and again the mean value and standard deviation have been calculated and plotted against mass, velocity and spring stiffness. See Figures 4.44 to 4.51.

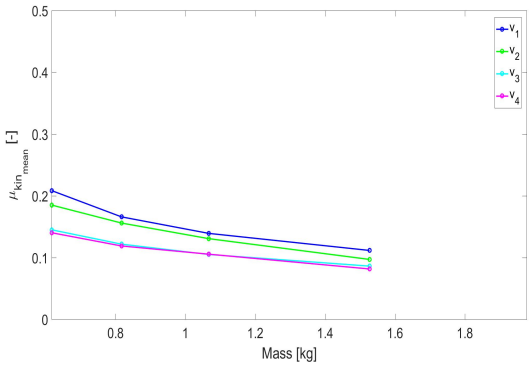

Figure 4.44: $\mu_{k_{mean}}$ for k_1

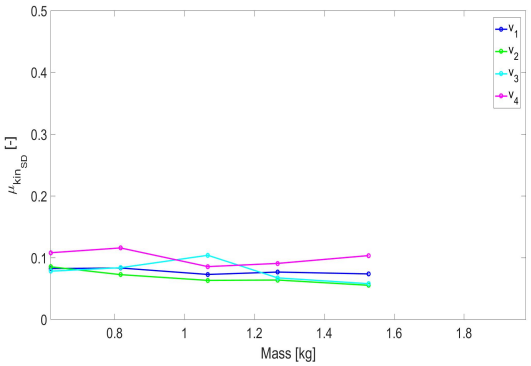

Figure 4.45: $\mu_{k_{SD}}$ for k_1

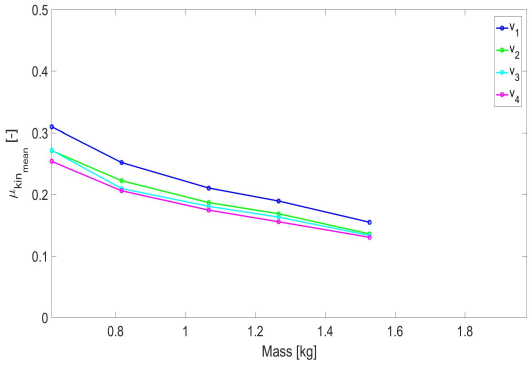

Figure 4.46: $\mu_{k_{mean}}$ for k_2

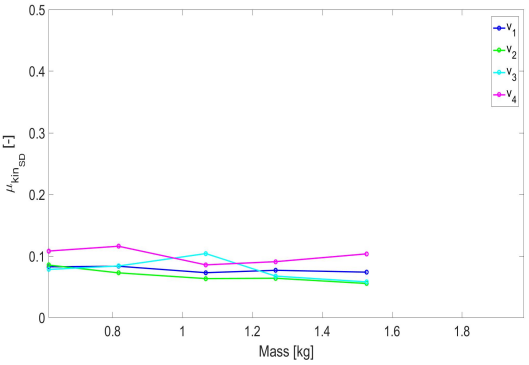

Figure 4.47: $\mu_{k_{SD}}$ for k_2

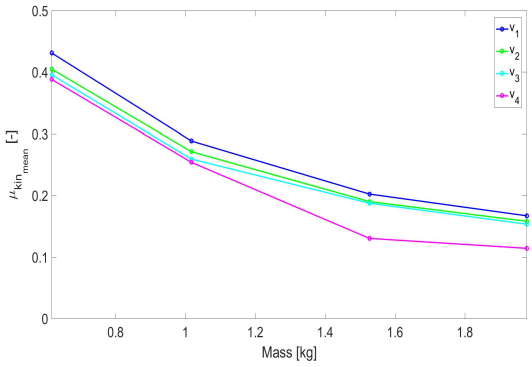

Figure 4.48: $\mu_{k_{mean}}$ for k_3

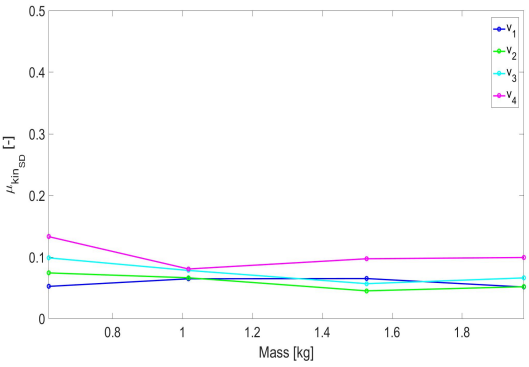

Figure 4.49: $\mu_{k_{SD}}$ for k_3

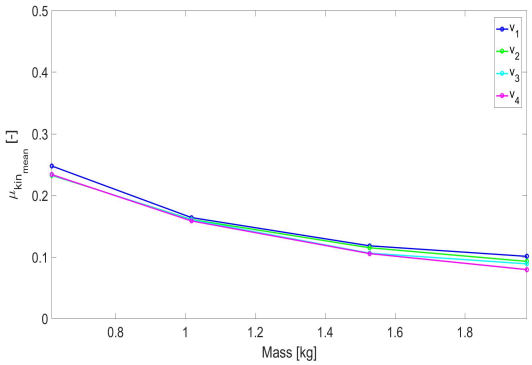

Figure 4.50: $\mu_{k_{mean}}$ for k_4

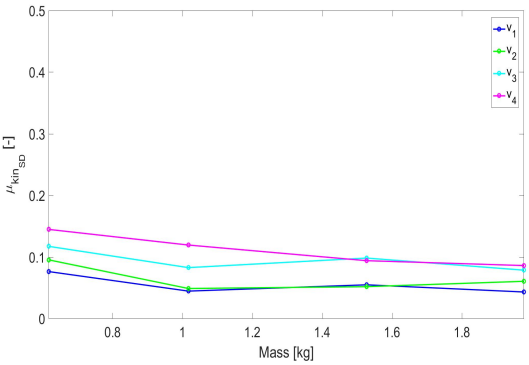

Figure 4.51: $\mu_{k_{SD}}$ for k_4

Figures 4.44, 4.46, 4.48 and 4.50 show a decreasing trend, indicating the decrease of the mean kinetic friction coefficient with increasing normal load. This corresponds to findings in literature [Fiorio, Meyssonnier, and Boulon 2002], [Moen et al. 2015]. It is also observed that an increase in velocity causes a decrease in kinetic friction coefficient, see Figure 4.44. This is consistent with findings in previous research [Martins, Oden, and Simoes 1990], [Saeki et al. 1986], [Moen et al. 2015]. The actual contact area diminishes because the surfaces are riding over each other, giving less opportunity for the asperities to lock into each other [Saeki et al. 1986]. Another explanation could be the development of a thin water layer due to frictional heating, lubricating the ice-concrete contact [Moen et al. 2015].

As for the static friction coefficients, again an overall increase in the kinetic friction coefficient with increasing spring stiffness is observed from k_1 to k_3 (Figures 4.44 - 4.48) but this trend does not follow through for spring type k_4, see Figure 4.50. The standard

deviation of the kinetic friction coefficient is larger than the standard deviation that was observed for the static friction coefficient, see Section 4.2.2. Once more, the spring stiffness, velocity and mass do not seem to have a significant influence. Compared to the static friction coefficient, the trends for the kinetic friction coefficient are smoother and the data is more complete, this is due to the much larger set of data points identified in slip mode.

4.2.4 Variation of kinetic friction coefficient over time

Although the kinetic friction coefficient is often represented as a constant, in reality it changes over time. In this section, the variation of the kinetic friction coefficient over time is discussed. Figure 4.52 shows the change of μ_k over time, for test $k_1v_1m_1$.

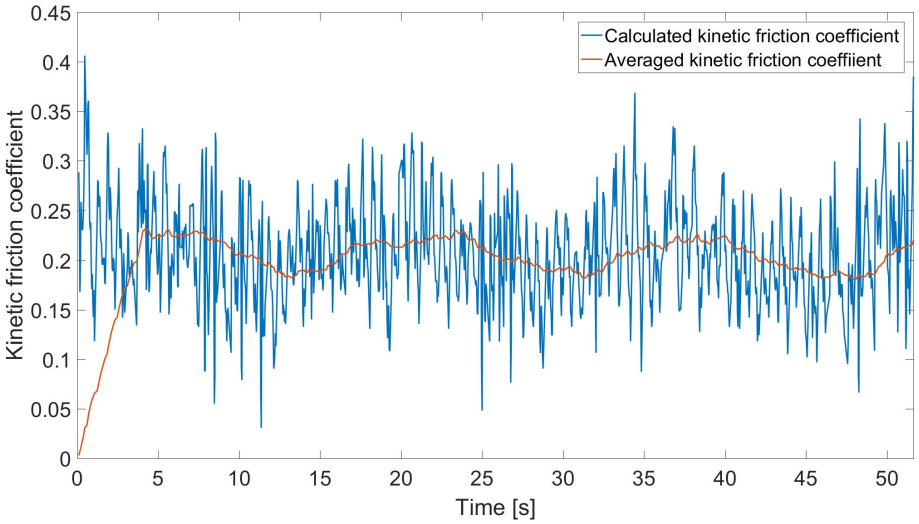

Figure 4.52: Kinetic friction coefficient over time, data set $k_1v_1m_1$

By averaging the curve of the kinetic friction coefficient per 100 data points, it also becomes clear that μ_k changes over time harmonically, with a period of about 18 seconds. The period of rotation of the concrete slab is about also about 18 seconds, which suggests that the change of μ_k is related to the position on the concrete slab. To see if this periodic behavior is also observed in other tests, the kinetic friction coefficient over time was analyzed for another example, see Figures 4.53.

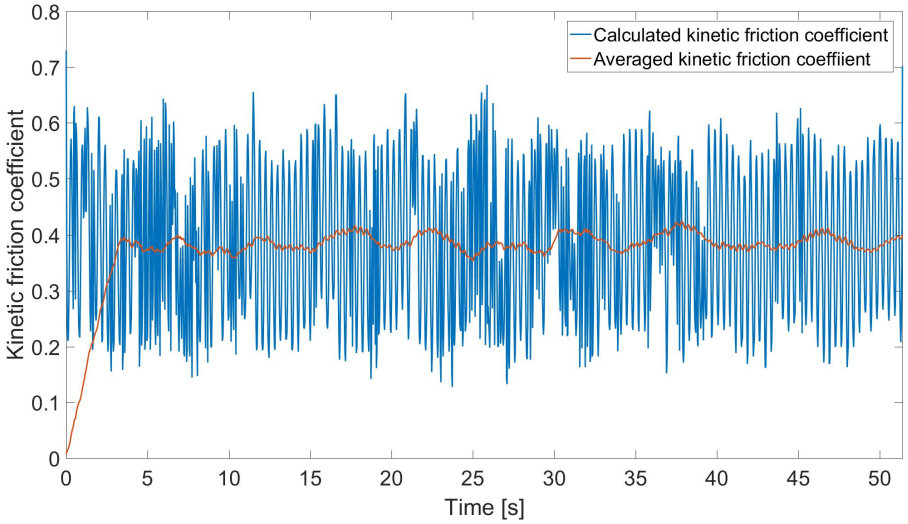

Figure 4.53: Kinetic friction coefficient over time, data set $k_3v_4m_1$

From Figure 4.53 the period visible over the averaged kinetic friction coefficient is estimated at 5 seconds, while for a concrete velocity "v_4", the period is:

$$T_{v_4} = \frac{60\text{s}}{11.7\text{RPM}} = 5.13s \tag{4.8}$$

It can therefore be concluded that the kinetic friction coefficient is influenced by the location along the circular path on the concrete slab. The change of roughness across the slab could cause this, even though the concrete was poured in a way to minimize this effect.

Apart from the periodicity, it is also seen in Figures 4.52 and 4.53, that the variation of the kinetic friction coefficient is large compared to its mean. This could be the result of how the kinetic friction coefficient was calculated, namely as follows:

$$\mu_k = \frac{m\ddot{x} + kx}{mg} \tag{4.9}$$

In theory, the terms $\frac{m\ddot{x}}{mg}$ and $\frac{kx}{mg}$ would be varying, but in the same order of magnitude. The displacement x was measured in the experiment, and the acceleration $\ddot{x}$ was calculated by taking the gradient of x over time twice. This introduces computational errors and might explain the large variation of μ_k over time. Therefore, the same plot was constructed with μ_k approximated by:

$$\mu_k = \frac{2kx}{mg} \tag{4.10}$$

The result is shown in Figure 4.54.

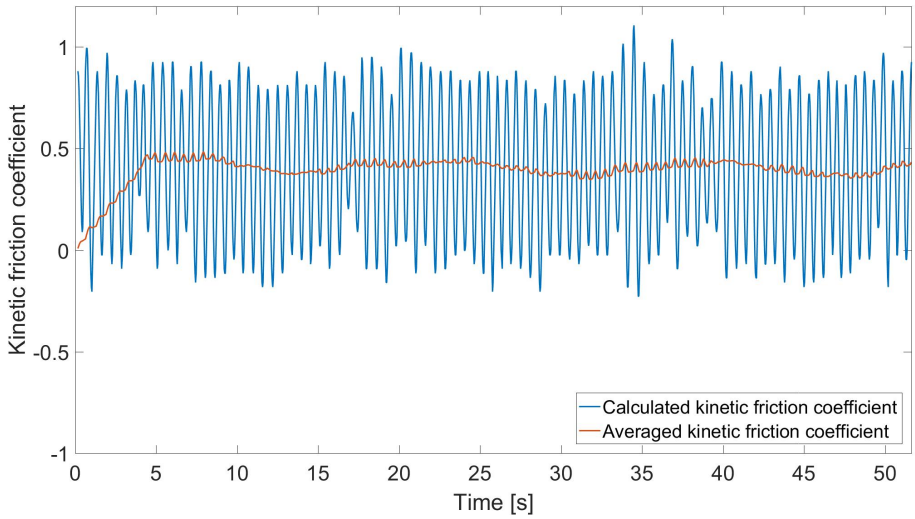

Figure 4.54: Kinetic friction coefficient over time, data set $k_1v_1m_1$, for $\mu_k = \frac{2kx}{mg}$

The figure above shows an even larger variation and indicates that the assumption that the two terms in Equation 4.9 are of equal magnitude, is not valid here. To investigate the influence of the second term, the kinetic friction coefficient was also calculated as:

$$\mu_k = \frac{2m\ddot{x}}{mg}. \tag{4.11}$$

The result is shown in Figure 4.55.

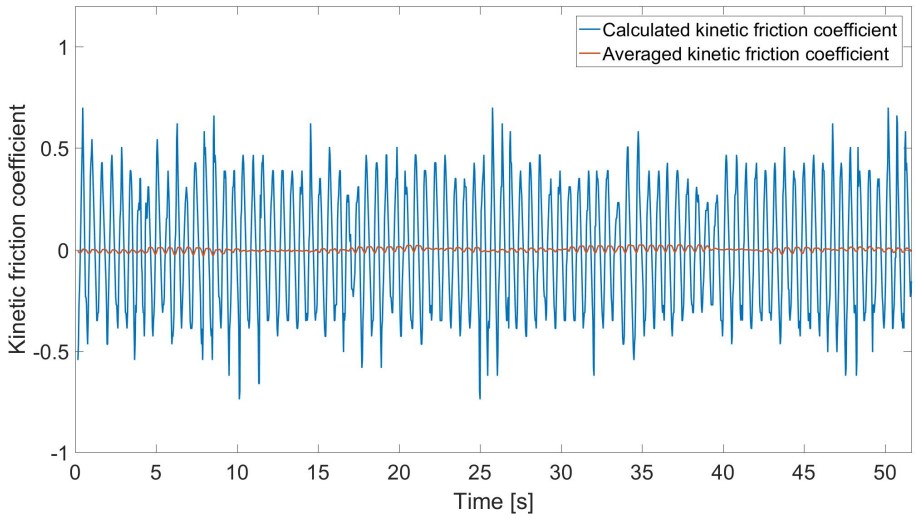

Figure 4.55: Kinetic friction coefficient over time, data set $k_1v_1m_1$, for $\mu_k = \frac{2m\ddot{x}}{mg}$

Figure 4.55 supports the conclusion made based on the outcome of Figure 4.54, namely that the Equation 4.9 can not be represented by either Equation 4.10 or 4.11. It can also be concluded that the large variation of μ_k during one test can not be explained by the computational error resulting from the calculation of the acceleration.

4.2.5 Ratio between static and kinetic friction coefficient

The ratio between the static and kinetic friction coefficient is calculated for every data set and the result is presented below. An overview of the test numbers and the corresponding test k, v and m is given in Appendix E.

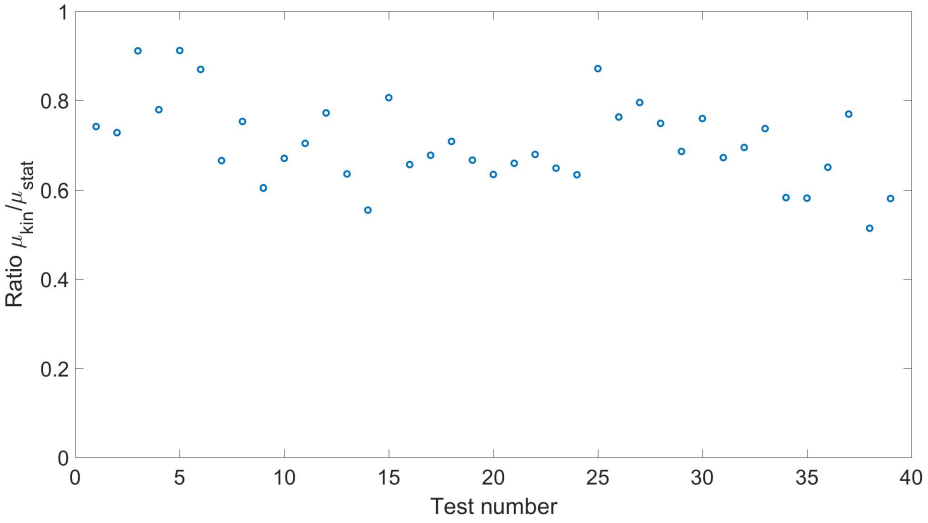

Figure 4.56: Ratio between kinetic and static friction coefficient for all tests

Figure 4.56 shows that the ratio: $\mu_{ratio} = \frac{\mu_k}{\mu_s}$ lies between 0.51 - 0.91 with an average of 0.70.

Chapter 5

Numerical model of stick-slip behavior between concrete and ice

The development of numerical models is an important aspect of research, as it allows for analysis anytime, anywhere, at low cost and with a controllable input. In this chapter, the numerical model that was developed to study stick-slip behavior is presented and discussed. The model is based on an example of a mass attached to a spring, which is resting on a moving conveyor belt. The experimentally obtained static and kinetic friction coefficients were used as input in the final stick-slip model. The lay-out of the model is presented in the first section after which the equations of motion, input of the model and the assumptions made are discussed. The model is verified by means of a preliminary comparison with the experimental data, as well as an analysis that investigates the sensitivity of the model to the input parameters.

5.1 The stick-slip model of a mass on a conveyor belt

The numerical model is based on the conveyor-belt model that was shown previously in Chapter 2, see Figure 5.1.

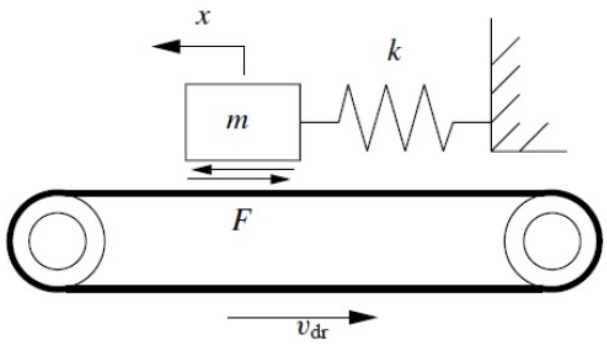

Figure 5.1: 1 DOF model with dry friction [Leine et al. 1998]

As seen in Figure 5.1, a block with mass m is positioned on a conveyor belt that runs at a speed v_{dr}, and a spring with stiffness k connects the block to a wall. It is assumed that the mass is initially placed on the conveyor belt at the equilibrium position such that there is no extension nor compression in the spring. Once the belt is switched on the mass will start moving with the belt in *stick mode*. The relative velocity between the two surfaces is then zero, because the static friction force prohibits the block from moving. Using the definition of the Coulomb model of friction it is known that the friction force is equal to the external forces that act on the block, until the critical static friction force is reached. The critical static friction force is related to the normal force:

$$F_{crit_{stat}} = \mu_s \cdot F_N = \mu_k \cdot m \cdot g \tag{5.1}$$

After this state is reached, the system will transition from *stick* to *slip mode*. In slip mode a kinetic friction force is acting on the body. The kinetic friction force is also related to the normal force as follows:

$$F_{kin} = \mu_k \cdot F_N = \mu_k \cdot m \cdot g \tag{5.2}$$

The mass will slip over the surface of the conveyor belt until the velocity of the mass is equal and in the same direction as v_{dr} again, after which it will transition back to *stick mode*. This process is repeated over and over as long as the belt keeps running. Summarizing, the *stick-slip motion* of the ice block can be described as follows:

Stick mode:

$$\begin{aligned} v_{ice} &= v_{dr} \\ x_{ice} &= x_{ice}(t_0) + v_{dr} \cdot (t - t_0) \\ a_{ice} &= 0 \end{aligned}$$

Stick-to-slip transition:

$$\begin{aligned} F_{ex} &= F_{crit_{stat}} \\ 4k \cdot x_{ice} &= \mu_s \cdot m \cdot g \end{aligned}$$

Slip mode:

$$\begin{aligned} F_{ex} &= F_{kin} \\ m \cdot a_{ice} + 4k \cdot x_{ice} &= \mu_k \cdot m \cdot g \end{aligned}$$

Slip-to-stick transition:

$$v_{ice} = v_{dr}$$

The spring stiffness in the model represents the four springs in the experiment, and therefore, the external force contains the term $4k \cdot x$. A numerical model describing these relations and solving the differential equations for the mass on the conveyor belt was created. The input needed for this model is:

- Mass, m $[kg]$
- Spring stiffness, k $[N/m]$
- Gravitational acceleration, g $[m/s^2]$
- Belt drive velocity, v_{dr} $[m/s]$
- Static friction coefficient, μ_s [-]
- Kinetic friction coefficient, μ_k [-]

The mass, spring stiffness and belt drive velocity are based on the values used in the experiment, and the static and kinetic friction coefficients are obtained from the experimental data analysis as presented in the previous chapter.

5.2 Verification of the numerical model

Throughout the development of the model, it was ensured that model output was in line with the conceptual specifications. In other words, the verification of the numerical model was a continuous process. The verification of the stick-slip model can be split up in two parts. First, a preliminary comparison of the model with the experimental data is presented in Section 5.2.1 which led to an improvement of the model through randomization of the static and kinetic friction coefficients as presented in Section 5.2.2. Secondly, a sensitivity analysis of the model to changes in the input parameters was performed, which is presented in Section 5.2.3.

5.2.1 Preliminary comparison with experiment

From the equations and conditions described in Section 5.1 a preliminary numerical model was constructed where all input parameters were treated as constants. A preliminary comparison between model and the experiment was made, where an example test case was taken from the test plan (see Section 3.3): $k_1 v_1 m_1$. Corresponding with this test case the following input was given to the preliminary numerical model:

- $m = 0.6171$ kg (only the ice sample and ice holder, no additional weights)
- $k = 20.17$ N/m
- $g = 9.81$ m/s^2
- $v_{dr} = 0.15$ m/s (local velocity of concrete, v_1)
- $\mu_s = 0.2815$ (mean static friction coefficient, Section 4.2.2 or Appendix B)
- $\mu_k = 0.2086$ (mean kinetic friction coefficient, Section 4.2.3 or Appendix C)

Figure 5.2 presents the displacement curve produced by the *model* and Figure 5.3 presents the displacement curve that was obtained from the *experimental data*.

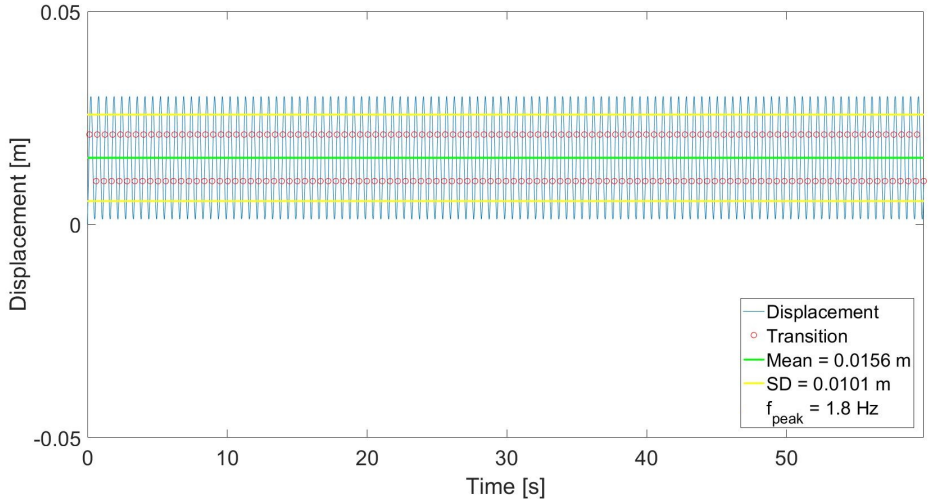

Figure 5.2: Displacement output of stick-slip model

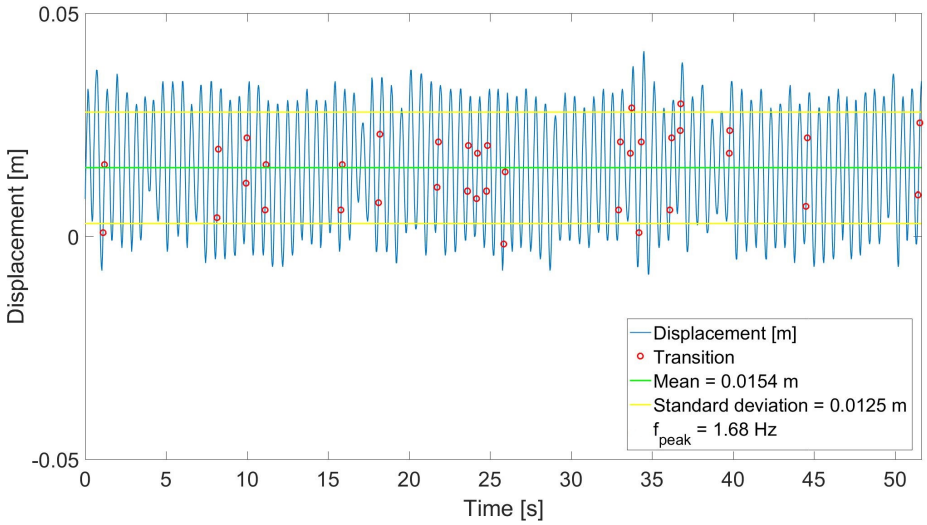

Figure 5.3: Displacement output of stick-slip experiment

The following observations are made when comparing the two displacement curves:

- The mean displacements show a high level of similarity, with only a difference of 0.1 mm
- The standard deviation of the displacement is slightly underestimated by the model and displays a difference of 2.4 mm with respect to the experiment
- The peak frequency determined by the model is 1.8 Hz while the experiment showed a frequency of 1.68 Hz
- The locations of stick-to-slip and slip-to-stick transition are not constant in the experiment, while they are constant in the model
- A stick mode is identified in every cycle in the numerical model, while this is not the case in the experiment
- The overall lay-out of the curve produced by the numerical model is smooth and regular, while the experimental data is not

Figures 5.4 and 5.5 display the velocity curves of the model and the experiment, respectively.

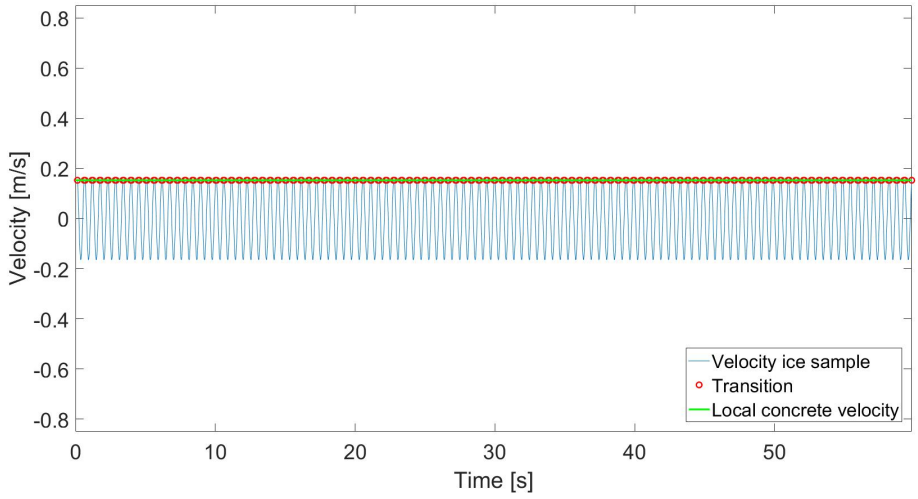

Figure 5.4: Velocity output of stick-slip model

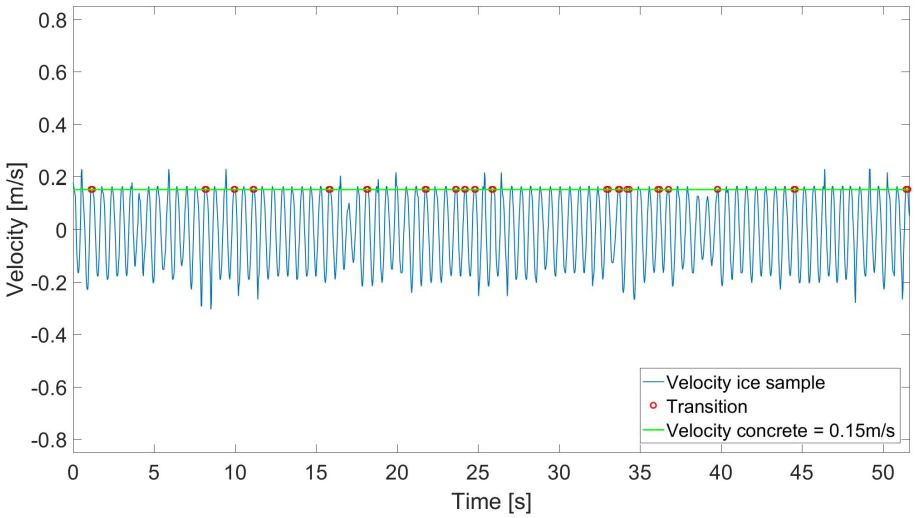

Figure 5.5: Velocity output of stick-slip experiment

When comparing the velocity curves, it is noticed that:

- In the numerical model the velocity of the sample does not exceed the local velocity of the concrete, while it does so in the experimental result and therefore does not exhibit stick mode in these cases
- During the experiment, the velocity of the concrete is sometimes not reached, while the numerical model predicts that the ice sample will always reach this velocity and will always continue to stick mode
- The maximum negative velocity that is reached is the same in every cycle according to the numerical model, while the experimental data depicts a much more irregular situation
- The overall lay-out of the curve produced by the numerical model is smooth and regular, while the curve obtained in the experiment is not

For the first three observations made when comparing the displacement curves, on the previous page, the quantitative discrepancies between the model and experiment are based on one example. In order to produce a more significant conclusion, a comparative statistical analysis is needed and therefore these observations are ignored in this preliminary comparison. What becomes clear however, is that the model produces a regular and smooth representation of what is a more irregular and perturbed situation in reality. A way that is proposed to enhance the output of the numerical model is the following:

"Introducing randomized static and kinetic friction coefficients will increase the similarity with the experiment"

Instead of treating the static and kinetic friction coefficients as constants, new friction coefficients will be randomly generated for each onset to stick- or slip-mode. This is more representative because in reality:

- The roughness of the concrete is not exactly the same everywhere
- The roughness of the ice sample may change over time
- A liquid layer may form between the ice and concrete surfaces over time due to frictional heating

All of this contributes to the fact that the static and kinetic friction coefficients are not constant, which was also clearly observed in the analysis of the friction coefficients in Chapter 4. The next section will elaborate on the improved model.

5.2.2 The updated numerical model: randomized friction coefficients

As concluded above, the numerical model needs to include randomized friction coefficients in order to represent reality better. From the analysis of the experimental data, the mean and standard deviation of the static and kinetic friction coefficients were found (see Chapter 4). In the updated numerical model, after each transition (stick-to-slip or slip-to-stick) the friction coefficients are generated randomly from a Gaussian distribution with the values for the mean and standard deviation of the friction coefficients as obtained from the experimental data analysis. The standard deviations ($\mu_{k_{SD}}$ and $\mu_{s_{SD}}$) found in the experimental data analysis were large compared to the mean friction coefficients, which could result in $\mu_k > \mu_s$, which is physically impossible. Therefore, it is made sure that the condition $\mu_k < \mu_s$ is met each time the friction coefficients are determined from the Gaussian distribution. The output of the updated model is as shown in Figures 5.6 and 5.7.

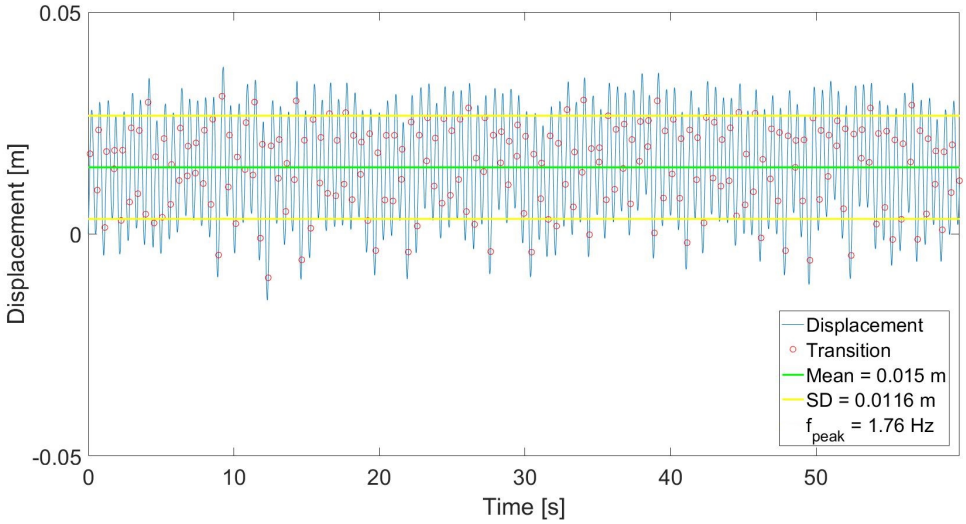

Figure 5.6: Displacement of stick-slip model

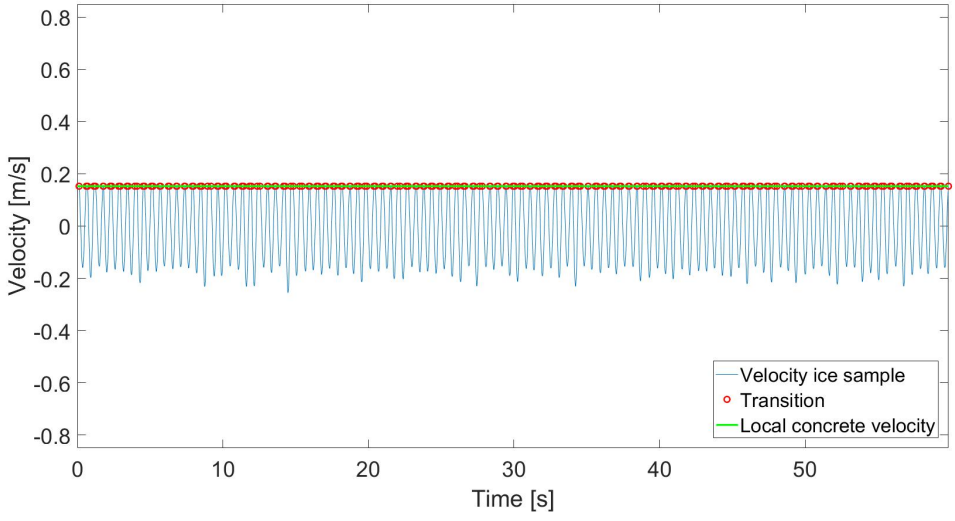

Figure 5.7: Velocity of stick-slip model

It can be seen that the behavior predicted by the model is now more similar to that of the experiment, see Figures 5.3 and 5.5. It becomes clear in the displacement curve that the stick-to-slip and slip-to-stick locations are not constant anymore, causing a more irregular behavior of the ice sample in terms of both displacement as well as velocity.

5.2.3 Influence of k, v and m on the motion of the ice sample

To verify that the numerical model produces the desired output, a sensitivity analysis was performed. In the same way as was done with the experimental data, the mean and standard deviation of the displacement as well as the peak frequency with which the ice sample oscillates, is plotted against the input variables (k, v and m). The values for k, v and m were taken from the test plan and the friction coefficients (mean and standard deviation) were obtained from the friction coefficient analyses performed in Chapter 4. Since not all test data allowed for the calculation of the static friction coefficient, not all tests from the test plan could be reproduced using the numerical model.

Figures 5.8 and 5.9 show the mean displacement and the standard deviation of the displacement that were calculated by the numerical model over a range of masses, for different concrete velocities and a constant spring stiffness k_1. Figures 5.10 to 5.15 show the same for spring stiffness k_2, k_3 and k_4 consecutively.

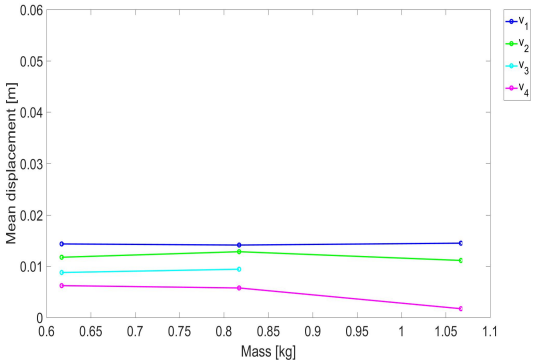

Figure 5.8: x_{mean} for k_1

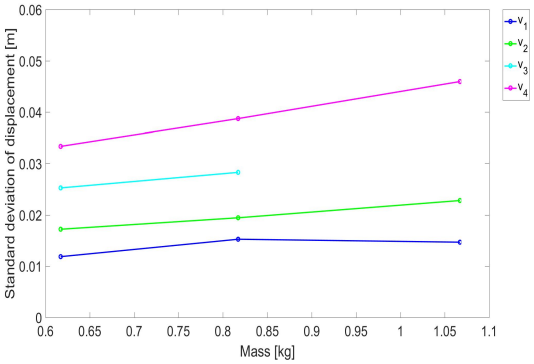

Figure 5.9: x_{SD} for k_1

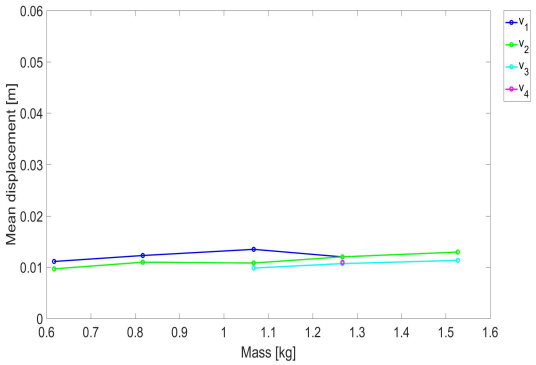

Figure 5.10: x_{mean} for k_2

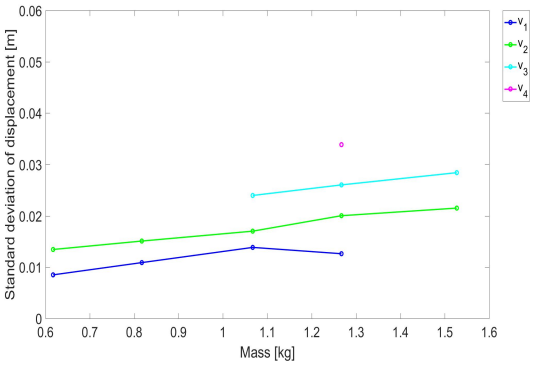

Figure 5.11: x_{SD} for k_2

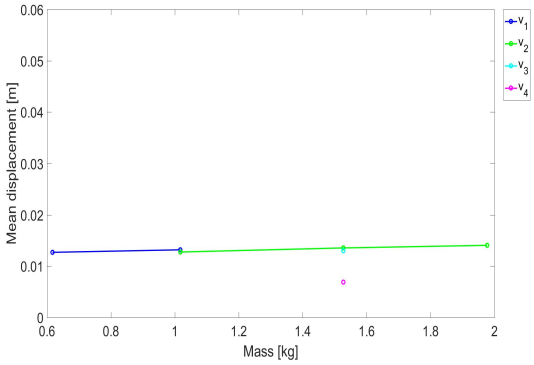

Figure 5.12: x_{mean} for k_3

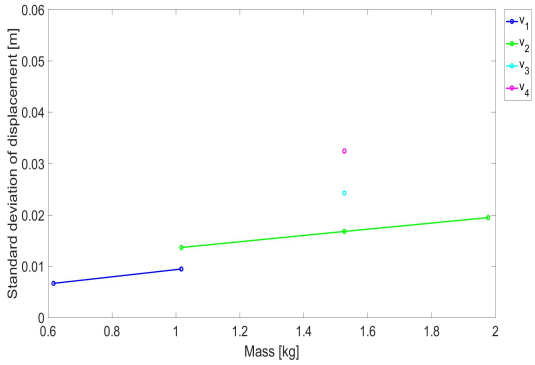

Figure 5.13: x_{SD} for k_3

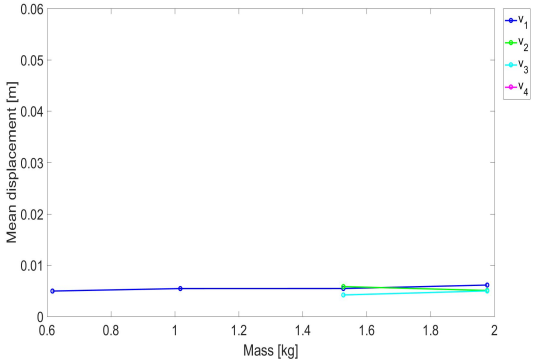

Figure 5.14: x_{mean} for k_4

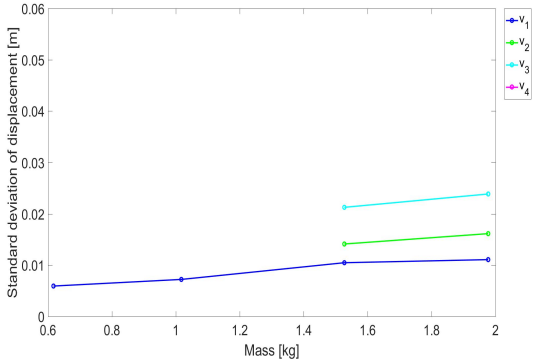

Figure 5.15: x_{SD} for k_4

In general the following can be observed in Figures 5.8 - 5.15:

- The mean displacement slightly increases with increasing mass for k_2 - k_4 (Figures 5.10, 5.12 and 5.14). However, in Figure 5.8 it is observed that the mean displacement stays constant under an increase in normal load or even decreases for velocities v_2 and v_4.
- Figures 5.9, 5.11, 5.13 and 5.15 clearly show a decreasing trend in x_{mean}. This indicates that the standard deviation of the displacement increases with increasing mass.
- Comparing the different velocities in Figures 5.8 and 5.9 it is observed that an increase in velocity causes a decrease in mean displacement, and an increase in the standard deviation of the displacement.
- When comparing Figures 5.8 - 5.15, in general, a tendency for an overall decrease of the parameters as the spring stiffness increases is observed for both x_{mean} and x_{SD}.

This is in accordance with the conclusions of Chapter 4. The behavior of the ice sample, expressed in x_{mean} and x_{SD}, with respect to k, v and m is similar.

Figures 5.16 until 5.19 show the variation of the peak frequency with mass, velocity and spring stiffness as calculated by the model.

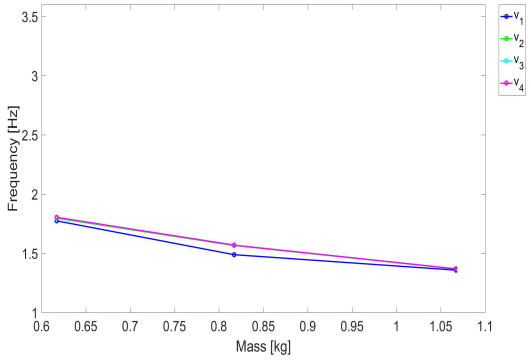

Figure 5.16: f_{peak} for k_1

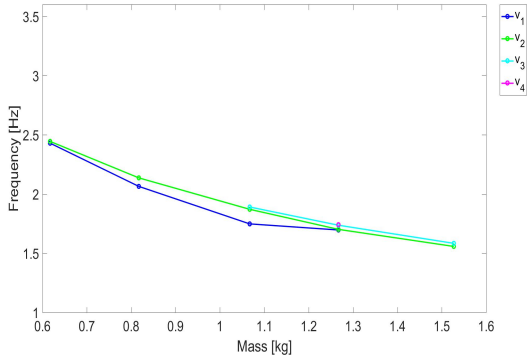

Figure 5.17: f_{peak} for k_2

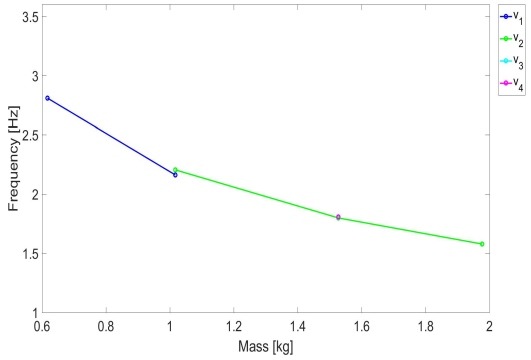

Figure 5.18: f_{peak} for k_3

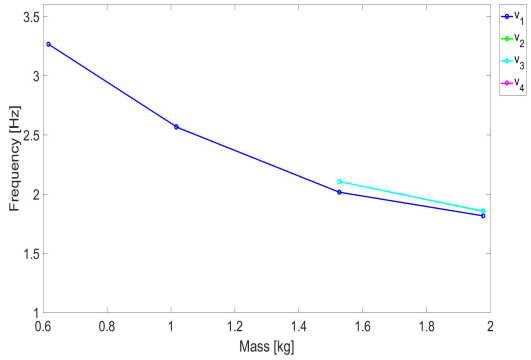

Figure 5.19: f_{peak} for k_4

The analysis shows that:

- An increase in mass causes a decrease in frequency. This is observed in the decreasing trend that is visible in all Figures 5.16 to 5.19.
- An increase in velocity does not influence the frequency significantly. For example in Figure 5.18 the different velocities almost form a continuous curve.
- An increase in spring stiffness causes an increase in frequency. Comparing Figures 5.16 and 5.17, it is observed that an increase in spring stiffness ($k_2 > k_1$) causes an upward shift of the curve. The same is seen in Figures 5.18 and 5.19.

As for the mean and standard deviation, this is in line with what the model is expected to do based on the experimental data. Therefore, the sensitivity analysis has verified the model is working properly. As mentioned above, the randomly chosen friction coefficients cause the numerical output to vary when the output is reproduced. For the input $k_1 v_1 m_1$ twenty different runs of the numerical model were performed. Figure 5.20 shows the variation of the mean displacement between different runs.

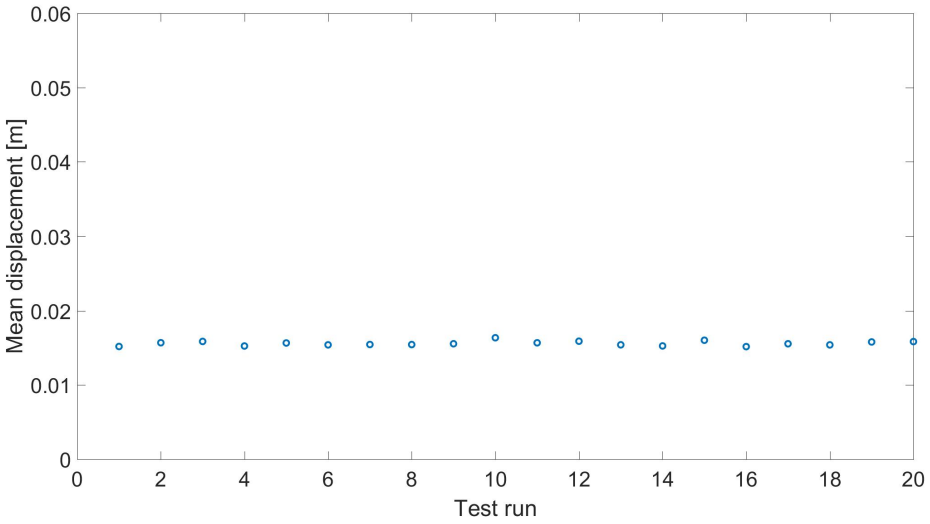

Figure 5.20: Sensitivity to randomness of mean displacement

The mean displacement varies only slightly, with respect to the range of mean displacements that is considered. It is concluded that the variation of the numerical output due to the randomization in friction coefficients, is acceptable.

Chapter 6

Validation of numerical model through comparison with experimental data

In this chapter, the validation process of the numerical model through comparison with the experimental data is discussed. In order to compare the experimental data to the output produced by the numerical model, first an overview is given of the differences between the model and the experiment, and the assumptions made, are discussed in Section 6.1. Section 6.2 continues with a quantitative comparison between the model output and experimental data, to statistically validate the model.

6.1 Discussion of the differences between model and experimental set-up

In order to validate the numerical model, which is done by comparing the output to the experimental data, awareness of the differences between model and experiment, and the assumptions made, is crucial. The differences are listed in Table 6.1 and are discussed in the sections below.

Table 6.1: Differences between numerical model and experimental set-up

Model	**Experiment**
1D behavior	2D behavior
Simulated randomness in friction coefficients	Natural randomness in friction coefficients
No time dependence of μ_k	Time dependence of μ_k
No memory effect incorporated	Memory effect / static strengthening
Dry friction	Dry and possibly wet friction

6.1.1 1D versus 2D behavior

In the numerical model the assumption is made that the mass only moves in x-direction and therefore exhibits 1D behavior. Figure 6.1 shows the side and topview of the conveyor belt model.

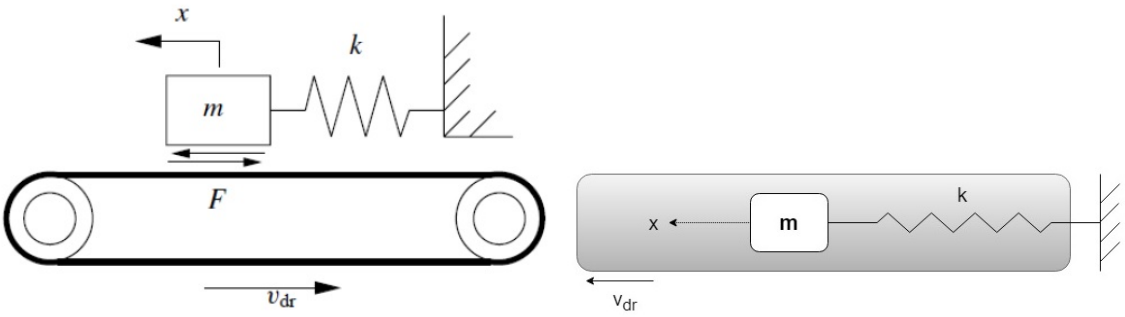

(a) Side view of conveyor belt model (b) Top view of conveyor belt model

Figure 6.1: Lay-out of the conveyor belt model

Since a conveyor belt with a concrete surface was not a feasible experimental set-up, a rotating concrete slab was used which by default introduces translation in more than one direction, leading to 2D behavior. Figure 6.2 shows the side and top view of the experimental set-up.

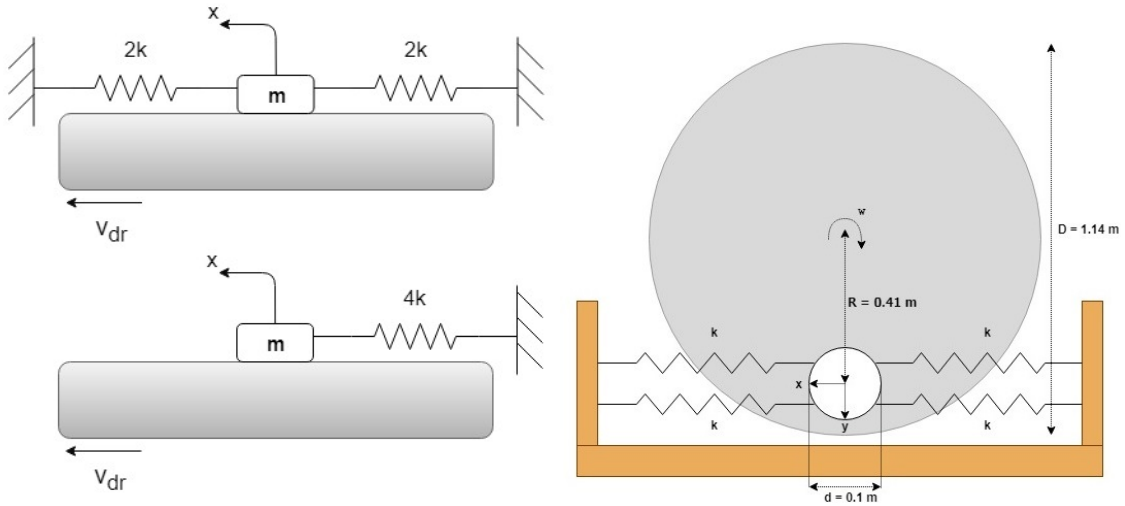

(a) Side view of experimental set-up (b) Top view of experimental set-up

Figure 6.2: Lay-out of the experimental set-up

In theory, when considering the side view of the experimental set-up, the four springs can be added and represented by one spring. By representing the experimental set-up this way, one could state that there are no differences between the experiment and the model. However, when comparing the top views as presented in Figure 6.1b and 6.2b it becomes clear that in the experimental set-up a displacement component in y-direction is present. This is due to the fact that in stick mode the ice sample moves in the same direction as the concrete and therefore has a rotational motion and thus has displacements in both x- and y-direction. The two springs on either side help in resisting this rotational motion but analysis of the experimental data has shown that a y-component is present, and that the ice sample rotates (see Chapter 4). This again influences the behavior of the springs and therefore the addition of the spring stiffness into one spring with value $4k$ is debatable.

6.1.2 Randomness in friction coefficients and time dependence of the kinetic friction coefficient

The static and kinetic friction coefficients were calculated from the experimental data. Over the course of one test, the friction coefficients varied and therefore the mean and standard deviations were calculated. These values were provided as input to the numerical model. For every onset to stick or slip mode, the static or kinetic friction coefficient is obtained from a Gaussian distribution. Large variations of the kinetic friction coefficient over the course of one test were observed in Chapter 4. It was concluded that this effect can not be explained by the computational error that is introduced by calculating the acceleration by taking the gradient of the displacement twice. In the following it is investigated if the randomized kinetic friction coefficients used in the model, agree with the kinetic friction coefficients obtained from the experiment, and if it is possible verify the calculation method of μ_k.

In the numerical model the input is known. In the same way as for the calculation of the kinetic friction coefficient from the experimental data, the coefficient is calculated from the *numerical* data, to verify that the output agrees with the input and that the calculation method for μ_k is valid. Therefore, for the numerical output, the stick and slip modes were identified and the kinetic friction coefficient was obtained as: $\mu_k = \frac{m\ddot{x}+kx}{mg}$. The result is shown in Figure 6.3

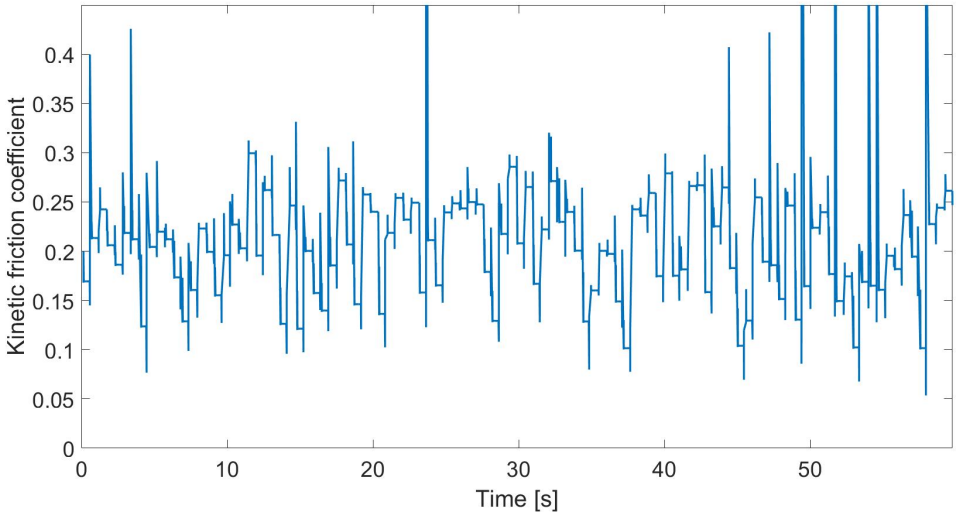

Figure 6.3: Kinetic friction coefficient calculated from the output of the model

The model was constructed such that for each onset of stick or slip mode, the static or, respectively, the kinetic friction coefficient was calculated from the Gaussian distribution, as explained in Chapter 5. One would therefore expect to see regions of constant μ_k in Figure 6.3 with gaps in between that indicate stick mode. To visualize this better, the plot was constructed as a scatter plot instead of a line plot, see Figure 6.4.

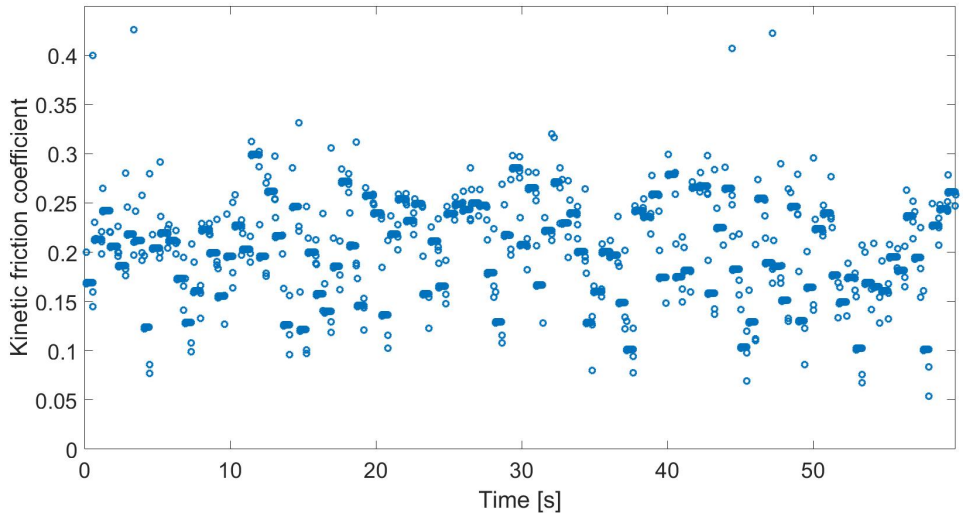

Figure 6.4: Kinetic friction coefficient calculated from the output of the model, scatter plot

Figure 6.4 shows that there are indeed periods of constant μ_k, which should be the case as the input was specified as such. A reason for the outliers could be found in the way that the slip mode is defined, according to Chapter 4:

"All data points for which $v < v_{concrete}$, are in slip mode"

However, transition from slip to stick happens *around* $v_{concrete}$, and therefore perhaps only the data points that are not exactly below, but that are well below $v_{concrete}$ should be taken into account. This reasoning was tested and the following definition of slip was used: *"All data points for which $v < 0.97 \cdot v_{concrete}$ are in slip mode"*. The result is shown in Figure 6.5.

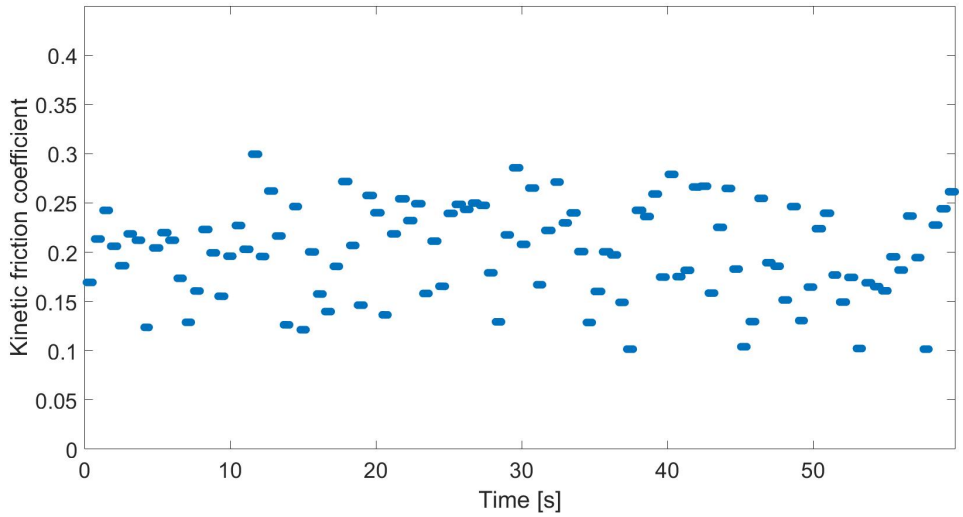

Figure 6.5: Kinetic friction coefficient calculated from the output of the model, with $v < 0.97 \cdot v_{concrete}$

All the outliers have been filtered out and the variation of μ_k is smaller when compared to Figure 6.4. This proves the hypothesis that the data points *around* $v_{concrete}$ should not be taken into account in the calculation of μ_k.

Using the numerical model, the calculation method of the kinetic friction coefficient

has been verified. The experimental data is now analyzed again. Figure 6.6 presents the result as was shown in Figure 4.52 but presented as a scatter plot. Slip mode is defined here as $v_{ice} < v_{concrete}$.

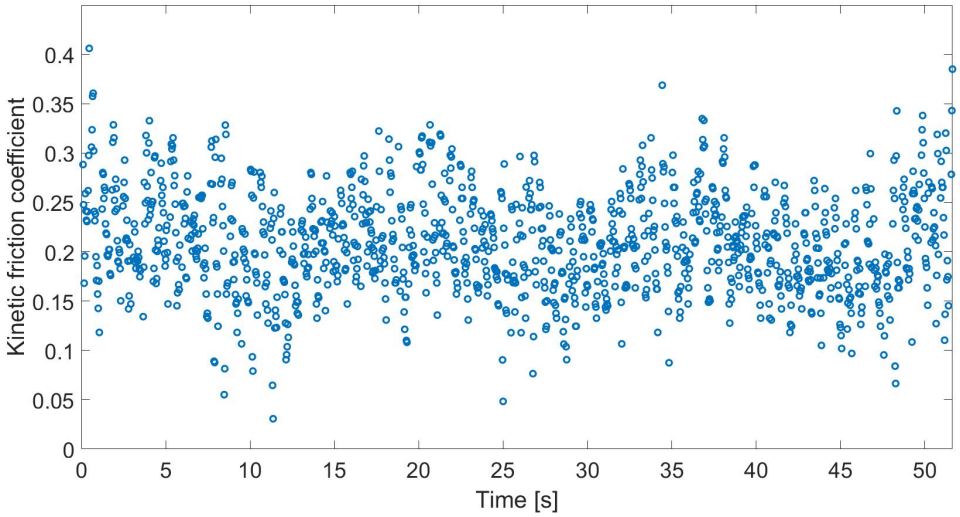

Figure 6.6: Kinetic friction coefficient calculated from the experimental data, scatter plot

Now, the same rationale as above is applied. Since there were fewer data points in the experimental data, there were no data points between $0.97 \cdot v_{concrete}$ and $v_{concrete}$. Therefore, the definition of slip mode in the experimental data was adapted to: $v_{ice} < 0.8 \cdot v_{concrete}$, see Figure 6.7

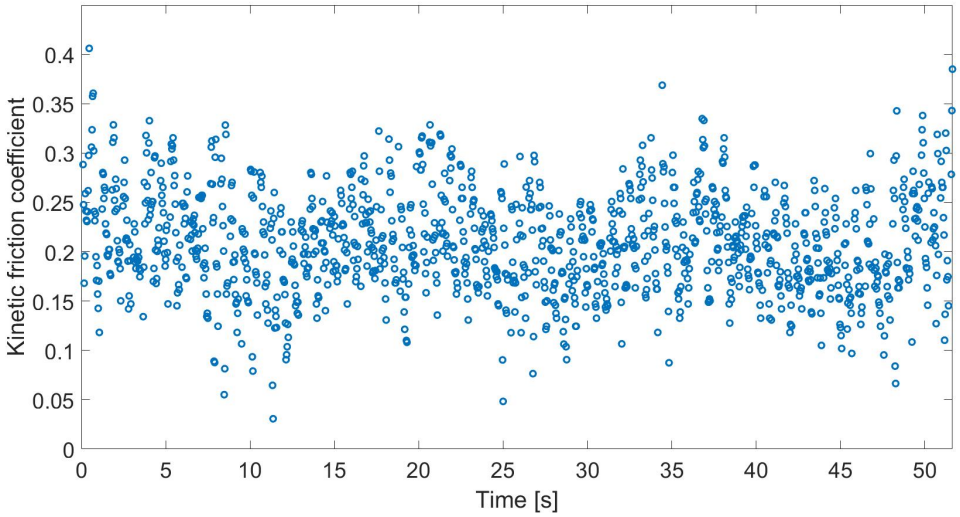

Figure 6.7: Kinetic friction coefficient calculated from the experimental data, $v < 0.8 \cdot v_{concrete}$

The difference is not visible right away, but the number of data points in Figure 6.6 is around 1200, while in Figure 6.7 the number of data points is reduced to about 900. However, it becomes apparent that the outliers have not been filtered out.

When comparing the friction coefficients from the experiment and from the numerical model, the spread of the kinetic friction coefficient is similar. In both Figures 6.5 and 6.6, the kinetic friction coefficient roughly varies between 0.1 and 0.3. In Chapter 4, it was also seen that the kinetic friction coefficient depends on the location of the ice sample along

the circular path on the concrete slab, possibly due to skewing of the slab or because of a certain pattern in roughness. The effect of the rotation of the slab was not taken into account in the numerical model.

As a conclusion, it can be stated that the calculation method of μ_k has been verified, with respect to the input and output of the numerical model. Next to that, the Gaussian distributed randomized friction coefficient in the numerical model, represents the kinetic friction coefficient from the experiment. Periodic effects have not been observed in the displacement, velocity and acceleration. Therefore, the fact that the periodicity of μ_k is not taken into account in the model is assumed valid.

6.1.3 Memory effect in friction

By calculating the friction coefficients from the experimetnal data, using the friction laws of Coulomb and Amonton, the effect of memory in friction is not considered. Therefore, in the numerical model this is not taken into account. The question is, by not including this memory effect in the numerical model, is it possible to accurately describe the stick-slip phenomenon? And by calculating the friction coefficients without memory effect, have they been calculated accurately? In the work of Schulson and Fortt [Schulson and Fortt 2013] it is noticed that static strengthening can be detected only after a certain threshold value for the holding time and that this threshold period decreases with increasing velocity. At a sliding velocity of 0.0001 m/s the effect is clearly visible after one second holding time. The lowest velocity used in the stick-slip experiments presented in this thesis, is 0.15 m/s which is 1500 times larger. This would suggest a serious decrease in the threshold period. The stick periods observed in the experiment lasted up to 0.13 seconds. Based on the work of Schulson one would therefore expect static strengthening to have played a role in the stick-slip behavior of the set-up used for this experiment.

Assuming static strengthening has played a role during the experiments, the coefficients that were calculated from the experimental data would have been the *final* static friction coefficients. Therefore, the possible effect of static strengthening is taken into account in the model through the friction coefficients. When a situation would be simulated with the numerical model, for which the friction coefficients are not known from the experiment, this might be a factor to consider.

6.1.4 Dry and wet friction

The numerical model is based on the assumption that the stick-slip phenomenon between concrete and ice can be described by *dry friction*. However, ice is subject to melting, and the ambient temperature as well as frictional heating of the ice surface can largely influence the state of the ice which brings the validity of the assumption of dry friction into question. During the experiment, it was made sure that the ambient temperature during testing stayed below zero, preferably around -2 ° C. The ice sample was inspected after testing and no signs of surface melting were visible with the unaided eye. It is known that wet friction lubricates the surfaces and decreases the friction. According to [Moen et al. 2015], this effect could potentially explain the effect of the velocity on the kinetic friction coefficient: a higher velocity yields a lower friction coefficient. However other explanations were also found in literature, which seem more likely due to the fact that no surface melting was observed. Nevertheless, since the friction coefficients were calculated from the experimental data and then implemented in the numerical model, the possible microscopic effect is taken into account by the effect it would have had on the friction coefficient. If surface melting had been such that the whole interface would have been lubricated with water, it could have prevented stick mode from happening. In this case, the stick-slip model would not be accurate. However, since surface melting was not visible,

it is concluded that the assumption of dry friction is valid.

6.2 Statistical comparison between output of the model and experimental data

To assess whether or not the output of the numerical model simulates the experiment with statistical significance, the output of the model was compared to the complete set of experimental data. In order to characterize the behavior of the ice sample under certain conditions, the mean and standard deviation of the displacement (x_{mean} and x_{SD}) and the peak frequency (f_{peak}) of the ice sample interacting with the concrete were determined for every data set from the test plan. The variables k, v, m were varied in the numerical model according to the experimental test plan, see Chapter 3. The static and kinetic friction coefficients were obtained from the corresponding experimental data. As was explained in Chapter 4, peaks were observed in the experimental velocity curves and therefore it was not possible to calculate the static friction coefficient for every data set. Therefore, not every test could be simulated with the numerical model. In total 39 tests could be simulated by the model and the data sets compared to the experimental data were assigned a test number of 1 to 39, see Appendix E for an overview.

For each characteristic parameter x_{mean}, x_{SD} or f_{freq}, the error was calculated. The error is defined as the difference between what was calculated by the model and what was observed in the experiments and is calculated as follows:

$$\text{Error} = \frac{\bar{x}_{model} - \bar{x}_{experiment}}{\bar{x}_{experiment}} \cdot 100\% \tag{6.1}$$

Where $\bar{x}$ represents either x_{mean}, x_{SD} or f_{freq}. Figure 6.8 shows the mean displacement for all tests that could be simulated by the model, and as found from the experimental data, and displays the error.

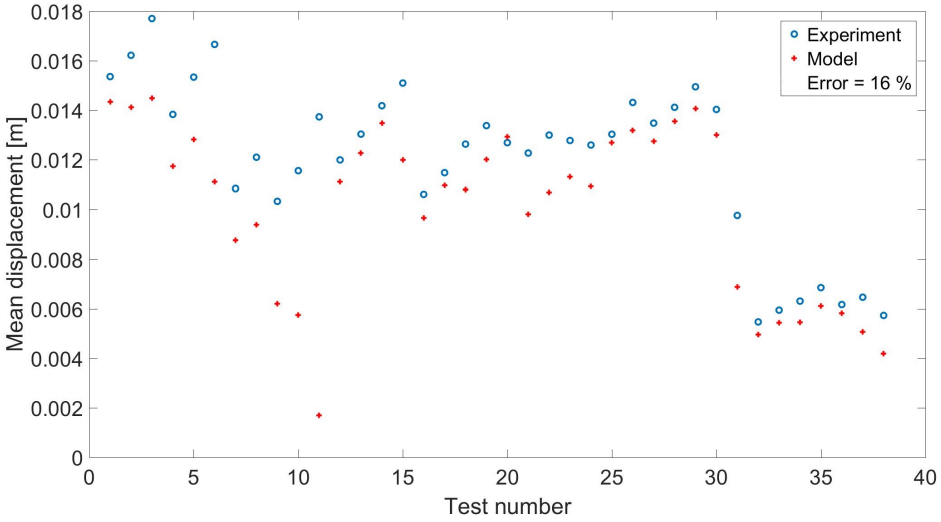

Figure 6.8: Mean displacement of experiment versus model

According to Figure 6.8 the mean displacement predicted by the model is on average underestimated by 16%. It can also be observed that for the lower test numbers 1-11, the trend observed in the experimental data is not followed by the numerical data points.

Figure 6.9 presents the comparison made between model and the experiment in terms of the standard deviation of the displacement.

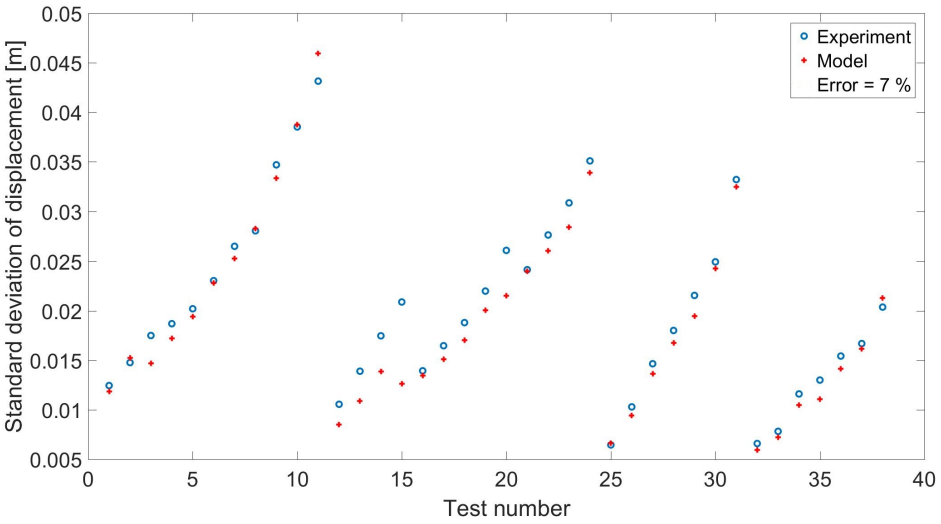

Figure 6.9: Standard deviation of displacement of experiment versus model

The standard deviation of the displacement is calculated with an error of 7% and the trends seen in the experimental data and the numerical output are similar. Lastly the peak frequencies are compared in Figure 6.10.

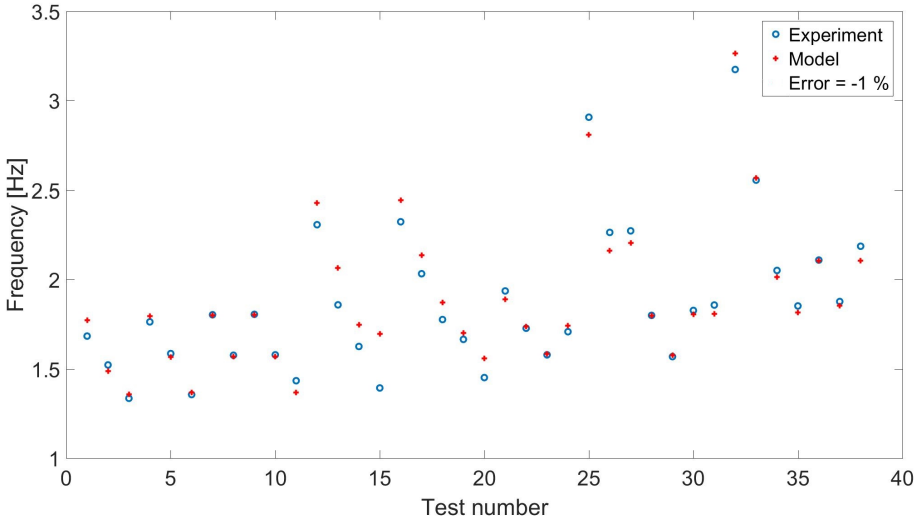

Figure 6.10: Frequency of experiment versus model

Figure 6.10 provides the insight that the peak frequency predicted by the numerical model is sometimes over- and sometimes underestimated, but on average the error is low, only -1%.

6.2.1 Discussion of the differences observed in statistical comparison

As was discussed in Section 6.1, several differences between the model and the experiment can be identified. This naturally results in a discrepancy between the output of the model and the experimental data. As explained in Section 6.1.2, it was observed in Chapter 4 that the calculated kinetic friction coefficient had a large standard deviation. This also causes a large variation in the slip mode in the numerical model and influences the output. To investigate this influence, the standard deviation of the kinetic friction coefficient was therefore decreased: $\mu_{kin_{SD_{new}}} = 0.5 \cdot \mu_{kin_{SD_{old}}}$. This influenced the results as shown in Figures 6.11, 6.12 and 6.13 respectively.

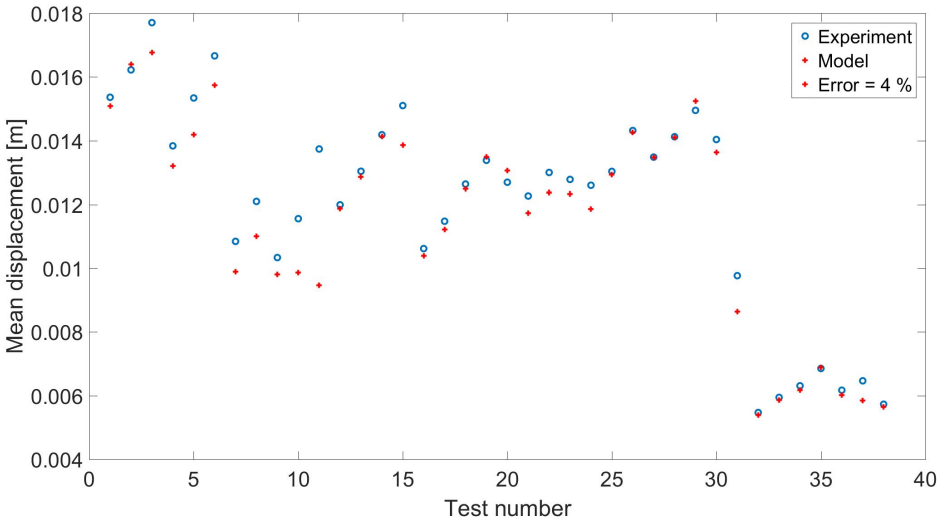

Figure 6.11: Mean displacement of experiment versus model ($0.5 \cdot \mu_{kinSD}$)

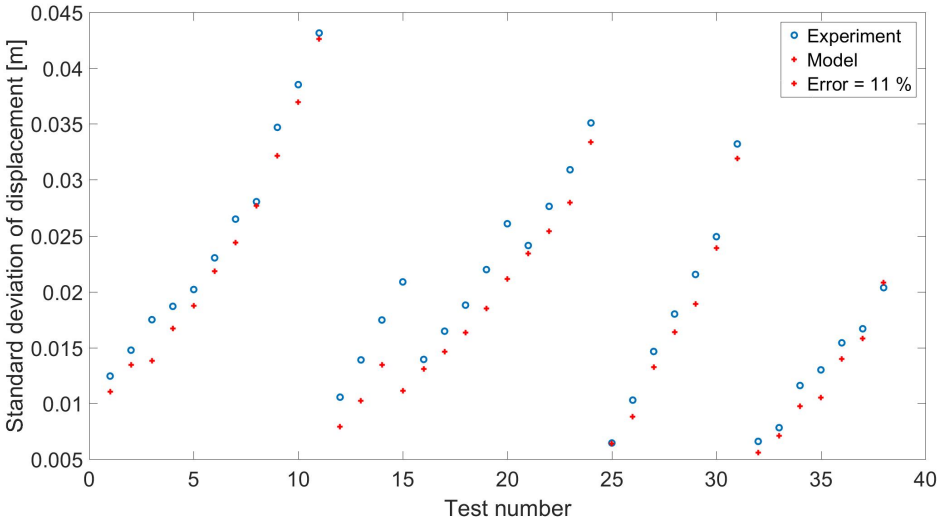

Figure 6.12: Standard deviation of displacement of experiment versus model ($0.5 \cdot \mu_{kinSD}$)

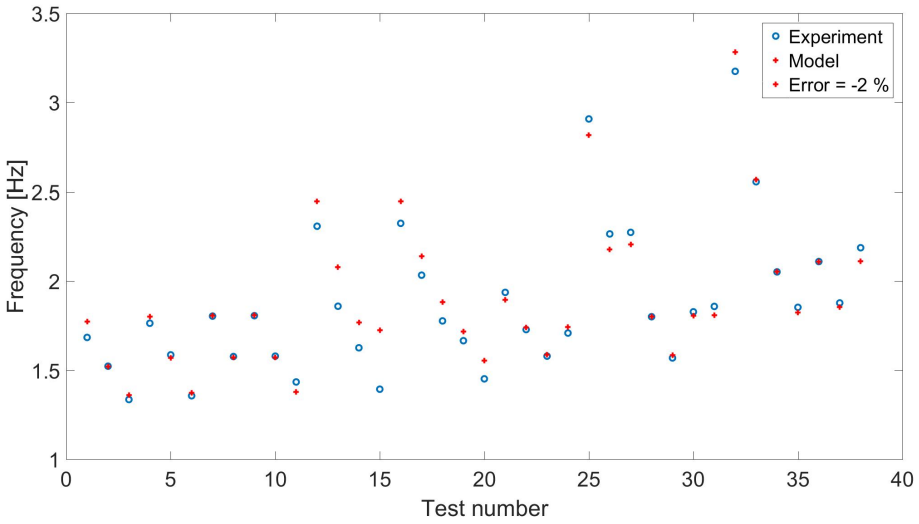

Figure 6.13: Frequency of experiment versus model ($0.5 \cdot \mu_{kinSD}$)

The effect of decreasing the standard deviation of the kinetic friction coefficient by 50 percent clearly benefits the prediction of the mean displacement of the ice sample, as the error has decreased from 16% to 4%, see Figure 6.11. Next to that the trends in the mean displacement predicted by the model are more similar to the trends observed in the numerical model. However, decreasing $\mu_{k_{SD}}$ does not benefit the numerically calculated standard deviation of the displacement, see Figure 6.12. The error has increased from 7% to 11%, but the trends are still predicted well. Figure 6.13 shows that the prediction of the peak frequency is not significantly affected going from 1% to 2% error. The overestimation of the variation of the kinetic friction coefficient over time seems to explain a large part of the discrepancies between the experimental and numerical output, and thus more research into the calculation of $\mu_{k_{SD}}$ is needed.

Chapter 7

Conclusions and Recommendations

A need exists for a more accurate identification of the static and kinetic friction coefficients. For this purpose, over a hundred experimental stick-slip tests have been carried out at Memorial University of Newfoundland, Canada. The static and kinetic friction coefficients were calculated and the influence of the normal load, velocity and spring stiffness was analyzed. Additionally, a numerical stick-slip model was created and validated using the experimental data. Section 7.1 summarizes the findings of the experimental work and section 7.2 recapitulates the numerical model. Section 7.3 contains a discussion about the types of friction that can be used to describe the stick-slip phenomenon, based on the observations in the experimental work as well as the numerical output. Lastly, section 7.4 ends with a list of recommendations for future research.

7.1 Observations and conclusions drawn from the experimental work

An experimental set-up was designed successfully, and stick-slip behavior of ice on a concrete surface was tested. The influence of the normal load on the ice sample (m), the velocity of the concrete (v) and the stiffness of the springs (k) on the behavior of the ice sample was analyzed. It was verified that the experimentally obtained data physically makes sense. For example, the ice sample traveled further when the normal load was higher, indicating an increase in frictional resistance. Next to that, the stick and slip modes were identified in the experimental data. The following definitions were used:

- When $v_{ice} = v_{concrete}$, the ice sample is in stick mdoe
- When $v_{ice} < v_{concrete}$, the ice sample is in slip

In the process of identifying the stick modes, unexpected peaks in the velocity curves were observed due to measurement errors and rotation of the ice sample. Wherever peaks in the velocity curve were observed it was not possible to identify a stick mode. Identification of the stick and slip modes in the experimental data allowed for the calculation of the static and kinetic friction coefficients. Because of the difficulty of identifying stick mode in some cases due to the peaks in the velocity curves, less data points were available for the calculation of the static friction coefficient, compared to the data that was available for the calculation of the kinetic friction coefficient. The static friction coefficients obtained over the whole range of tests varied from 0.1 to 0.5. The kinetic friction coefficient found varied from 0.08 to 0.4 and is on average equal to 0.7 times the static friction coefficient. The influence of m, v and k on the friction coefficients was also investigated, where the mean of the friction coefficients showed a clear dependence, but the standard deviation

of both the static and the kinetic friction coefficients did not seem to be influenced. The influence of the m, v and k on the mean friction coefficients is summarized in Sections 7.1.1, 7.1.2 and 7.1.3 respectively.

7.1.1 Influence of normal load on μ_s and μ_k

- The overall friction force $F_{fric} = \mu_s F_N$ was observed to increase with an increase in normal load, leading to leading to larger displacements of the ice sample. However, analysis of the static friction coefficient demonstrated that an increase in weight added on top of the ice sample decreased the static friction coefficient. Since the decrease in the friction coefficient is of a smaller magnitude than the increase in the normal force F_N, the overall friction force increases.

- The obtained kinetic friction coefficient was observed to decrease as a result of an increase in normal load, which is supported by literature [Fiorio, Meyssonnier, and Boulon 2002], [Moen et al. 2015].

7.1.2 Influence of concrete velocity on μ_s and μ_k

- An increase in velocity slightly decreases the static friction coefficient, according to the analysis of the experimental data performed in this thesis. In literature it is also found that the static friction coefficient decreases with increasing velocity [Saeki et al. 1986]. In [Saeki et al. 1986], it is suggested that this influence decreases with increasing velocity, especially from around 0.1 m/s upwards, which supports the findings in this thesis.

- For the kinetic friction coefficient it was more clearly observed that an increase in velocity caused a decrease in the kinetic friction coefficient. Literature points out that an increase in velocity causes an increase of the effects of frictional heating, namely the development of a thin water layer [Moen et al. 2015]. This effect lowers the friction between the two surfaces. Even though dry friction was assumed in this thesis, and surface melting was not visible, this effect may have occurred on a microscopic level. [Saeki et al. 1986] advocate the fact that higher velocities cause the surfaces to ride over each other.

7.1.3 Influence of spring stiffness on μ_s and μ_k

The influence of spring stiffness was not identified, as the results of the analysis were contradicting. In the lower range of spring stiffnesses, an increase caused in k caused an increase in the static as well as the kinetic friction coefficient. A further increase in spring stiffness, however, caused a decrease in both the static and kinetic friction coefficients.

7.2 Performance of the numerical model

The experimentally obtained means and standard deviations of the static and kinetic friction coefficients, were included in the model by randomly determining the static and kinetic friction coefficients for each onset to stick or slip mode from a Gaussian distribution. It was shown that the behavior of the ice predicted by the model, with respect to the influence of m, v and k, corresponds with the behavior observed during the experiments. For example, increasing the normal load in the model shows larger displacements of the ice sample, as was also observed in the experiment. A statistical comparison was made between the model output and the experimental data for three output parameters that characterize the behavior of the ice sample: the mean displacement x_{mean}, the standard deviation of the displacement x_{SD} and the peak frequency of the system f_{peak}. The comparison showed that the mean displacement predicted by the numerical model deviates

16% from what was seen in the experiment. The standard deviation of the displacement is predicted with a 7% error and the peak frequency is slightly overestimated by 1%. The error in the mean displacement could be explained by the large variation in the kinetic friction coefficient. Possible explanations for the large variation of the kinetic friction coefficient were investigated. The influence of the computational error introduced by the calculation of the acceleration was investigated but no indications were found that this explains the large variation. Next to that, the way the kinetic friction coefficient was studied by using the numerical model. The input in the model was known, and the output was calculated. The output was in line with the expectations based on the input. Based on this, it was concluded that neither the calculation method explains the large variations. The effect of diminishing the variation of the kinetic friction coefficient with 50 %, on the output was investigated and showed a promising result. Therefore, improvements can be made to the model, and more research into the calculation of the friction coefficients could provide insight and improve the input of the model. Nevertheless, in general it can be concluded that the conveyor belt type numerical stick-slip model is valid for predicting the stick-slip behavior as observed during the experiment.

7.3 Identification of the type of friction that can describe the stick-slip phenomenon

In the numerical model it was assumed that the behavior of ice on a concrete surface can be described by dry friction without memory effect, where the friction coefficients are randomly obtained from a Gaussian distribution for each onset to stick or slip mode. It can be concluded that for the conditions of the experiment presented in this thesis (e.g. the ranges of m, v and k used):

- A Gaussian distributed randomization of the friction coefficients shows a promising result, however, the experimentally obtained variation of the kinetic friction coefficient may be too large. It was also shown that the kinetic friction coefficient depends on the location of the ice sample along the circular path on the concrete slab, and this is not taken into account in the model. However, since no periodic effects were observed in the output, it is concluded that the Gaussian distribution suffices.
- The memory effect can be neglected in the numerical model. If static strengthening has occurred during the experiment, this effect is incorporated in the calculation of the static friction coefficient. Therefore, indirectly the effect is taken into account in the model. Under different circumstances, e.g. when the friction coefficients are not known experimentally, this effect should be looked into.
- The assumption of dry friction is valid, since surface melting was not observed. If it has occurred on a microscopic level, the effect is taken into account through the friction coefficients.

7.4 Recommendations for future research

For future research into the identification of the static and kinetic friction coefficients for ice interacting with concrete surfaces during stick-slip, it is recommended to:

- obtain a more accurate estimation of the static friction coefficient, by removing the possibility for peaks in the velocity curve so that more stick modes can be identified. This can be achieved by further minimizing the possibility for 2D behavior in the experiment, which could for example be accomplished by investigating stick-slip behavior along a linear, instead of rotational, path. The peaks in the velocity could also be reduced by including the 2D behavior in the numerical model, where the ice

sample has three degrees of freedom: x, y and θ. If a similar set-up is used with a similar displacement measurement technique, the displacement of the ice sample should be measured from its center of rotation, as opposed to the edge of the ice sample, as was done in this work.

- research more extensively into the variation μ_k, by further analyzing the way μ_k was calculated. Other methods for the calculation of μ_k can be considered, for example by expressing the equations of motion following the Lagrange method.
- investigate the possibility for extrapolation with the numerical model, to make it suitable for researching stick-slip behavior outside the boundaries considered in this thesis (e.g. the ranges for m, v and k). Another possibility could be to experimentally investigate the boundaries for m, v and k for which stick-slip behavior is observed, and investigate the possibility of interpolation
- investigate other parameters that influence the stick-slip behavior, and therewith the friction coefficients. In literature dependency on for example surface roughness and ambient temperature is investigated, but as for the influences of sliding velocity and normal load, more research is needed.
- make an extensive comparison between findings in literature with respect to the static and kinetic friction coefficients. And obtain a clear overview of the possible physical mechanisms involved, such as frictional heating or the crushing of asperities due to increased normal load.
- experimentally investigate the physical mechanisms involved further, by for example using microscopic images and thermal imagery.

List of Figures

List of Tables

Appendix A

Experimental data

Table A.1: Experimental data for spring type k_1

k	**v**	**m**	x_{mean} [m]	x_{SD} [m]	f_{peak} [Hz]
k_1	v_1	m_1	0.0154	0.0125	1.68
k_1	v_1	m_2	0.0162	0.0148	1.52
k_1	v_1	m_3	0.0177	0.0175	1.34
k_1	v_1	m_6	0.0202	0.0231	1.06
k_1	v_2	m_1	0.0138	0.0187	1.76
k_1	v_2	m_2	0.0153	0.0202	1.59
k_1	v_2	m_4	0.0167	0.0230	1.36
k_1	v_2	m_6	0.0175	0.0314	1.16
k_1	v_3	m_1	0.0108	0.0265	1.80
k_1	v_3	m_2	0.0121	0.0281	1.58
k_1	v_3	m_4	0.0135	0.0327	1.36
k_1	v_3	m_6	0.0152	0.0415	1.17
k_1	v_4	m_1	0.0103	0.0347	1.81
k_1	v_4	m_2	0.0116	0.0385	1.58
k_1	v_4	m_4	0.0137	0.0431	1.43
k_1	v_4	m_6	0.0143	0.0541	1.21
k_1	v_5	m_1	0.0101	0.0410	1.83
k_1	v_5	m_2	0.0116	0.0479	1.65
k_1	v_5	m_4	0.0136	0.0535	1.41
k_1	v_5	m_6	0.0196	0.0667	1.29
k_1	v_6	m_1	0.0100	0.0523	1.81
k_1	v_6	m_2	0.0115	0.0583	1.65
k_1	v_6	m_4	0.0134	0.0637	1.45
k_1	v_6	m_6	0.0280	0.0739	1.38

Table A.2: Experimental data for spring type k_2

k	**v**	**m**	x_{mean} [m]	x_{SD} [m]	f_{peak} [Hz]
k_2	v_1	m_1	0.0120	0.0106	2.31
k_2	v_1	m_2	0.0130	0.0139	1.86
k_2	v_1	m_4	0.0142	0.0175	1.63
k_2	v_1	m_5	0.0151	0.0209	1.39
k_2	v_1	m_6	0.0153	0.0257	1.29
k_2	v_2	m_1	0.0106	0.0139	2.32
k_2	v_2	m_2	0.0115	0.0165	2.03
k_2	v_2	m_4	0.0126	0.0188	1.78
k_2	v_2	m_5	0.0134	0.0220	1.67
k_2	v_2	m_6	0.0127	0.0261	1.45
k_2	v_3	m_1	0.0107	0.0175	2.42
k_2	v_3	m_2	0.0109	0.0206	2.12
k_2	v_3	m_4	0.0123	0.0241	1.94
k_2	v_3	m_5	0.0130	0.0277	1.73
k_2	v_3	m_6	0.0128	0.0309	1.58
k_2	v_4	m_1	0.0100	0.0231	2.48
k_2	v_4	m_2	0.0108	0.0271	2.22
k_2	v_4	m_4	0.0120	0.0309	1.86
k_2	v_4	m_5	0.0126	0.0351	1.71
k_2	v_4	m_6	0.0132	0.0396	1.58
k_2	v_5	m_1	0.0086	0.0297	2.54
k_2	v_5	m_2	0.0091	0.0351	2.22
k_2	v_5	m_4	0.0096	0.0303	2.03
k_2	v_5	m_5	0.0108	0.0439	1.81
k_2	v_5	m_6	0.0113	0.0495	1.63
k_2	v_6	m_1	0.0084	0.0346	2.46
k_2	v_6	m_2	0.0096	0.0430	2.14
k_2	v_6	m_4	0.0101	0.0324	2.03
k_2	v_6	m_5	0.0112	0.0494	1.75
k_2	v_6	m_6	0.0151	0.0592	1.72

Table A.3: Experimental data for spring type k_3

k	**v**	**m**	x_{mean} [m]	x_{SD} [m]	f_{peak} [Hz]
k_3	v_1	m_1	0.0130	0.0065	2.91
k_3	v_1	m_3	0.0143	0.0103	2.26
k_3	v_1	m_6	0.0150	0.0128	1.90
k_3	v_1	m_7	0.0158	0.0159	1.49
k_3	v_2	m_1	0.0122	0.0108	2.86
k_3	v_2	m_3	0.0135	0.0147	2.27
k_3	v_2	m_6	0.0141	0.0180	1.80
k_3	v_2	m_7	0.0149	0.0216	1.57
k_3	v_3	m_1	0.0120	0.0156	2.76
k_3	v_3	m_3	0.0130	0.0208	2.22
k_3	v_3	m_6	0.0140	0.0249	1.83
k_3	v_3	m_7	0.0148	0.0296	1.60
k_3	v_4	m_1	0.0117	0.0210	2.82
k_3	v_4	m_3	0.0126	0.0271	2.21
k_3	v_4	m_6	0.0098	0.0332	1.86
k_3	v_4	m_7	0.0119	0.0380	1.70
k_3	v_5	m_1	0.0083	0.0264	2.82
k_3	v_5	m_3	0.0091	0.0334	2.29
k_3	v_5	m_6	0.0037	0.0254	1.82
k_3	v_5	m_7	0.0041	0.0373	1.66
k_3	v_6	m_1	0.0021	0.0303	2.88
k_3	v_6	m_3	0.0029	0.0306	2.26
k_3	v_6	m_6	0.0037	0.0328	1.86
k_3	v_6	m_7	0.0047	0.0578	1.68

Table A.4: Experimental data for spring type k_4

k	**v**	**m**	x_{mean} [m]	x_{SD} [m]	f_{peak} [Hz]
k_4	v_1	m_1	0.00547	0.0066	3.17
k_4	v_1	m_3	0.00595	0.0078	2.55
k_4	v_1	m_6	0.00631	0.0116	2.05
k_4	v_1	m_7	0.00685	0.0130	1.85
k_4	v_2	m_1	0.00514	0.0096	3.27
k_4	v_2	m_3	0.00589	0.0108	2.69
k_4	v_2	m_6	0.00617	0.0154	2.11
k_4	v_2	m_7	0.00647	0.0167	1.88
k_4	v_3	m_1	0.00517	0.0133	3.43
k_4	v_3	m_3	0.00583	0.0161	2.71
k_4	v_3	m_6	0.00573	0.0204	2.19
k_4	v_3	m_7	0.00624	0.0232	1.99
k_4	v_4	m_1	0.00514	0.0167	3.52
k_4	v_4	m_3	0.00577	0.0183	2.77
k_4	v_4	m_6	0.00559	0.0222	2.23
k_4	v_4	m_7	0.00561	0.0269	1.99
k_4	v_5	m_1	0.00525	0.0171	3.48
k_4	v_5	m_3	0.00546	0.0205	2.69
k_4	v_5	m_6	0.00511	0.0240	2.32
k_4	v_5	m_7	0.00559	0.0229	1.99
k_4	v_6	m_1	0.00512	0.0147	3.41
k_4	v_6	m_3	0.00528	0.0209	2.69
k_4	v_6	m_6	0.00539	0.0179	2.26
k_4	v_6	m_7	0.00557	0.0182	1.93

Appendix B

Static friction coefficients

Table B.1: Static friction coefficients, spring type k_1

k	**v**	**m**	$\mu_{s_{mean}}$	$\mu_{s_{SD}}$
k_1	v_1	m_1	0.2815	0.0538
k_1	v_1	m_2	0.2282	0.0726
k_1	v_1	m_4	0.1529	0.0441
k_1	v_1	m_6		
k_1	v_2	m_1	0.2377	0.0640
k_1	v_2	m_2	0.1711	0.0493
k_1	v_2	m_4	0.1504	0.0449
k_1	v_2	m_6		
k_1	v_3	m_1	0.2183	0.0631
k_1	v_3	m_2	0.1619	0.0431
k_1	v_3	m_4		
k_1	v_3	m_6		
k_1	v_4	m_1	0.2324	0.0129
k_1	v_4	m_2	0.1775	0.0449
k_1	v_4	m_4	0.1501	0.0288
k_1	v_4	m_6		

Table B.2: Static friction coefficients, spring type k_2

k	**v**	**m**	$\mu_{s_{mean}}$	$\mu_{s_{SD}}$
k_2	v_1	m_1	0.4010	0.0818
k_2	v_1	m_2	0.3965	0.0725
k_2	v_1	m_4	0.3791	0.0904
k_2	v_1	m_5	0.2347	0.0434
k_2	v_1	m_6		
k_2	v_2	m_1	0.4134	0.1505
k_2	v_2	m_2	0.3285	0.1183
k_2	v_2	m_4	0.2636	0.0899
k_2	v_2	m_5	0.2531	0.1070
k_2	v_2	m_6	0.2142	0.1194
k_2	v_3	m_1		
k_2	v_3	m_2		
k_2	v_3	m_4	0.2740	0.0436
k_2	v_3	m_5	0.2402	0.0825
k_2	v_3	m_6	0.2057	0.0580
k_2	v_4	m_1		
k_2	v_4	m_2		
k_2	v_4	m_4		
k_2	v_4	m_5	0.2456	0.0398
k_2	v_4	m_6		

Table B.3: Static friction coefficients, spring type k_3

k	**v**	**m**	$\mu_{s_{mean}}$	$\mu_{s_{SD}}$
k_3	v_1	m_1	0.4946	0.0632
k_3	v_1	m_3	0.3780	0.0495
k_3	v_1	m_6		
k_3	v_1	m_7		
k_3	v_2	m_1		
k_3	v_2	m_3	0.3407	0.0424
k_3	v_2	m_6	0.2537	0.0448
k_3	v_2	m_7	0.2303	0.0277
k_3	v_3	m_1		
k_3	v_3	m_3		
k_3	v_3	m_6	0.2465	0.0316
k_3	v_3	m_7		
k_3	v_4	m_1		
k_3	v_4	m_3		
k_3	v_4	m_6	0.1937	0.0217
k_3	v_4	m_7		

Table B.4: Static friction coefficients, spring type k_4

k	**v**	**m**	$\mu_{s_{mean}}$	$\mu_{s_{SD}}$
k_4	v_1	m_1	0.3570	0.0572
k_4	v_1	m_3	0.2225	0.0636
k_4	v_1	m_6	0.2025	0.0898
k_4	v_1	m_7	0.1735	0.0524
k_4	v_2	m_1		
k_4	v_2	m_3		
k_4	v_2	m_6	0.1767	0.0555
k_4	v_2	m_7	0.1205	0.0468
k_4	v_3	m_1		
k_4	v_3	m_3		
k_4	v_3	m_6	0.2065	0.0471
k_4	v_3	m_7	0.1527	0.0365
k_4	v_4	m_1		
k_4	v_4	m_3		
k_4	v_4	m_6		
k_4	v_4	m_7		

Appendix C

Kinetic friction coefficients

Table C.1: Kinetic friction coefficients, spring type k_1

k	**v**	**m**	$\mu_{k_{mean}}$	$\mu_{k_{SD}}$
k_1	v_1	m_1	0.2086	0.0510
k_1	v_1	m_2	0.1661	0.0523
k_1	v_1	m_4	0.1393	0.0469
k_1	v_1	m_6	0.1117	0.0517
k_1	v_2	m_1	0.1852	0.0674
k_1	v_2	m_2	0.1561	0.0566
k_1	v_2	m_4	0.1308	0.0587
k_1	v_2	m_6	0.0971	0.0838
k_1	v_3	m_1	0.1451	0.0898
k_1	v_3	m_2	0.1218	0.0691
k_1	v_3	m_4	0.1051	0.0815
k_1	v_3	m_6	0.0863	0.0844
k_1	v_4	m_1	0.1403	0.1176
k_1	v_4	m_2	0.1189	0.1169
k_1	v_4	m_4	0.1056	0.1284
k_1	v_4	m_6	0.0816	0.1499

Table C.2: Kinetic friction coefficients, spring type k_2

k	**v**	**m**	$\mu_{k_{mean}}$	$\mu_{k_{SD}}$
k_2	v_1	m_1	0.3095	0.0823
k_2	v_1	m_2	0.2517	0.0832
k_2	v_1	m_4	0.2103	0.0727
k_2	v_1	m_5	0.1892	0.0766
k_2	v_1	m_6	0.1548	0.0736
k_2	v_2	m_1	0.2712	0.0851
k_2	v_2	m_2	0.2223	0.0724
k_2	v_2	m_4	0.1866	0.0631
k_2	v_2	m_5	0.1685	0.0637
k_2	v_2	m_6	0.1358	0.0552
k_2	v_3	m_1	0.2717	0.0780
k_2	v_3	m_2	0.2096	0.0836
k_2	v_3	m_4	0.1805	0.1038
k_2	v_3	m_5	0.1630	0.0671
k_2	v_3	m_6	0.1333	0.0578
k_2	v_4	m_1	0.2537	0.1079
k_2	v_4	m_2	0.2059	0.1157
k_2	v_4	m_4	0.1744	0.0854
k_2	v_4	m_5	0.1555	0.0906
k_2	v_4	m_6	0.1303	0.1033

Table C.3: Kinetic friction coefficients, spring type k_3

k	**v**	**m**	$\mu_{k_{mean}}$	$\mu_{k_{SD}}$
k_3	v_1	m_1	0.4309	0.0521
k_3	v_1	m_3	0.2883	0.0644
k_3	v_1	m_6	0.2021	0.0648
k_3	v_1	m_7	0.1668	0.0511
k_3	v_2	m_1	0.4048	0.0740
k_3	v_2	m_3	0.2709	0.0661
k_3	v_2	m_6	0.1899	0.0449
k_3	v_2	m_7	0.1579	0.0516
k_3	v_3	m_1	0.3954	0.0984
k_3	v_3	m_3	0.2589	0.0780
k_3	v_3	m_6	0.1872	0.0565
k_3	v_3	m_7	0.1532	0.0659
k_3	v_4	m_1	0.3880	0.1330
k_3	v_4	m_3	0.2537	0.0804
k_3	v_4	m_6	0.1301	0.0970
k_3	v_4	m_7	0.1139	0.0990

Table C.4: Kinetic friction coefficients, spring type k_4

k	**v**	**m**	$\mu_{k_{mean}}$	$\mu_{k_{SD}}$
k_4	v_1	m_1	0.2478	0.0762
k_4	v_1	m_3	0.1639	0.0444
k_4	v_1	m_6	0.1180	0.0546
k_4	v_1	m_7	0.1009	0.0430
k_4	v_2	m_1	0.2326	0.0952
k_4	v_2	m_3	0.1608	0.0487
k_4	v_2	m_6	0.1149	0.0516
k_4	v_2	m_7	0.0927	0.0603
k_4	v_3	m_1	0.2332	0.1172
k_4	v_3	m_3	0.1601	0.0826
k_4	v_3	m_6	0.1061	0.0981
k_4	v_3	m_7	0.0887	0.0785
k_4	v_4	m_1	0.2338	0.1447
k_4	v_4	m_3	0.1585	0.1193
k_4	v_4	m_6	0.1054	0.0939
k_4	v_4	m_7	0.0794	0.0859

Appendix D

Output of numerical model

Table D.1: Output of the numerical model for spring type k_1

k	**v**	**m**	x_{mean} [m]	x_{SD} [m]	f_{peak} [Hz]
k_1	v_1	m_1	0.0143	0.0119	1.77
k_1	v_1	m_2	0.0141	0.0153	1.49
k_1	v_1	m_4	0.0145	0.0147	1.36
k_1	v_1	m_6			
k_1	v_2	m_1	0.0117	0.0172	1.80
k_1	v_2	m_2	0.0128	0.0194	1.57
k_1	v_2	m_4	0.0111	0.0228	1.37
k_1	v_2	m_6			
k_1	v_3	m_1	0.0088	0.0253	1.80
k_1	v_3	m_2	0.0094	0.0283	1.57
k_1	v_3	m_4			
k_1	v_3	m_6			
k_1	v_4	m_1	0.0062	0.0334	1.80
k_1	v_4	m_2	0.0057	0.0387	1.57
k_1	v_4	m_4	0.0017	0.0459	1.37
k_1	v_4	m_6			

Table D.2: Output of the numerical model for spring type k_2

k	**v**	**m**	x_{mean} [m]	x_{SD} [m]	f_{peak} [Hz]
k_2	v_1	m_1	0.0111	0.0085	2.43
k_2	v_1	m_2	0.0134	0.0109	2.07
k_2	v_1	m_4	0.0135	0.0139	1.75
k_2	v_1	m_5	0.0120	0.0126	1.70
k_2	v_1	m_6			
k_2	v_2	m_1	0.0097	0.0134	2.45
k_2	v_2	m_2	0.0110	0.0151	2.14
k_2	v_2	m_4	0.0108	0.0170	1.87
k_2	v_2	m_5	0.0120	0.0200	1.70
k_2	v_2	m_6	0.0129	0.0215	1.56
k_2	v_3	m_1			
k_2	v_3	m_2			
k_2	v_3	m_4	0.0098	0.0240	1.89
k_2	v_3	m_5	0.0107	0.0260	1.74
k_2	v_3	m_6	0.0113	0.0284	1.58
k_2	v_4	m_1			
k_2	v_4	m_2			
k_2	v_4	m_4			
k_2	v_4	m_5	0.0109	0.0339	1.74
k_2	v_4	m_6			

Table D.3: Output of the numerical model for spring type k_3

k	**v**	**m**	x_{mean} [m]	x_{SD} [m]	f_{peak} [Hz]
k_3	v_1	m_1	0.0127	0.0066	2.81
k_3	v_1	m_3	0.0132	0.0094	2.16
k_3	v_1	m_6			
k_3	v_1	m_7			
k_3	v_2	m_1			
k_3	v_2	m_3	0.0128	0.0136	2.20
k_3	v_2	m_6	0.0136	0.0168	1.80
k_3	v_2	m_7	0.0141	0.0195	1.58
k_3	v_3	m_1			
k_3	v_3	m_3			
k_3	v_3	m_6	0.0130	0.0243	1.81
k_3	v_3	m_7			
k_3	v_4	m_1			
k_3	v_4	m_3			
k_3	v_4	m_6	0.0069	0.0325	1.81
k_3	v_4	m_7			

Table D.4: Output of the numerical model for spring type k_4

k	**v**	**m**	x_{mean} [m]	x_{SD} [m]	f_{peak} [Hz]
k_4	v_1	m_1	0.0055	0.0059	3.26
k_4	v_1	m_3	0.0054	0.0072	2.57
k_4	v_1	m_6	0.0054	0.0105	2.02
k_4	v_1	m_7	0.0061	0.0111	1.82
k_4	v_2	m_1			
k_4	v_2	m_3			
k_4	v_2	m_6	0.0058	0.0141	2.11
k_4	v_2	m_7	0.0051	0.0161	1.85
k_4	v_3	m_1			
k_4	v_3	m_3			
k_4	v_3	m_6	0.0042	0.0213	2.11
k_4	v_3	m_7	0.0050	0.0239	1.86
k_4	v_4	m_1			
k_4	v_4	m_3			
k_4	v_4	m_6			
k_4	v_4	m_7			

Appendix E

Overview of test numbers

Table E.1: Definition of test number based on experimental variables k,v and m

Test number	**k**	**v**	**m**
1	k_1	v_1	m_1
2	k_1	v_1	m_2
3	k_1	v_1	m_4
4	k_1	v_2	m_1
5	k_1	v_2	m_2
6	k_1	v_2	m_4
7	k_1	v_3	m_1
8	k_1	v_3	m_2
9	k_1	v_4	m_1
10	k_1	v_4	m_2
11	k_1	v_4	m_4
12	k_2	v_1	m_1
13	k_2	v_1	m_2
14	k_2	v_1	m_4
15	k_2	v_1	m_5
16	k_2	v_2	m_1
17	k_2	v_2	m_2
18	k_2	v_2	m_4
19	k_2	v_2	m_5
20	k_2	v_2	m_6
21	k_2	v_3	m_4
22	k_2	v_3	m_5
23	k_2	v_3	m_6
24	k_2	v_4	m_5
25	k_3	v_1	m_1
26	k_3	v_1	m_3
27	k_3	v_2	m_3
28	k_3	v_2	m_6
29	k_3	v_2	m_7
30	k_3	v_3	m_6
31	k_3	v_4	m_6
32	k_4	v_1	m_1
33	k_4	v_1	m_3
34	k_4	v_1	m_6
35	k_4	v_1	m_7
36	k_4	v_2	m_6
37	k_4	v_2	m_7
38	k_4	v_3	m_6
39	k_4	v_3	m_7

Bibliography

Bose, Arindam (2013). *How to detect and track red objects in live video in Matlab*. URL: http://arindambose.com/?p=587.

Bruneau, S. E., A.K. Dillenburg, and S. Ritter (2012). "Ice sample production techniques and indentation tests for laboratory experiments simulating ship collisions with ice". In: International Society of Offshore and Polar Engineers.

Fiorio, B. and J. Meyssonnier (1997). "Experimental study of the friction of ice over concrete at the centimeter scale". In: International Society of Offshore and Polar Engineers, pp. 466 –472.

Fiorio, B., J. Meyssonnier, and M. Boulon (2002). "Experimental study of the friction of ice over concrete under simplified ice-structure interaction conditions". In: *Canadian Journal of Civil Engineering* 29, pp. 347–359.

Galvanetto, U. and S.R. Bishop (1994). "Stick-slip vibrations of a two degree-of-freedom geophysical fault model". In: *International Journal of Mechanical Sciences* 36.8, pp. 683–698.

Hoving, J. (2019). "Boundary formulations for discrete lattices to describe the non-smooth dynamic behaviour of solid media in the time domain". PhD thesis. Delft University of Technology.

Huovinen, S. (1990). "Abrasion of concrete by ice in arctic sea structures". In: *Rakenteiden mekaniikka* 23, pp. 23–25.

Itoh, Y. et al. (1988). "An experimental study on abrasion of concrete due to sea ice". In: Offshore Technology Conference, pp. 61–68.

Jacobsen, S., L.V. Kim, and E.E. Pomnikov (2012). "Concrete destructure due to ice-indentation pore pressure". In: International Society of Offshore and Polar Engineers.

Leine, R.I. et al. (1998). "Stick-slip vibrations induced by alternate friction models". In: *Nonlinear Dynamics* 16, pp. 41–54.

Martins, J.A.C., J.T. Oden, and F.M.F. Simoes (1990). "A study of static and kinetic friction". In: *International Journal of Engineering Science* 28.1, pp. 29–92.

Moen, E. et al. (2015). "Experimental study of concrete abrasion due to ice friction - Part I: Set-up, ice abrasion vs. material properties and exposure conditions". In: *Cold Regions Science and Technology* 110, pp. 183–201.

Nakazawa, N. et al. (1993). "Factors Influencing the Coefficient of Friction between Sea Ice and Various Materials". In: Port and Ocean Engineering Under Arctic Conditions, pp. 97–105.

Newhook, J. and D. McGuinn (2007). "Ice abrasion assessment - piers of confederation bridge". In: *Confedeation Bridge Engineering Summit Canadian Society of Civil Engineering*, pp. 145–157.

Oestreich, M., N. Hinrichs, and K. Popp (1996). "Bifurcation and stability analysis for a non-smooth friction oscillator". In: *Archive of Applied Mechanics* 66, pp. 301–314.

Popov, V.L. (2017). *Contact mechanics and friction: physical principles and applications*. Springer.

Ryan, A., S. Bruneau, and Bruce Colbourne (2017). "Conceptual Design for Testing Ice Abrasion on Offshore Concrete Surfaces". In: *Proceedings of the Twenty-seventh (2017) International Ocean and Polar Engineering Conference*. International Society of Offshore and Polar Engineers, pp. 1292–1298.

Saeki, H. et al. (1986). "The coefficient of friction between sea ice and various materials used in offshore structures". In: *Journal of Energy Resources Technology* 108, pp. 65–71.

Schulson, E.M. and A.L. Fortt (2013). "Static strengthening of frictional surfaces of ice". In: *Acta Materialia* 61, pp. 1616–1623.

Tijsen, J.N.W. (2015). "Experimental study on the development of abrasion at offshore concrete structures in ice conditions". MA thesis. Delft University of Technology.